SUSPENSION MECHANICS:

I. INERTIAL AND NON-NEWTONIAN MIGRATION OF NEUTRALLY BUOYANT RIGID SPHERES IN TWO-DIMENSIONAL UNIDIRECTIONAL FLOWS;

II. THE EFFECT OF VISCOELASTICITY ON THE CREEPING MOTION OF A TRAIN OF NEUTRALLY BUOYANT NEWTONIAN DROPS THROUGH A CIRCULAR TUBE.

Thesis by
Bosco Po-Wai Ho

In Partial Fulfillment of the Requirement
for the Degree of
Doctor of Philosophy

California Institute of Technology
Pasadena, California
1975

(Submitted December 10, 1974)

This thesis is dedicated to my parents.

ACKNOWLEDGEMENT

I wish to express my deepest gratitude to my research advisor, Dr. L. G. Leal, who has given me timeless effort, encouragement and patience throughout the course of this research.

I would like to extend my sincere thanks to the financial supports of California Institute of Technology, the Petroleum Research Fund administered by the American Chemical Society, Union Oil Company Foundation, and National Science Foundation.

Also, I appreciate all the help from George Griffith, Raymond Reed, Seichi Nakawatase, Bill Schuelke, and from my colleagues Grant Robertson, Erdinc Zana and Tom McMillen.

While words cannot express all the thanks I owe my parents, I must acknowledge their wisdom in sending me to college eight years ago and their continuous financial support, encouragement, patience and love throughout my college years. To my father and mother, YOU have made all these possible for me.

ABSTRACT

The lateral migration of neutrally buoyant rigid spheres in two-dimensional unidirectional flows was studied theoretically. The cases of both inertia-induced migration in a Newtonian fluid and normal stress-induced migration in a second-order fluid were considered. Analytical results for the lateral velocities were obtained, and the equilibrium positions and trajectories of the spheres compared favorably with the experimental data available in the literature. The effective viscosity was obtained for a dilute suspension of spheres which were simultaneously undergoing inertia-induced migration and translational Brownian motion in a plane Poiseuille flow. The migration of spheres suspended in a second-order fluid inside a screw extruder was also considered.

The creeping motion of neutrally buoyant concentrically located Newtonian drops through a circular tube was studied experimentally for drops which have an undeformed radius comparable to that of the tube. Both a Newtonian and a viscoelastic suspending fluid were used in order to determine the influence of viscoelasticity. The extra pressure drop due to the presence of the suspended drops, the shape and velocity of the drops, and the streamlines of the flow were obtained for various viscosity ratios,

total flow rates, and drop sizes. The results were compared with existing theoretical and experimental data.

TABLE OF CONTENTS

Chapter 1

INTRODUCTION

Studies involving multiphase systems undergoing bulk motion have encompassed broad lines of disciplines in science and engineering. Multiphase flow, in this context, refers to the relative motion of discrete particles (either solid or fluid phases) in a suspending fluid medium and to the flow of interstitial fluid, or fluids, through a matrix of solid materials. The former includes particles moving through a stagnant fluid (e.g. sedimentation), fluid flowing through 'stationary' particles (e.g. fluidized beds), and particles undergoing translational and rotational motion in a flowing medium (e.g. shearing motion of a suspension). The latter refers to flow through porous media or packed beds. Studies on these systems include various transport processes of momentum, heat and mass, chemical kinetics, and electric charge and ionic transfer.

Flowing multiphase systems are found in many industrial processes such as polymer processing in the plastic industry, fluidized beds, pulp and paper making, magnetic tape manufacture, separation processes in metallurgy, and pollution abatement. Also in nature, there occur flowing multiphase systems such as aerosols in the atmosphere,

sediments in water, the flow through porous media, and biological fluids. Discussions of many natural and technological processes involving multiphase systems may be found in the texts by Happel & Brenner (1973) and Soo (1967). Understanding the fundamental principles of the flow of these systems is useful for their description, in optimization and design in industry, and the innovation and systematic development of new products and processes.

The investigations of various processes occurring in multiphase systems have followed two methods of approach: (i) treating the detailed physical and chemical processes on the scale of one or few particles and then trying to extend the results to the entire system as a whole, and (ii) modifying the continuum mechanics of single-phase systems on a macroscopic scale in such a manner as to account for the presence of the particles. In this dissertation, the dynamics and kinematics of two types of two-phase systems (i.e. suspensions) are studied on the microscopic scale to provide a fundamental understanding of the fluid mechanics of such systems, and some of these results are extended to macroscopic properties.

It is now worthwhile to point out several usages of the dynamics and kinematics of the flow fields of suspensions. In many instances, the flow fields govern the behavior of other transport processes such as the forced

convection of heat and mass, and chemical reactions that are occurring in the system. Of course, if the flow fields are coupled with other processes, the solutions to these problems have to be solved simultaneously. Also, the rheological properties of the suspension on a macroscopic scale can be derived (at least in principle) from the flow fields and the spatial, orientation and shape distributions of suspended particles. This last application is often called "microrheology", a terminology first used by Goldsmith & Mason (1966) who reviewed the dynamics and kinematics of flow fields and particles on the microscopic scale. Recent developments on the extension of the microscopic details to macroscopic variables are summarized by Brenner (1970) and Batchelor (1974). Naturally, the rheological properties of a multiphase system can be studied from a continuum approach also. However, this latter approach suffers the disadvantage that there exist many unknown material coefficients which are sometimes difficult or impossible to obtain. In addition, no insight is obtained as to which constitutive model is applicable to a given suspension. On the other hand, microrheology is able to provide a detailed relationship between microstructure and bulk properties. Unfortunately, every system will have to be treated separately (at least at the present stage of development)

and many complicated systems may not have tractable solutions. Attempts to relate the constitutive equations derived from the microrheological and the continuum approaches appear to be a worthwhile endeavor (see Barthés-Biesel & Acrivos (1973)).

To obtain the flow fields on the microscopic scale in the absence of other transport or chemical processes (or if these processes are uncoupled from momentum transfer), the solutions to the momentum and mass conservation equations are required. The nonlinear features of these differential equations and the required boundary conditions often render the problems formidable. The nonlinearity may arise from three sources. First of all, the momentum equation has a nonlinear term arising from the inertia of the fluid. Secondly, if the fluid is non-Newtonian in nature, the viscous stresses in the momentum equation become nonlinear. Finally, if any boundary is nonrigid such that the shape of the boundary is part of the solution, the problem is also nonlinear. If the nonlinearity is small, analytical results can often be obtained either by neglecting the nonlinear terms completely or by using perturbation methods to obtain higher order corrections to the linear solutions. If the nonlinearity is large, experimental results are necessary. Often, the nonlinear effects are most interesting, such as

in the problems treated in this dissertation. Chapter II deals theoretically with the inertia-induced lateral migration of a neutrally buoyant rigid sphere in a Newtonian fluid. Chapter III considers analytically the lateral migration of a neutrally buoyant rigid sphere suspended in a non-Newtonian second-order fluid. Chapter IV involves experimental studies of the motion of liquid drops suspended in both Newtonian and viscoelastic fluids in a tube and suffering large deformation.

REFERENCES

Barthés-Biesel, D. & Acrivos, A. 1973 The rheology of suspensions and its relation to phenomenological theories for non-Newtonian fluids. Int. J. Multiphase Flow 1, 1.

Batchelor, G. K. 1974 Transport Properties of Two-Phase Materials with Random Structure. In Annual Review of Fluid Mechanics (ed. Van Dyke, M., et.al.), vol. 6. Annual Reviews Inc.

Brenner, H. 1970 Rheology of Two-Phase Systems. In Annual Review of Fluid Mechanics (ed. Van Dyke, M., et.al.) Vol. 2. Annual Reviews Inc.

Goldsmith, H. L. & Mason, S. G. 1967 The Microrheology of Dispersions. In Rheology: Theory and Applications (ed. F. R. Eirich), Vol. 4 Academic.

Happel, J. & Brenner, H. 1973 Low Reynolds Number Hydrodynamics. Noordhoff.

Soo, S. L. 1967 Fluid Dynamics of Multiphase Systems. Blaisdell.

Chapter II

INERTIAL MIGRATION OF RIGID SPHERES IN TWO-DIMENSIONAL UNIDIRECTIONAL FLOWS

The nonlinear inertial term in the momentum equation can cause several interesting effects in the motion of suspended particles. Neutrally buoyant spherical particles suspended in a Newtonian fluid undergoing unidirectional flow can migrate across streamlines under the influence of inertia and the bounding walls. This chapter theoretically studies such a phenomenon. The text of Chapter II consists of an article (coauthor, Dr. L. G. Leal) which has appeared in print in the Journal of Fluid Mechanics. Some of the details omitted in the text for brevity are given in Appendix A.

J. Fluid Mech. (1974), *vol.* 65, *part* 2, *pp.* 365–400
Printed in Great Britain

Inertial migration of rigid spheres in two-dimensional unidirectional flows

By B. P. HO AND L. G. LEAL
Chemical Engineering, California Institute of Technology, Pasadena

(Received 4 September 1973)

The familiar Segré–Silberberg effect of inertia-induced lateral migration of a neutrally buoyant rigid sphere in a Newtonian fluid is studied theoretically for simple shear flow and for two-dimensional Poiseuille flow. It is shown that the spheres reach a stable lateral equilibrium position independent of the initial position of release. For simple shear flow, this position is midway between the walls, whereas for Poiseuille flow, it is 0·6 of the channel half-width from the centre-line. Particle trajectories are calculated in both cases and compared with available experimental data. Implications for the measurement of the rheological properties of a dilute suspension of spheres are discussed.

1. Introduction

The phenomenon of inertia-induced cross-stream migration of small suspended particles in flowing suspensions has occupied a central position in the rheology and mechanics of such materials since the classical investigations of Segré & Silberberg (1962*a*, *b*, 1963). Though there had been occasional prior reports in the literature of non-uniform concentration distributions of particles in pipe flow (cf. Starkey 1956), these authors provided the first conclusive demonstration that neutrally buoyant rigid spheres in Poiseuille flow could, under appropriate circumstances, migrate across streamlines. More surprising than the existence of migration, however, was Segré & Silberberg's observation that the spheres eventually attained an equilibrium position at approximately 0·6 of the tube radius from the tube centre-line.

Following Segré & Silberberg, many subsequent experimental studies have been reported in which either the bulk flow configuration or the particle properties differed from those of the original work. Many of these are summarized in two excellent review articles, one by Goldsmith & Mason (1966) and the other by Brenner (1966). More recent investigations have been reported by Tachibana (1973) and Halow & Wills (1970*a*, *b*). These various studies show that the general behaviour for rigid *spheres* depends strongly on the specific bulk flow geometry and on whether or not the particle is neutrally buoyant. For Couette flow, neutrally buoyant rigid spheres migrate to the centre-line, while for both two- and three-dimensional Poiseuille flow, the sphere ultimately attains an equilibrium position which is approximately 60 % of the way from the centre-line to the vessel walls. On the other hand, a non-neutrally buoyant sphere subjected

to Poiseuille flow through a vertical flow channel is found to migrate towards the walls if its velocity is greater than the undisturbed fluid velocity evaluated at the same point, but towards the centre-line if the particle velocity lags behind the undisturbed fluid velocity.

In the present paper, we consider the case of a neutrally buoyant rigid sphere suspended in a Newtonian fluid which is undergoing either simple shear flow or a two-dimensional Poiseuille flow between two infinite plane boundaries. Many previous investigations have attempted to provide a theoretical description of the migration phenomenon. Experimentally, it has been recognized for some time that a neutrally buoyant rigid sphere suspended in a laminar unidirectional flow will rotate and translate *without* crossing the undisturbed streamlines, provided that the appropriate particle Reynolds number is sufficiently small. Indeed, Bretherton (1962) has shown theoretically that, if the inertia terms of the equations of motion are completely neglected, no lateral force can exist for a body of revolution in a unidirectional flow. Theoretical treatment of the migration problem thus requires inclusion of inertia effects. All investigators to date have used asymptotic expansions for small but non-zero values of the Reynolds number as a means of estimating the inertial contribution to the lateral motion of the particle. The two best known studies are those of Rubinow & Keller (1961) and Saffman (1965). Rubinow & Keller (1961) considered the case of a rigid sphere which is simultaneously spinning with an angular velocity $\mathbf{\Omega}_s$ and translating (in a perpendicular direction) at a velocity $\mathbf{U}_s$ through an unbounded stationary fluid at small (but non-zero) Reynolds number. The lateral force resulting in this case is

$$\mathbf{F}_L = \pi a^3 \rho_0 \mathbf{\Omega}_s \times \mathbf{U}_s, \tag{1.1}$$

in which ρ_0 is the fluid density and a is the radius of the spherical particle. Saffman (1965) considered the case of a uniform shear flow (with shear rate β^*) of an unbounded fluid of viscosity μ_0. The sphere was assumed to rotate with an angular velocity $\mathbf{\Omega}_s$ parallel to the vorticity vector of the undisturbed shear flow, and to translate with a velocity V relative to the local undisturbed velocity of the suspending fluid. The magnitude of the lateral force for this 'slip–shear' case is

$$F_L = 6{\cdot}46\mu_0 V a^2 (\beta^* \rho_0/\mu_0)^{\frac{1}{2}}, \tag{1.2}$$

which differs radically from that predicted by the 'slip–spin' mechanism of Rubinow & Keller (1961). In particular, the magnitude of the lateral force given by (1.2) is completely independent of the rate of rotation of the particle. The direction of the force (1.2) is such that a sphere lagging behind the local undisturbed fluid would migrate in the direction of the larger, undisturbed velocity, while a sphere leading the undisturbed flow would migrate in the opposite direction. Although a number of attempts have been made to use the theories of Rubinow & Keller (1961) and of Saffman (1965) to explain or correlate experimental observations of lateral migration, neither furnishes a satisfactory fundamental explanation of the phenomenon for the motion of neutrally buoyant particles in tubes or other bounded flow systems. Cox & Brenner (1968) were the first to consider the complete three-dimensional Poiseuille problem taking

account of the presence of the walls and the non-uniformity of the shear. These authors used the method of matched asymptotic expansions with two small parameters, the Reynolds number and the ratio a/R_0 of the sphere radius to the tube radius, to solve for the inertia-induced force and torque on the sphere. Unfortunately, however, the solution is not given in explicit form, but rather involves a number of very complex integral functions. As a result, no definite conclusions can be reached regarding the direction of the lateral force, its precise magnitude at any given radial position or even the presence or absence of an equilibrium position corresponding to the original observation of Segré & Silberberg.

Two-dimensional Poiseuille flow was previously studied experimentally and theoretically by Repetti & Leonard (1966), who attempted to explain the observed phenomenon of intermediate equilibrium positions by means of the Rubinow–Keller slip–spin theory. Most recently, Tachibana (1973) reported experimental results for two- and three-dimensional Poiseuille flow and concluded that the equilibrium positions are identical for both cases. Couette flow was investigated, both experimentally and theoretically, by Halow & Wills (1970*a*, *b*). The experimental work of these authors included a determination of equilibrium positions, as well as detailed measurements of the particle trajectories, prior to reaching equilibrium. The theory proposed was based upon the solution of Saffman (1965) and was represented as providing agreement with the particle trajectories. However, this agreement must be considered fortuitous since it was only achieved after multiplying Saffman's original (corrected) lift force by an empirical factor of 5. Our present analysis is closely similar to that of Cox & Brenner (1968). Specifically, we use the method of reflexions (equivalent to the formal expansion in a/R_0) to obtain the necessary solutions of the fluid motion. The lateral force on and velocity of the sphere are evaluated from these solutions using the generalized reciprocal theorem of Lorentz. By restricting our attention to two-dimensional flows between plane boundaries, we have been able to evaluate the magnitude and direction of the lateral force. In the next section of the paper, we outline the general method of solution and derive the necessary governing equations. The third section outlines the solution for creeping motion of a sphere suspended in a general quadratic bulk flow between two plane walls when the sphere is located at an arbitrary position between them (though not too close to either wall). The fourth section considers the related problem of the creeping motion of a sphere normal to two parallel walls when the sphere is again located at an arbitrary position between them. In the fifth section, we use these two solutions and the generalized reciprocal theorem to calculate the lateral force on the particle for both the simple shear and two-dimensional Poiseuille flow configurations. Finally, in the last two sections we provide trajectory calculations for a sphere and consider the steady-state concentration distribution for various bulk flow rates in the presence of translational Brownian motion. The trajectory calculations are compared with available experimental data in the Couette and two-dimensional Poiseuille systems. The non-uniform concentration distributions lead to an apparent non-Newtonian viscosity behaviour for two-dimensional Poiseuille flow, the behaviour depending on the

specific apparatus. This result is discussed in light of current theories of suspension rheology and of the related experimental data of Segré & Silberberg (1963) for apparent viscosities in tube flow of a dilute suspension of rigid spheres.

2. The basic equations

We consider a neutrally buoyant rigid sphere of radius a freely suspended in an incompressible Newtonian fluid which is confined between two parallel infinite plane walls separated by a distance d. The suspending fluid is assumed to be undergoing either a simple shear flow or a two-dimensional Poiseuille flow. We denote the fluid viscosity by μ_0 and its density by ρ_0. The basic flow geometry and remaining physical variables for the problem are depicted in figure 1. Of particular importance is d_1, the distance from the stationary wall in shear flow or from the bottom wall in two-dimensional Poiseuille flow to the centre of the particle. Also, as indicated, we employ co-ordinate axes fixed with respect to the particle for the basic analysis, with x^* in the direction of the undisturbed velocity, y^* in the direction of the undisturbed vorticity and z^* in the cross-stream direction. The origin of the co-ordinate system is coincident with the centre of the particle, hence, the walls in this system are located at $z^* = -d_1$ and $z^* = d - d_1$, respectively. We assume that the sphere is translating at a velocity $\mathbf{U}_s^*$ and rotating with an angular velocity $\boldsymbol{\Omega}_s^*$. As we have noted in the introduction, there can be no lateral (z) component to $\mathbf{U}_s^*$ in the absence of inertial effects in the disturbance flow induced by the particle. The prime objective of the present work is the calculation of the first inertia-induced contribution to the z component U_{sz}^*. In the following analysis, all variables will be non-dimensionalized with respect to the characteristic length scale a and an as yet unspecified velocity scale V_c^*. Variables with the superscript * are dimensional and all others non-dimensional, except for the obvious dimensional length scales a, d and d_1. The Reynolds number is then defined as $Re \equiv \rho_0 V_c^* a/\mu_0$.

We begin the detailed analysis with the full dimensionless governing equations and boundary conditions for the velocity and pressure fields $\mathbf{U}$ and P expressed in the particle-fixed co-ordinates indicated previously:

$$\left.\begin{aligned} &\nabla^2\mathbf{U} - \nabla P = Re\,(\mathbf{U}.\nabla\mathbf{U}), \quad \nabla.\mathbf{U} = 0, \\ &\mathbf{U} = \boldsymbol{\Omega}_s \times \mathbf{r} \quad \text{on} \quad r = 1, \\ &\mathbf{U} = \mathbf{V}_w - \mathbf{U}_s \quad \text{on} \quad \text{the walls}, \\ &\mathbf{U} \to \mathbf{V} \quad \text{as} \quad r \to \infty. \end{aligned}\right\} \tag{2.1}$$

Here, $\mathbf{V}$ represents the dimensionless undisturbed bulk flow while $\mathbf{V}_w$ is the dimensionless velocity of the walls. The undisturbed flow $(\mathbf{V}, Q)$ is measured relative to the particle-fixed co-ordinate system described earlier. In order to consider the simple shear and two-dimensional Poiseuille flows simultaneously, the undisturbed velocity and pressure fields will thus be expressed in the general form

$$\mathbf{V} = (\alpha + \beta z + \gamma z^2)\,\mathbf{e}_x - \mathbf{U}_s, \quad Q = 2\gamma x, \tag{2.2}$$

where α, β and γ in simple shear flow are given by

$$\alpha = V_w s, \quad \beta = V_w \kappa, \quad \gamma = 0, \tag{2.3}$$

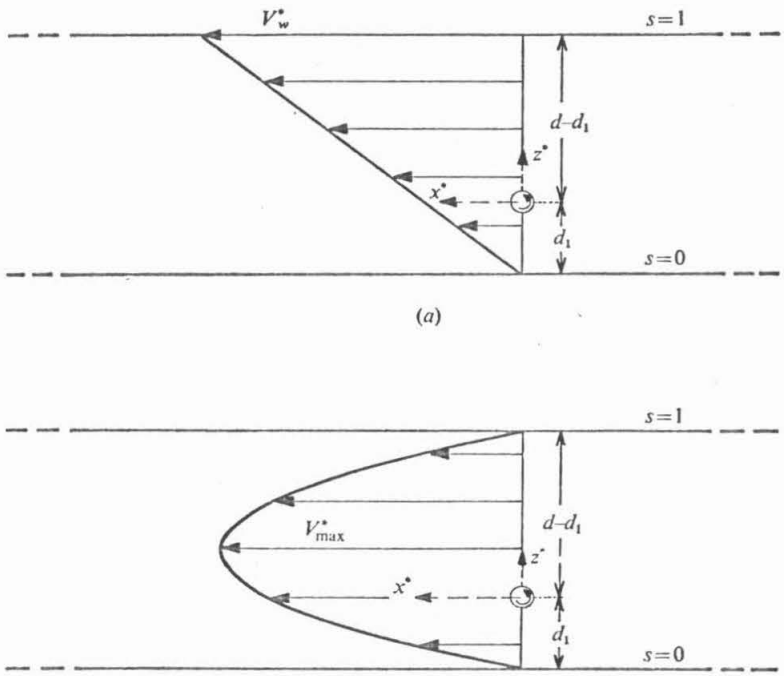

FIGURE 1. The physical system for (*a*) simple shear flow and (*b*) two-dimensional Poiseuille flow.

and in two-dimensional Poiseuille flow take the form

$$\alpha = 4V_{\max}s(1-s), \quad \beta = 4V_{\max}(1-2s)\kappa, \quad \gamma = -4V_{\max}\kappa^2. \tag{2.4}$$

In the above $s = d_1/d$ and $\kappa = a/d$, with d_1 defined in figure 1. Both V_w and $V_{\max}$ are non-dimensionalized with respect to V_c^*.

The solution of (2.1) is aided by introducing the disturbance velocity and pressure fields $\mathbf{v} = \mathbf{U} - \mathbf{V}$ and $q = P - Q$. Since the undisturbed fields $\mathbf{V}$ and Q themselves satisfy the equations and boundary condition

$$\left.\begin{aligned} &\nabla^2\mathbf{V} - \nabla Q = 0, \quad \nabla.\mathbf{V} = 0, \\ &\mathbf{V} = \mathbf{V}_w - \mathbf{U}_s \quad \text{on} \quad \text{the walls} \end{aligned}\right\} \tag{2.5}$$

for all values of the mean (bulk flow) Reynolds number,† it is straightforward to obtain the governing differential equations and boundary conditions for the disturbance fields:

$$\left.\begin{aligned} &\nabla^2\mathbf{v} - \nabla q = Re\,(\mathbf{v}.\nabla\mathbf{v} + \mathbf{v}.\nabla\mathbf{V} + \mathbf{V}.\nabla\mathbf{v}), \\ &\nabla.\mathbf{v} = 0, \\ &\mathbf{v} = \boldsymbol{\Omega}_s \times \mathbf{r} - \mathbf{V} \quad \text{on} \quad r = 1, \\ &\mathbf{v} = 0 \quad \text{on} \quad \text{the walls}, \\ &\mathbf{v} \to 0 \quad \text{as} \quad r \to \infty. \end{aligned}\right\} \tag{2.6}$$

† The inertia terms vanish identically for the unidirectional flows considered here.

In addition, since the disturbance flow is generated by the shear field acting on the sphere, it is clear that the appropriate characteristic velocity V_c^* defining the Reynolds number in (2.1) and (2.6) is the shear velocity $V_w^*(a/d)$ for simple shear flow and $V_{\max}^*(a/d)$ for two-dimensional Poiseuille flow.† Thus, the appropriate Reynolds number for the disturbance flow $(\mathbf{v}, q)$ is $Re \equiv \rho_0 V_w^* \kappa a/\mu_0$ for simple shear flow and $Re \equiv \rho_0 V_{\max}^* \kappa a/\mu_0$ for two-dimensional Poiseuille flow. The present paper is concerned with the solution of (2.6) in the double limit $Re \to 0$ with κ fixed, followed by $\kappa \to 0$. We shall soon see that it is necessary to have $Re \ll \kappa^2$ for the present method of solution. It is also worthwhile to note that the Reynolds number for the bulk flow $(\mathbf{V}, Q)$, say $\overline{Re} \equiv \rho_0 V_w^* d/\mu_0$ for the simple shear flow, is $\overline{Re} = Re\,\kappa^{-2}$. Thus, the condition $Re \ll \kappa^2$ also implies that $\overline{Re} \ll 1$.

Following the approach of Cox & Brenner (1968), we thus proceed by postulating the existence of an asymptotic expansion for $\mathbf{v}$, q, $\mathbf{U}_s$ and $\boldsymbol{\Omega}_s$ of the form

$$\left.\begin{aligned} \mathbf{v} &= \mathbf{v}^{(0)} + Re\,\mathbf{v}^{(1)} + \ldots, \qquad q = q^{(0)} + Re\,q^{(1)} + \ldots, \\ \mathbf{U}_s &= \mathbf{U}_s^{(0)} + Re\,\mathbf{U}_s^{(1)} + \ldots, \quad \boldsymbol{\Omega}_s = \boldsymbol{\Omega}_s^{(0)} + Re\,\boldsymbol{\Omega}_s^{(1)} + \ldots, \end{aligned}\right\} \tag{2.7}$$

in which the individual terms $(\mathbf{v}^{(0)}, q^{(0)})$ and $(\mathbf{v}^{(1)}, q^{(1)})$ satisfy the equations

$$\left.\begin{aligned} \nabla^2\mathbf{v}^{(0)} - \nabla q^{(0)} = 0, \quad \nabla\cdot\mathbf{v}^{(0)} = 0, \\ \mathbf{v}^{(0)} = \boldsymbol{\Omega}_s^{(0)} \times \mathbf{r} - (\alpha + \beta z + \gamma z^2)\,\mathbf{e}_x + \mathbf{U}_s^{(0)} \quad \text{on} \quad r = 1, \\ \mathbf{v}^{(0)} = 0 \quad \text{on} \quad \text{the walls}, \\ \mathbf{v}^{(0)} \to 0 \quad \text{as} \quad r \to \infty \end{aligned}\right\} \tag{2.8}$$

and

$$\left.\begin{aligned} \nabla^2\mathbf{v}^{(1)} - \nabla q^{(1)} = \mathbf{v}^{(0)}\cdot\nabla\mathbf{v}^{(0)} + \mathbf{v}^{(0)}\cdot\nabla\mathbf{V} + \mathbf{V}\cdot\nabla\mathbf{v}^{(0)}, \\ \nabla\cdot\mathbf{v}^{(1)} = 0, \\ \mathbf{v}^{(1)} = \boldsymbol{\Omega}_s^{(1)} \times \mathbf{r} + \mathbf{U}_s^{(1)} \quad \text{on} \quad r = 1, \\ \mathbf{v}^{(1)} = 0 \quad \text{on} \quad \text{the walls}, \\ \mathbf{v}^{(1)} \to 0 \quad \text{as} \quad r \to \infty. \end{aligned}\right\} \tag{2.9}$$

The condition for large r in (2.9) requires justification since it is well known that, to solve the Navier–Stokes equations by perturbation expansion, an outer expansion is generally required and a matching of the inner and outer expansions is necessary to obtain higher-order corrections. In the present case, however, Cox & Brenner (1968) have shown that the first term in the outer expansion is of smaller order than the Reynolds number to the first power, so that 'matching' for $Re\,\mathbf{v}^{(1)}$ is accomplished by simple application of the *natural* boundary condition, namely $\mathbf{v}^{(1)} \to 0$ as $\mathbf{r} \to \infty$. Alternatively, it may be verified from the solution for $(\mathbf{v}^{(0)}, q^{(0)})$ that the ratio of inertia to viscous terms is $Re\,\kappa^{-1}(r^*/a)$. Hence, close to and within the walls $r^* = O(d)$, the Stokes solution, provides a uniformly valid first approximation provided that $Re \ll \kappa^2$. In any case, it is clear that the outer expansion in Re is not required to obtain the lateral velocity to $O(Re)$.

† However, if the sphere is not neutrally buoyant, so that an appreciable slip velocity is introduced, the dominant disturbance may be generated by this slip velocity and the appropriate characteristic velocity for the Reynolds number would be the slip velocity.

The particle satisfies the usual equations of rigid-particle dynamics with no external force and torque. Because of the $O(Re)$ migration, the particle does suffer translational and angular accelerations, but these are $O(Re^2)$. Hence, there is no net hydrodynamic force or torque on the particle at $O(1)$ and $O(Re)$, and this fact is used to calculate $\mathbf{U}_s$ and $\boldsymbol{\Omega}_s$ to $O(Re)$. The zeroth-order terms $\mathbf{U}_s^{(0)}$ and $\boldsymbol{\Omega}_s^{(0)}$ are the translational and angular velocity of the sphere in the absence of inertia and can be written as

$$\mathbf{U}_s^{(0)} = U_{sx}^{(0)}\,\mathbf{e}_x, \quad \boldsymbol{\Omega}_s^{(0)} = \Omega_{sy}^{(0)}\,\mathbf{e}_y. \tag{2.10}$$

The first-order correction, taking inertia into account, contributes the additional translational and angular velocities $\mathbf{U}_s^{(1)}$ and $\boldsymbol{\Omega}_s^{(1)}$. At present,we are interested in calculating the lateral migration velocity $U_{sz}^{(1)}$, which is the z component of $\mathbf{U}_s^{(1)}$. Clearly, $U_{sz}^{(1)}$ could be determined by solving for $\mathbf{v}^{(1)}$ leaving $\mathbf{U}_s^{(1)}$ and $\boldsymbol{\Omega}_s^{(1)}$ unspecified and then applying the conditions of zero net external force and torque on the freely suspended particle; however, it can be shown that a complete solution for $\mathbf{v}^{(1)}$ is not necessary for this purpose. Instead, a version of the well-known reciprocal theorem of Lorentz which we shall outline in the next paragraph can be employed; this allows the migration velocity to be expressed in terms of a certain volume integral over the total fluid volume. Careful application of the reciprocal theorem also provides a proof of the fact that the lateral velocity calculated in the manner outlined above produces results identical to those of the approach outlined by Cox & Brenner (1968), in which one, in effect, first calculates the force required to prevent migration.

Suppose that $\boldsymbol{\tau}^{(1)}$ is the stress tensor corresponding to the velocity and pressure fields $\mathbf{v}^{(1)}$ and $q^{(1)}$ and $\mathbf{f}$ is the inhomogeneous part of the governing equation for $(\mathbf{v}^{(1)}, q^{(1)})$, that is

$$\boldsymbol{\tau}^{(1)} = -q^{(1)}\mathbf{I} + \nabla\mathbf{v}^{(1)} + (\nabla\mathbf{v}^{(1)})^T, \tag{2.11}$$

$$\mathbf{f} = \mathbf{v}^{(0)}.\nabla\mathbf{v}^{(0)} + \mathbf{v}^{(0)}.\nabla\mathbf{V} + \mathbf{V}.\nabla\mathbf{v}^{(0)}, \tag{2.12}$$

where $\mathbf{I}$ is the idemfactor and the superscript T stands for the transpose of the dyadic; then we can write

$$\nabla.\boldsymbol{\tau}^{(1)} - \mathbf{f} = 0, \tag{2.13}$$

or in summation notation

$$\tau_{jl,j}^{(1)} - f_l = 0. \tag{2.14}$$

Now let us define a new velocity field $(\mathbf{u}, p)$ according to the equations

$$\left.\begin{aligned} &\nabla^2\mathbf{u} - \nabla p = 0, \quad \nabla.\mathbf{u} = 0,\\ &\mathbf{u} = \mathbf{e}_z \quad \text{on} \quad r = 1,\\ &\mathbf{u} = 0 \quad \text{on} \quad \text{the walls},\\ &\mathbf{u} \to 0 \quad \text{as} \quad r \to \infty, \end{aligned}\right\} \tag{2.15}$$

which is the velocity field for a sphere translating with unit velocity perpendicular to the walls in a quiescent fluid. Denoting the corresponding stress tensor as $\mathbf{t}$, we can write

$$\nabla.\mathbf{t} = 0, \quad \text{or} \quad t_{ij,i} = 0. \tag{2.16}$$

Equations (2.14) and (2.16) then lead trivially to the equations

$$(\tau_{jl,j}^{(1)} - f_l)\,u_l = 0, \quad t_{ij,i}\,v_j^{(1)} = 0. \tag{2.17a, b}$$

On subtracting (2.17*b*) from (2.17*a*) and integrating over the entire fluid volume,

$$\int_{V_f} (\tau^{(1)}_{jl,j} u_l - t_{ij,i} v^{(1)}_j)\, dV = \int_{V_f} f_l u_l\, dV,$$

and rearranging, we obtain

$$\int_{V_f} \left\{ \frac{\partial}{\partial x_j}(\tau^{(1)}_{jl} u_l) - \tau^{(1)}_{jl} \frac{\partial u_l}{\partial x_j} - \frac{\partial}{\partial x_i}(t_{ij} v^{(1)}_j) + t_{ij} \frac{\partial v^{(1)}_j}{\partial x_i} \right\} dV = \int_{V_f} f_l u_l\, dV.$$

Use of the divergence theorem on the first and third terms yields

$$-\int_A n_i(\tau^{(1)}_{ij} u_j - t_{ij} v^{(1)}_j)\, dA - \int_{V_f} \left(\tau^{(1)}_{jl} \frac{\partial u_l}{\partial x_j} - t_{jl} \frac{\partial v^{(1)}_l}{\partial x_j} \right) dV = \int_{V_f} f_l u_l\, dV. \quad (2.18)$$

Here **n** denotes the unit vector pointing from the walls and particle surface into the surrounding fluid. By use of the definitions of $\tau^{(1)}_{jl}$ and t_{jl} and the equation of continuity, the integrand in the second integral can be shown to be identically zero. Hence, applying the boundary conditions

$$\mathbf{v}^{(1)} = \mathbf{u} = 0 \quad \text{on} \quad \text{the walls},$$

$$\mathbf{v}^{(1)} \to 0, \quad \mathbf{u} \to 0 \quad \text{as} \quad r \to \infty$$

and

$$v^{(1)}_j = (U^{(1)}_s)_j + \epsilon_{jmk} r_k (\Omega^{(1)}_s)_m, \quad u_j = \delta_{zj} \quad \text{on} \quad r = 1$$

we obtain

$$\int_A n_i \tau^{(1)}_{iz}\, dA - (U^{(1)}_s)_j \int_A n_i t_{ij}\, dA - \epsilon_{jmk} (\Omega^{(1)}_s)_m \int_A r_k n_i t_{ij}\, dA = -\int_{V_f} f_l u_l\, dV. \quad (2.19)$$

The first term on the left-hand side is the z component of the force on the sphere due to the velocity field $(\mathbf{v}^{(1)}, q^{(1)})$. Since the sphere is neutrally buoyant and freely suspended, we require this force to be identically zero, i.e.

$$\int_A n_i \tau^{(1)}_{iz}\, dA = 0.$$

The integral in the second term is nothing more than the hydrodynamic force on the sphere due to $(\mathbf{u}, p)$, i.e. the force on a sphere which translates between and normal to two infinite plane boundaries in a quiescent fluid, while the integral in the third term is the corresponding torque due to $(\mathbf{u}, p)$. The latter is clearly zero in view of the symmetries of the problem (2.15), while we shall show in § 4 that the former is of the form

$$\int_A n_i t_{ij}\, dA = -6\pi[1 + O(\kappa)]\, \delta_{zj}.$$

It thus follows that the migration velocity $U^{(1)}_{sz}$ is given by

$$U^{(1)}_{sz} = -\frac{1}{6\pi} \int_{V_f} f_l u_l\, dV. \quad (2.20)$$

The function **f** can be determined completely once the zeroth-order solution $\mathbf{v}^{(0)}$ is available, and the solution of (2.15) is straightforward. Hence, the reciprocal theorem, in the form (2.20), offers a considerably simplified scheme for calculating

the lateral migration velocity, especially when compared with the alternative calculation of the full first-order velocity field $\mathbf{v}^{(1)}$.

It is significant that the same result for the migration velocity $U_{sz}^{(1)}$ can also be obtained to the present level of approximation by a 'two-step' procedure in which one first calculates the force on the sphere with $U_{sz}^{(1)} \equiv 0$. In this case, (2.19) becomes

$$\int_A n_i \tau_{iz}^{(1)}\, dA = -\int_{V_f} f_l u_l\, dV.$$

Thus, the inertia-induced force is given by

$$F_L = -Re \int_{V_f} f_l u_l\, dV. \tag{2.21}$$

Clearly, upon adding the hydrodynamic drag associated with lateral motion

$$-6\pi[1+O(\kappa)]\, Re\, U_{sz}^{(1)}$$

and equating the sum to zero, the expression (2.20) is again obtained. The direct approach represented by the original development leading to (2.20) and the Cox & Brenner (1968) approach involving an intermediate calculation of F_L thus produce identical results to the *present order of approximation*. In view of the historical development of the problem, we shall adopt the latter, two-step calculation.

In the following two sections, we consider solutions of the problems (2.8) and (2.15) for $\mathbf{v}^{(0)}$ and $\mathbf{u}$ which are necessary for evaluation of (2.21).

3. Solution for $(\mathbf{v}^{(0)}, q^{(0)})$

Here we consider the creeping motion of a rigid sphere which is translating with a velocity $U_{sx}^{(0)}\,\mathbf{e}_x$ and rotating with an angular velocity $\Omega_{sy}^{(0)}\,\mathbf{e}_y$ in either simple shear or two-dimensional Poiseuille flow between two parallel plane boundaries. As we have seen, the corresponding velocity field $(\mathbf{v}^{(0)}, q^{(0)})$ is required to evaluate F_L using the reciprocal theorem, equation (2.21).

The solution is found by means of the iterative method of reflexions in which the complete solution $(\mathbf{v}^{(0)}, q^{(0)})$ is constructed as a sum of terms which alternately satisfy boundary conditions on the sphere surface and on the walls. A detailed description is given in Happel & Brenner (1973, chap. 7). The procedure actually produces a sequence of terms of increasing order in $\kappa\ (\equiv a/d)$ which is convergent for κ small, provided that the sphere is not too close to the walls. Expressing the velocity and pressure fields in the form

$$\left.\begin{aligned} \mathbf{v}^{(0)} &= \mathbf{v}_1^{(0)} + \mathbf{v}_2^{(0)} + \mathbf{v}_3^{(0)} + \ldots, \\ q^{(0)} &= q_1^{(0)} + q_2^{(0)} + q_3^{(0)} + \ldots, \end{aligned}\right\} \tag{3.1}$$

the method of reflexions is defined by the sequence of problems

$$\left.\begin{aligned} &\nabla^2 \mathbf{v}_1^{(0)} - \nabla q_1^{(0)} = 0, \quad \nabla \cdot \mathbf{v}_1^{(0)} = 0, \\ &\mathbf{v}_1^{(0)} = \Omega_{sy}^{(0)}\,\mathbf{e}_y \times \mathbf{r} - (\alpha + \beta z + \gamma z^2 - U_{sx}^{(0)})\,\mathbf{e}_x \quad \text{on} \quad r = 1, \\ &\mathbf{v}_1^{(0)} \to 0 \quad \text{as} \quad r \to \infty; \end{aligned}\right\} \tag{3.2}$$

$$\left.\begin{aligned}&\nabla^2\mathbf{v}_2^{(0)}-\nabla q_2^{(0)}=0,\quad \nabla.\mathbf{v}_2^{(0)}=0,\\&\mathbf{v}_2^{(0)}=-\mathbf{v}_1^{(0)}\quad\text{on}\quad\text{the walls;}\end{aligned}\right\}\tag{3.3}$$

$$\left.\begin{aligned}&\nabla^2\mathbf{v}_3^{(0)}-\nabla q_3^{(0)}=0,\quad \nabla.\mathbf{v}_3^{(0)}=0,\\&\mathbf{v}_3^{(0)}=-\mathbf{v}_2^{(0)}\quad\text{on}\quad r=1,\\&\mathbf{v}_3^{(0)}\to 0\quad\text{as}\quad r\to\infty.\end{aligned}\right\}\tag{3.4}$$

The quantities $\Omega_{sy}^{(0)}$ and $U_{sx}^{(0)}$ are as yet unknowns, which we shall shortly evaluate by equating the net force and torque acting on the sphere owing to $\mathbf{v}^{(0)}$ identically to zero. The field $(\mathbf{v}_1^{(0)}, q_1^{(0)})$ satisfies the boundary condition on the sphere surface, but in doing so generates non-zero terms at the walls. The second term $(\mathbf{v}_2^{(0)}, q_2^{(0)})$ cancels these terms at the wall, but in the process generates a non-zero contribution at the sphere surface which must be cancelled by the third term $(\mathbf{v}_3^{(0)}, q_3^{(0)})$, and so on to higher orders.

The solution for $(\mathbf{v}_1^{(0)}, q_1^{(0)})$ is found by using the general solution of Lamb. The result is

$$\mathbf{v}_1^{(0)}=(u_1^{(0)}, v_1^{(0)}, w_1^{(0)}),$$

$$\begin{aligned}u_1^{(0)}=&-\frac{A_1}{2}\left(1+\frac{x^2}{r^2}\right)\frac{1}{r}-B_1\left(1-\frac{3x^2}{r^2}\right)\frac{1}{r^3}-C_1\frac{z}{r^3}\\&+\frac{3D_1}{2}\left(\frac{zx^2}{r^5}\right)+3E_1\left(1-\frac{5x^2}{r^2}\right)\frac{z}{r^5}+3F_1\left(\frac{z^2-y^2}{r^2}\right)\frac{1}{r^3}\\&-\frac{G_1}{10}\left(1-\frac{13x^2}{r^2}-\frac{5z^2}{r^2}+\frac{75z^2x^2}{r^4}\right)\frac{1}{r^3}+3H_1\left(1-\frac{5x^2}{r^2}-\frac{5z^2}{r^2}+\frac{35z^2x^2}{r^4}\right)\frac{1}{r^5},\end{aligned}\tag{3.5a}$$

$$\begin{aligned}v_1^{(0)}=&-\frac{A_1}{2}\left(\frac{xy}{r^3}\right)+3B_1\frac{xy}{r^5}+\frac{3D_1}{2}\left(\frac{xyz}{r^5}\right)-15E_1\frac{xyz}{r^7}+3F_1\frac{xy}{r^5}\\&+\frac{G_1}{10}\left(13-\frac{75z^2}{r^2}\right)\frac{xy}{r^5}-15H_1\left(1-\frac{7z^2}{r^2}\right)\frac{xy}{r^7},\end{aligned}\tag{3.5b}$$

$$\begin{aligned}w_1^{(0)}=&-\frac{A_1}{2}\left(\frac{zx}{r^3}\right)+3B_1\frac{zx}{r^5}+C_1\frac{x}{r^3}+\frac{3D_1}{2}\left(\frac{z^2x}{r^5}\right)+3E_1\left(1-\frac{5z^2}{r^2}\right)\frac{x}{r^5}-3F_1\frac{zx}{r^5}\\&+\frac{G_1}{10}\left(23-\frac{75z^2}{r^2}\right)\frac{zx}{r^5}-15H_1\left(3-\frac{7z^2}{r^2}\right)\frac{zx}{r^7},\end{aligned}\tag{3.5c}$$

where

$$\left.\begin{aligned}&A_1=-\tfrac{3}{2}(U_{sx}^{(0)}-\alpha-\tfrac{1}{3}\gamma),\quad B_1=-\tfrac{1}{4}(U_{sx}^{(0)}-\alpha-\tfrac{3}{5}\gamma),\quad C_1=-(\Omega_{sy}^{(0)}-\tfrac{1}{2}\beta),\\&D_1=-\tfrac{5}{3}\beta,\quad E_1=-\tfrac{1}{6}\beta,\quad F_1=-\tfrac{1}{9}\gamma,\quad G_1=\tfrac{7}{12}\gamma,\quad H_1=\tfrac{1}{24}\gamma.\end{aligned}\right\}\tag{3.6}$$

The solution for $(\mathbf{v}_2^{(0)}, q_2^{(0)})$ is found by requiring $\mathbf{v}_2^{(0)}=-\mathbf{v}_1^{(0)}$ on the walls. Since the walls are a distance of order κ^{-1} from the sphere, it is convenient to introduce outer variables defined by

$$x'=\kappa x,\quad y'=\kappa y,\quad z'=\kappa z\quad (r'=\kappa r).\tag{3.7}$$

It is then necessary to re-express the field $(\mathbf{v}^{(0)}, q^{(0)})$ in a form appropriate to the region near the walls. This is accomplished by introducing the relationship

$$\frac{1}{r'}=\frac{1}{2\pi}\int_{-\infty}^{\infty}\int_{-\infty}^{\infty}\exp\{i\Omega-|\Lambda|\}\frac{d\xi\,d\eta}{2\zeta},\tag{3.8}$$

where $\Omega = \frac{1}{2}(\xi x' + \eta y')$, $\Lambda = \frac{1}{2}\zeta z'$ and $\zeta^2 = \xi^2 + \eta^2$, so that the velocity field $\mathbf{v}_1^{(0)}$ can be expressed in integral form as

$$u_1^{(0)} = \frac{1}{2\pi}\int_{-\infty}^{\infty}\int_{-\infty}^{\infty} \exp\{i\Omega - |\Lambda|\}\left[g_1 + \frac{\xi^2}{\zeta^2}(g_2 + |\Lambda|\, g_3)\right] d\xi\, d\eta, \tag{3.9a}$$

$$v_1^{(0)} = \frac{1}{2\pi}\int_{-\infty}^{\infty}\int_{-\infty}^{\infty} \exp\{i\Omega - |\Lambda|\}[g_2 + |\Lambda|\, g_3]\frac{\xi\eta}{\zeta^2}\, d\xi f\eta, \tag{3.9b}$$

$$w_1^{(0)} = \frac{1}{2\pi}\int_{-\infty}^{\infty}\int_{-\infty}^{\infty} \exp\{i\Omega - |\Lambda|\}[g_1 + g_2 + g_3 + |\Lambda|\, g_3]\frac{i\xi}{\zeta}\frac{z'}{|z'|}\, d\xi\, d\eta, \tag{3.9c}$$

where

$$g_1 = -\frac{\kappa}{2\zeta}A_1 - \frac{\kappa^2}{4}\left(C_1 - \frac{D_1}{2}\right)\frac{z'}{|z'|} + \frac{\kappa^3}{4}\left(F_1 - \frac{G_1}{6}\right)\zeta, \tag{3.10a}$$

$$g_2 = \frac{\kappa}{4\zeta}A_1 - \frac{\kappa^3}{8}(B_1 + F_1 + \tfrac{13}{30}G_1)\zeta + \frac{\kappa^4}{16}E_1\frac{z'}{|z'|}\zeta^2 - \frac{\kappa^5}{32}H_1\zeta^3, \tag{3.10b}$$

$$g_3 = \frac{\kappa}{4\zeta}A_1 - \frac{\kappa^2 D_1}{8}\frac{z'}{|z'|} + \frac{\kappa^3 G_1}{16}\zeta. \tag{3.10c}$$

In view of the expressions (3.9), the field $\mathbf{v}_2^{(0)}$ may be assumed to have the following form, which satisfies the Stokes and continuity equations:

$$\mathbf{v}_2^{(0)} = (u_2^{(0)}, v_2^{(0)}, w_2^{(0)}),$$

$$u_2^{(0)} = \frac{1}{2\pi}\int_{-\infty}^{\infty}\int_{-\infty}^{\infty} \exp(i\Omega)\left\{\exp(-\Lambda)\left[g_4 + \frac{\xi^2}{\zeta^2}(g_5 + \Lambda g_6)\right] + \exp(\Lambda)\left[g_7 + \frac{\xi^2}{\zeta^2}(g_8 - \Lambda g_9)\right]\right\} d\xi\, d\eta, \tag{3.11a}$$

$$v_2^{(0)} = \frac{1}{2\pi}\int_{-\infty}^{\infty}\int_{-\infty}^{\infty} \exp(i\Omega)\{\exp(-\Lambda)[g_5 + \Lambda g_6] + \exp(\Lambda)[g_8 - \Lambda g_9]\}\frac{\xi\eta}{\zeta^2}\, d\xi\, d\eta, \tag{3.11b}$$

$$w_2^{(0)} = \frac{1}{2\pi}\int_{-\infty}^{\infty}\int_{-\infty}^{\infty} \exp(i\Omega)\{\exp(-\Lambda)[g_4 + g_5 + g_6 + \Lambda g_6] - \exp(\Lambda)[g_7 + g_8 + g_9 - \Lambda g_9]\}\frac{i\xi}{\zeta}\, d\xi\, d\eta. \tag{3.11c}$$

Here, $g_4, g_5, \ldots, g_9$ are unknown functions of ξ and η which are evaluated by applying the boundary conditions $\mathbf{v}_1^{(0)} + \mathbf{v}_2^{(0)} = 0$ on the walls $z' = -s$ and $z' = 1 - s$. In the interest of brevity, the detailed results are not presented here (see Ho 1974); however, results to lowest order in κ will appear in § 5. For our present purposes, it is sufficient to note that $g_4, g_5, \ldots, g_9$ depend on ξ and η only in the combination $\zeta\,[= (\xi^2 + \eta^2)^{\frac{1}{2}}]$ and that they can be expressed in terms of g_1, g_2 and g_3.

In order to solve for $(\mathbf{v}_3^{(0)}, q_3^{(0)})$, it is necessary to evaluate $\mathbf{v}_2^{(0)}$ in the vicinity of the sphere where x' and y' are of order κ. This is achieved by expanding the integrand for small values of $x'^2 + y'^2$. The results are

$$u_2^{(0)} = \tfrac{1}{2}(2I_1 + I_4) - \tfrac{1}{2}\kappa(2I_2 + I_5 - I_7)z + \ldots, \tag{3.12a}$$

$$v_2^{(0)} = 0 + \ldots, \tag{3.12b}$$

$$w_2^{(0)} = -\tfrac{1}{2}\kappa(I_2 + I_5 + I_7)x + \ldots, \tag{3.12c}$$

where
$$\left.\begin{aligned} I_1 &= \int_0^\infty \zeta(g_4+g_7)\,d\zeta, \quad I_4 = \int_0^\infty \zeta(g_5+g_8)\,d\zeta, \\ I_2 &= \int_0^\infty \tfrac{1}{2}\zeta^2(g_4-g_7)\,d\zeta, \quad I_5 = \int_0^\infty \tfrac{1}{2}\zeta^2(g_5-g_8)\,d\zeta, \\ I_7 &= \int_0^\infty \tfrac{1}{2}\zeta^2(g_6-g_9)\,d\zeta. \end{aligned}\right\} \tag{3.13}$$

With $\mathbf{v}_2^{(0)}$ expressed in this form, $\mathbf{v}_3^{(0)}$ too can be found easily using Lamb's general solution. The result is identical to (3.5) with $A_1, B_1, \ldots, H_1$ replaced by $A_3, B_3, \ldots, H_3$, where

$$\left.\begin{aligned} &A_3 = \tfrac{3}{2}(I_1+\tfrac{1}{2}I_4), \quad B_3 = \tfrac{1}{4}(I_1+\tfrac{1}{2}I_4), \\ &C_3 = -\tfrac{1}{2}\kappa(\tfrac{1}{2}I_2-I_7), \quad D_3 = \tfrac{5}{3}\kappa(\tfrac{3}{2}I_2+I_5), \\ &E_3 = \tfrac{1}{6}\kappa(\tfrac{3}{2}I_2+I_5), \quad F_3, G_3, H_3 = \text{higher order in } \kappa. \end{aligned}\right\} \tag{3.14}$$

This process of satisfying boundary conditions on the sphere and on the walls can be repeated to yield corrections of higher order in κ. For the present purposes, it suffices to stop at $\mathbf{v}_3^{(0)}$.

The hydrodynamic force and torque (dimensionless) acting on the body can be calculated using the formulae (see Happel & Brenner 1973, p. 308)

$$F_x = 4\pi(A_1+A_3+\ldots), \quad T_y = 8\pi(C_1+C_3+\ldots), \tag{3.15a, b}$$

for which the coefficients A_1, A_3, C_1 and C_3 are previously listed in (3.6) and (3.14). It is obvious that, since $(\mathbf{v}^{(0)}, p^{(0)})$ corresponds to Stokes flow, the force and torque on the sphere are in the x direction and y direction, respectively. It is most convenient to re-express the coefficients A_3 and C_3 in terms of A_1, C_1 and D_1, i.e.

$$A_3 \equiv \tfrac{3}{2}(I_1+\tfrac{1}{2}I_4) = \kappa A_1 K_A + \kappa^2 C_1 K_C + \kappa^2 D_1 K_D + \ldots, \tag{3.16a}$$

$$C_3 \equiv -\tfrac{1}{2}\kappa(\tfrac{1}{2}I_2-I_7) = \kappa^2 A_1 L_A + \kappa^3 C_1 L_C + \kappa^3 D_1 L_D + \ldots. \tag{3.16b}$$

Thus, substituting for A_1, C_1 and D_1 from (3.6), the force and torque may be written as

$$F_x/4\pi = -\tfrac{3}{2}(U_{sx}^{(0)}-\alpha-\tfrac{1}{3}\kappa^2\gamma')(1+\kappa K_A) - \kappa^2(\Omega_{sy}^{(0)}-\tfrac{1}{2}\kappa\beta')K_C - \tfrac{5}{3}\kappa^3\beta' K_D + \ldots, \tag{3.17a}$$

$$T_y/8\pi = -(\Omega_{sy}^{(0)}-\tfrac{1}{2}\kappa\beta')(1+\kappa^3 L_C) - \tfrac{3}{2}\kappa^2(U_{sx}^{(0)}-\alpha-\tfrac{1}{3}\kappa^2\gamma')L_A - \tfrac{5}{3}\kappa^4\beta' L_D + \ldots. \tag{3.17b}$$

The coefficients K_A, K_C, K_D, L_A, L_C and L_D are integrals over ζ which are of order κ^0, and are dependent only on the parameter s. In addition, $\beta' = \beta/\kappa = O(1)$ and $\gamma' = \gamma/\kappa^2 = O(1)$. Equations (3.17$a$) and (3.17$b$) may be used to calculate the force and torque acting on a sphere which is translating and rotating at a known *specified* rate in either Couette or two-dimensional Poiseuille flow. Alternatively, the force and torque may be specified and (3.17a) and (3.17b) used to determine the corresponding translational and rotational velocities $U_{sx}^{(0)}$ and $\Omega_{sy}^{(0)}$.

s	Present theory, $-\frac{10}{9}K_D$	Halow & Wills, $\frac{5}{16}[1/(1-s)^2-1/s^2]$	Wakiya
0·10	−30·834	−30·864	—
0·20	−7·199	−7·324	—
0·25	−4·315	−4·444	−4·315
0·30	−2·717	−2·835	—
0·40	−1·018	−1·085	—
0·50	0·0	0·0	—

TABLE 1. The slip velocity $U_p/V_w\kappa^3$ of a neutrally buoyant sphere freely suspended in a simple shear flow bounded between two walls, $K_D(s) = -K_D(1-s)$.

The specific case of primary interest in the present context is $F_x = T_y = 0$, corresponding to a freely suspended neutrally buoyant particle. In this case, it can be shown from (3.17a) and (3.17b) that

$$U_{sx}^{(0)} - \alpha = \tfrac{1}{3}\kappa^2\gamma' - \tfrac{10}{9}\kappa^3\beta' K_D, \tag{3.18a}$$

$$\Omega_{sy}^{(0)} - \tfrac{1}{2}\kappa\beta' = -\tfrac{5}{3}\kappa^4\beta' L_D. \tag{3.18b}$$

Thus, the sphere rotates with the vorticity of the fluid to within a small correction $O(\kappa^4)$. In two-dimensional Poiseuille flow

$$\alpha = 4V_{\max}s(1-s), \quad \beta' = 4V_{\max}(1-2s), \quad \gamma' = -4V_{\max}.$$

Hence, the slip velocity $U_p \equiv U_{sx}^{(0)} - \alpha$ becomes

$$U_p = -\tfrac{4}{3}V_{\max}\kappa^2 - \tfrac{40}{9}V_{\max}\kappa^3(1-2s)\,K_D + O(\kappa^4). \tag{3.19}$$

This expression is consistent with the similar result given in Happel & Brenner (1973, chap. 3) for motion through a circular tube, and predicts that a small sphere (i.e. $\kappa \ll 1$) will lag behind the surrounding fluid for all positions s. In simple shear flow

$$\alpha = V_w s, \quad \beta' = V_w, \quad \gamma' = 0,$$

so that

$$U_p = -\tfrac{10}{9}V_w\kappa^3 K_D + O(\kappa^4). \tag{3.20}$$

We have numerically evaluated K_D for various values of s and the results are listed in table 1. It is evident that the sphere *leads* the fluid for $s > 0{\cdot}5$ and *lags* behind it for $s < 0{\cdot}5$. We note also the expected symmetry in K_D:

$$K_D(s) = -K_D(1-s).$$

These results for simple shear flow may be compared with the similar calculation of Wakiya (1956), who solved the same problem but evaluated U_p only for $s = 0{\cdot}25$ and $0{\cdot}75$. As indicated in table 1, our calculated values are essentially identical to his at those values of s. More recently, Halow & Wills (1970a) used an *ad hoc* method in which the contributions of the two individual walls were summed to estimate the force acting on a sphere between two plane walls. The resulting formula for F_x is

$$\frac{F_x}{6\pi} = -(U_{sx}^{(0)} - \alpha)\left\{1 + \tfrac{9}{16}\kappa\left[\frac{1}{s} + \frac{1}{1-s}\right]\right\} - \tfrac{5}{16}V_w k^3\left[\frac{1}{s^2} - \frac{1}{(1-s)^2}\right]. \tag{3.21}$$

	(a)			(b)		
s	Present theory, K_A	Halow & Wills, $\frac{9}{16}[1/s+1/(1-s)]$	Faxen	Present theory, L_A	Faxen	Wakiya
0·10	5·709	6·250	—	0·236	—	—
0·20	3·073	3·516	—	0·286	—	—
0·25	2·611	3·000	2·610	0·270	0·267	0·270
0·30	2·338	2·679	—	0·235	—	—
0·40	2·076	2·344	—	0·129	—	—
0·50	2·008	2·250	—	0·0	—	—

TABLE 2. (*a*) Additional hydrodynamic resistance on a sphere translating parallel to two infinite plane walls, $K_A(s) = K_A(1-s)$; and (*b*) the induced angular velocity, $L_A(s) = -L_A(1-s)$.

The corresponding values for $U_p/V_w\kappa^3$ are also listed in table 1 for the case in which $F_x = T_y = 0$. Sufficiently near the walls, $s < 0{\cdot}15$ or $s > 0{\cdot}85$, *both* theories reduce, in effect, to the motion of a sphere near a single plane wall and agreement between them is expected. Surprisingly, however, the simple addition of the two single-wall corrections gives results which compare quite well with our present 'exact' results for *all* values of s.

Although not required in the present context, it is also of general interest to use (3.17*a*) and (3.17*b*) to calculate the force and torque on a sphere which is translating in the x direction and/or rotating in the y direction between two infinite plane walls in a quiescent fluid. In these circumstances, since

$$\alpha = \beta' = \gamma' = 0,$$

$$F_x = -6\pi U^{(0)}_{sx}(1+\kappa K_A) - 4\pi\kappa^2\Omega^{(0)}_{sy} K_C, \tag{3.22a}$$

$$T_y = -8\pi\Omega^{(0)}_{sy}(1+\kappa^3 L_C) - 12\pi\kappa^2 U^{(0)}_{sx} L_A. \tag{3.22b}$$

In particular, a freely rotating sphere which is rising (or settling) through a quiescent fluid will experience the usual Stokes drag force modified by the additional term κK_A, and in addition will undergo an induced rotation at a rate

$$\Omega^{(0)}_{sy} = -\tfrac{3}{2}\kappa^2 U^{(0)}_{sx} L_A. \tag{3.23}$$

The coefficients K_A and L_A are listed in table 2 for various values of s. The values of the term corresponding to K_A, i.e. $\frac{9}{16}[1/s+1/(1-s)]$, from the approximate method, equation (3.21), are also listed in the same table. Wakiya (1956) and Faxen (see Happel & Brenner 1973, chap. 7) also reported the coefficients K_A and L_A for $s = 0{\cdot}25$ and $0{\cdot}75$ (see table 2).

4. Solution for $(\mathbf{u}, p)$

We now consider the creeping motion of a rigid sphere which is translating in a quiescent fluid between two parallel plane boundaries in the direction perpendicular to them. This velocity field $(\mathbf{u}, p)$ is required in the integral

expression (2.21) for the lateral force. The method of solution is identical to that of the preceding section, hence only the results will be given. We express $(\mathbf{u}, p)$ as

$$\left.\begin{aligned}\mathbf{u} &= \mathbf{u}_1+\mathbf{u}_2+\mathbf{u}_3+\ldots,\\ p &= p_1+p_2+p_3+\ldots.\end{aligned}\right\} \tag{4.1}$$

The solution $\mathbf{u}_1$ satisfying the boundary condition on the sphere, i.e. $\mathbf{u}_1 = \mathbf{e}_z$ at $r = 1$, is

$$\mathbf{u}_1 = (u_1, v_1, w_1),$$

$$u_1 = -\frac{A_1}{2}\frac{zx}{r^3}+3B_1\frac{zx}{r^5}, \quad v_1 = -\frac{A_1}{2}\frac{yz}{r^3}+3B_1\frac{yz}{r^5}, \tag{4.2a, b}$$

$$w_1 = -\frac{A_1}{2}\left(1+\frac{z^2}{r^2}\right)\frac{1}{r}-B_1\left(1-\frac{3z^2}{r^2}\right)\frac{1}{r^3}, \tag{4.2c}$$

and

$$A_1 = -\tfrac{3}{2}, \quad B_1 = -\tfrac{1}{4}. \tag{4.3}$$

Using (3.8), an integral form for $\mathbf{u}_1$ can be obtained in terms of the outer variables x', y', z' and r':

$$u_1 = \frac{1}{2\pi}\int_{-\infty}^{\infty}\int_{-\infty}^{\infty}\exp\{i\Omega-|\Lambda|\}\left[|z'|f_1+\frac{2}{\zeta}f_2\right]\frac{i\xi}{2}\frac{z'}{|z'|}\,d\xi\,d\eta, \tag{4.4a}$$

$$v_1 = \frac{1}{2\pi}\int_{-\infty}^{\infty}\int_{-\infty}^{\infty}\exp\{i\Omega-|\Lambda|\}\left[|z'|f_1+\frac{2}{\zeta}f_2\right]\frac{i\eta}{2}\frac{z'}{|z'|}\,d\xi\,d\eta, \tag{4.4b}$$

$$w_1 = \frac{-1}{2\pi}\int_{-\infty}^{\infty}\int_{-\infty}^{\infty}\exp\{i\Omega-|\Lambda|\}[f_1+f_2+|\Lambda|f_1]\,d\xi\,d\eta, \tag{4.4c}$$

where

$$f_1 = \kappa A_1/4\zeta, \quad f_2 = -\tfrac{1}{8}\kappa^3 B_1\zeta. \tag{4.5a, b}$$

Again, $\mathbf{u}_2$ is assumed to have the form $\mathbf{u}_2 = (u_2, v_2, w_2)$, with

$$u_2 = \frac{1}{2\pi}\int_{-\infty}^{\infty}\int_{-\infty}^{\infty}\exp(i\Omega)\left\{\exp(-\Lambda)\left[z'f_3+\frac{2}{\zeta}f_4\right]+\exp(\Lambda)\left[z'f_5-\frac{2}{\zeta}f_6\right]\right\}\frac{i\xi}{2}\,d\xi\,d\eta, \tag{4.6a}$$

$$v_2 = \frac{1}{2\pi}\int_{-\infty}^{\infty}\int_{-\infty}^{\infty}\exp(i\Omega)\left\{\exp(-\Lambda)\left[z'f_3+\frac{2}{\zeta}f_4\right]+\exp(\Lambda)\left[z'f_5-\frac{2}{\zeta}f_6\right]\right\}\frac{i\eta}{2}\,d\xi\,d\eta, \tag{4.6b}$$

$$w_2 = \frac{-1}{2\pi}\int_{-\infty}^{\infty}\int_{-\infty}^{\infty}\exp(i\Omega)\{\exp(-\Lambda)[f_3+f_4+\Lambda f_3] + \exp(\Lambda)[f_5+f_6-\Lambda f_5]\}\,d\xi\,d\eta. \tag{4.6c}$$

The coefficients f_3, f_4, f_5 and f_6 are found by satisfying the boundary condition $\mathbf{u}_1+\mathbf{u}_2 = 0$ on the walls $z' = -s$ and $z' = 1-s$. As before, the detailed results are omitted (see Ho 1974) while the expressions to the lowest order in κ are given in § 5. Again, f_3, f_4, f_5 and f_6 are found to be dependent on ζ. Near the sphere $\mathbf{u}_2$ can be simplified to the form

$$u_2 = -\tfrac{1}{2}\kappa J_2 x+O(\kappa^3), \quad v_2 = -\tfrac{1}{2}\kappa J_2 y+O(\kappa^3), \tag{4.7a, b}$$

$$w_2 = -(J_1+J_4)+\kappa J_2 z+O(\kappa^3), \tag{4.7c}$$

where

$$\left.\begin{aligned}J_1 = \int_0^{\infty}\zeta(f_4+f_6)\,d\zeta, \quad J_4 &= \int_0^{\infty}\zeta(f_3+f_5)\,d\zeta,\\ J_2 &= \int_0^{\infty}\tfrac{1}{2}\zeta^2(f_4-f_6)\,d\zeta.\end{aligned}\right\} \tag{4.8}$$

s	K_A	$\frac{9}{8}[1/s+1/(1-s)]$
0·1	11·2	12·50
0·2	5·65	7·03
0·25	4·560	6·000
0·3	3·864	5·357
0·4	3·117	4·688
0·5	2·902	4·500

TABLE 3. Additional hydrodynamic resistance on a sphere translating perpendicular to two infinite plane walls, $K_A(s) = K_A(1-s)$.

Hence, the solution $\mathbf{u}_3$ satisfying the boundary condition $\mathbf{u}_2+\mathbf{u}_3 = 0$ on $r = 1$ is the same as (4.2) with A_1 and B_1 replaced by A_3 and B_3, where

$$A_3 = -\tfrac{3}{2}(J_1+J_4), \quad B_3 = -\tfrac{1}{4}(J_1+J_4). \tag{4.9}$$

This completes the solution to the order of approximation required for our purposes.

As in the previous case, the force acting on the particle can be calculated from the coefficients A_1 and A_3 for any given imposed velocity. The torque is identically zero. The general form for the force is

$$F_z = 4\pi(A_1+A_3+\ldots). \tag{4.10}$$

Hence, substituting for A_1 and A_3 from (4.3) and (4.9), and noting that

$$A_3 \equiv -\tfrac{3}{2}(J_1+J_4) = \kappa A_1 K_A + \kappa^3 B_1 K_B, \tag{4.11}$$

we obtain

$$F_z/6\pi = -(1+\kappa K_A), \tag{4.12}$$

where the coefficient K_A is an integral over ζ which is $O(1)$ in κ, and is a function of the single parameter s. Thus, to a first approximation we obtain the usual Stokes force, with a correction $O(\kappa)$ due to the presence of the walls. The coefficient K_A is listed as a function of s in table 3. So far as we are aware, the only directly comparable results for two walls are from the study of Halow & Wills (1970*a*), who approximated the drag force as the sum of two single-wall calculations. This approach yields

$$\frac{F_z}{6\pi} = -\left[1+\tfrac{9}{8}\kappa\left(\frac{1}{s}+\frac{1}{1-s}\right)\right], \tag{4.13}$$

which is to be compared with (4.12). We have listed the correction term from (4.13) in a form comparable with the coefficient K_A in table 3. Unlike the previous example, where the *ad hoc* method of Halow & Wills produces reasonably accurate results, the comparison in this case is very poor with the values of the exact calculation being as much as 50 % lower than the values from (4.13). As one would expect, the greatest differences occur near the centre of the gap, where the influences of the walls are comparable. When the particle is close to one wall, the influence of the other is apparently weak and the one-wall approximation is adequate.

5. The lateral force

To calculate the lateral force, the volume integral (2.21) must be evaluated using the velocity fields $\mathbf{v}^{(0)}$ and $\mathbf{u}$ of the preceding two sections, i.e. we require

$$F_L = -Re\int_{V_f} \mathbf{u}.[\mathbf{v}^{(0)}.\nabla\mathbf{v}^{(0)} + \mathbf{v}^{(0)}.\nabla\mathbf{V} + \mathbf{V}.\nabla\mathbf{v}^{(0)}]\,dV,$$

where V_f is the fluid volume outside the sphere and bounded between the walls:

$$V_f = \{\mathbf{r}|r \geqslant 1,\ x < \infty,\ y < \infty,\ -s/\kappa \leqslant z \leqslant (1-s)/\kappa\}.$$

Motivated by the fact that the lower limit of integration is $O(1)$ while the upper limit is $O(1/\kappa)$, we divide the region of integration into two domains V_1 and V_2 such that

$$V_1 = \{\mathbf{r}|1 \leqslant r < \lambda\kappa^{\chi-1}\}, \tag{5.1}$$

$$V_2 = \{\mathbf{r}|\lambda\kappa^{\chi-1} \leqslant r < \infty,\ -s/\kappa \leqslant z \leqslant (1-s)/\kappa\}, \tag{5.2}$$

where $0 < \chi < 1$ and λ is a constant of order κ^0. Hence

$$F_L = -Re\int_{V_1} \mathbf{u}.\mathbf{f}\,dV - Re\int_{V_2} \mathbf{u}.\mathbf{f}\,dV. \tag{5.3}$$

Let us now investigate the magnitude of the first integral in (5.3). The solutions of the previous two sections and the general form (2.2) of the undisturbed flow field give the following orders of magnitude in κ and the radial position r:

$$\left.\begin{aligned} \mathbf{u} &= \mathbf{u}_1 + \mathbf{u}_2 + \mathbf{u}_3 + \ldots, \\ \mathbf{u}_1 &\sim O(1/r) + O(1/r^3), \\ \mathbf{u}_2 &\sim O(\kappa) + O(\kappa^2 r) + \ldots, \\ \mathbf{u}_3 &\sim O\left(\frac{\kappa}{r}\right) + O\left(\frac{\kappa}{r^3}\right) + O\left(\frac{\kappa^2}{r^2}\right) + O\left(\frac{\kappa^2}{r^4}\right) + \ldots, \end{aligned}\right\} \tag{5.4a}$$

$$\left.\begin{aligned} \mathbf{v}^{(0)} &= \mathbf{v}_1^{(0)} + \mathbf{v}_2^{(0)} + \mathbf{v}_3^{(0)} + \ldots, \\ \mathbf{v}_1^{(0)} &\sim O\left(\frac{\kappa}{r^2}\right) + O\left(\frac{\kappa}{r^4}\right) + O\left(\frac{\kappa^2}{r^3}\right) + O\left(\frac{\kappa^2}{r^5}\right) + O\left(\frac{\kappa^3}{r}\right) + O\left(\frac{\kappa^3}{r^3}\right) + \ldots, \\ \mathbf{v}_2^{(0)} &\sim O(\kappa^3) + O(\kappa^4 r) + \ldots, \\ \mathbf{v}_3^{(0)} &\sim O\left(\frac{\kappa^3}{r}\right) + O\left(\frac{\kappa^3}{r^3}\right) + O\left(\frac{\kappa^4}{r^2}\right) + O\left(\frac{\kappa^4}{r^4}\right) + \ldots, \end{aligned}\right\} \tag{5.4b}$$

$$\mathbf{V} \sim O(\kappa r) + O(\kappa^2 r^2). \tag{5.4c}$$

It follows, therefore, that the integrand behaves as

$$\mathbf{u}.\mathbf{f} \sim \kappa^2 O\left(\frac{1}{r^3}, \frac{1}{r^5}, \frac{1}{r^7}\right) + \kappa^3 O\left(\frac{1}{r^2}, \frac{1}{r^3}, \frac{1}{r^4}, \ldots\right) + \ldots. \tag{5.5}$$

It can be shown that the volume integral over a spherical shell (i.e. $1 \leqslant r < \lambda\kappa^{\chi-1}$) of the first term in (5.5) is identically zero. Thus, the dominant term derives from the term of order κ^3/r^2 in the integrand and the magnitude of the integral over V_1 is

$$\int_{V_1} \mathbf{u}.\mathbf{f}\,dV = O(\kappa^{\chi+2}). \tag{5.6}$$

Now let us investigate the second integral in (5.3). Here, in estimating the magnitudes of the various velocity fields, it is convenient to use the outer variables x', y', z' and r'. It is then easily shown that

$$\mathbf{u}_1 \sim O(\kappa), \quad \mathbf{u}_2 \sim O(\kappa), \quad \mathbf{u}_3 \sim O(\kappa^2), \tag{5.7}$$

$$\mathbf{v}_1^{(0)} \sim O(\kappa^3), \quad \mathbf{v}_2^{(0)} \sim O(\kappa^3), \quad \mathbf{v}_3^{(0)} \sim O(\kappa^4), \tag{5.8}$$

$$\mathbf{V} \sim O(1). \tag{5.9}$$

Hence, neglecting terms $O(\kappa^3)$ and smaller, the second volume integral of (5.3) can be written as

$$-Re\int_{V_2} \mathbf{u}.\mathbf{f}\,dV = -Re\,\kappa^{-2}\int_{V_2} (\mathbf{u}_1+\mathbf{u}_2).[(\mathbf{v}_1^{(0)}+\mathbf{v}_2^{(0)}).\nabla\mathbf{V} + \mathbf{V}.\nabla(\mathbf{v}_1^{(0)}+\mathbf{v}_2^{(0)})]\,dV + O(\kappa^3), \tag{5.10}$$

where the velocities are expressed in *outer variables* and V_2 is the volume element defined by

$$\lambda\kappa^{\chi} \leqslant r'$$

and

$$x' < \infty, \quad y' < \infty, \quad -s \leqslant z' \leqslant (1-s). \tag{5.11}$$

Now, the dominant term in the integrand of (5.10), as $r' \to 0$, is $O(\kappa^4/r'^2)$, hence if the lower limit $r' = \lambda\kappa^{\chi}$ were replaced by $r' = 0$, an error would be introduced which would be of the same order of magnitude as the contribution from V_1, i.e. $\kappa^{-2}\int O(\kappa^4/r'^2)\,dr'^3 = O(\kappa^{2+\chi})$. But the volume integral over V_2 is of order κ^2, hence to a first approximation, it is permissible to put $r' = 0$ as the lower limit and neglect the integral over V_1 entirely. We note that the resultant expression for F_L, equation (5.10), involves only $\mathbf{u}_1$ and $\mathbf{u}_2$ of $\mathbf{u}$, $\mathbf{v}_1^{(0)}$ and $\mathbf{v}_2^{(0)}$ of $\mathbf{v}^{(0)}$, and a single term of $\mathbf{V}$. Let us rewrite these various velocity fields (in terms of outer variables x', y', z' and r'). First, $\mathbf{u}$ is given by $\mathbf{u} = \mathbf{u}_1 + \mathbf{u}_2$, with

$$\mathbf{u}_1 = (u_1, v_1, w_1),$$

$$u_1 = \kappa\, 3z'x'/4r'^3 + O(\kappa^3), \quad v_1 = \kappa\, 3y'z'/4r'^3 + O(\kappa^3), \tag{5.12a, b}$$

$$w_1 = \kappa\frac{3}{4}\left(1+\frac{z'^2}{r'^2}\right)\frac{1}{r'} + O(\kappa^3), \tag{5.12c}$$

$$\mathbf{u}_2 = (u_2, v_2, w_2),$$

$$u_2 = -\frac{x'}{\rho'}\int_0^{\infty} J_1(W)\,[\exp(-\Lambda)\,(\Lambda f_3 + f_4) + \exp(\Lambda)\,(\Lambda f_5 - f_6)]\,\zeta\,d\zeta, \tag{5.13a}$$

$$v_2 = -\frac{y'}{\rho'}\int_0^{\infty} J_1(W)\,[\exp(-\Lambda)\,(\Lambda f_3 + f_4) + \exp(\Lambda)\,(\Lambda f_5 - f_6)]\,\zeta\,d\zeta, \tag{5.13b}$$

$$w_2 = -\int_0^{\infty} J_0(W)\,[\exp(-\Lambda)\,(f_3 + f_4 + \Lambda f_3) + \exp(\Lambda)\,(f_5 + f_6 - \Lambda f_5)]\,\zeta\,d\zeta, \tag{5.13c}$$

where

$$f_3 = (3\kappa/8\Delta\zeta)\,[(t_2-1)\,(t-1) + (1-s)\,\zeta t_2 - \zeta t + s\zeta t_2 t - (1-s)\,\zeta^2 t] + O(\kappa^3), \tag{5.14a}$$

$$f_4 = (-3\kappa/16\Delta\zeta)\,[(1-s)^2\,\zeta^2 t_2 - (1-2s)\,\zeta^2 t - s^2\zeta^2 t_2 t + s(1-s)\,\zeta^3 t] + O(\kappa^3), \tag{5.14b}$$

$$f_5 = (3\kappa/8\Delta\zeta)\,[(t_1-1)\,(t-1) + s\zeta t_1 - \zeta t + (1-s)\,\zeta t_1 t - s\zeta^2 t] + O(\kappa^3), \tag{5.14c}$$

$$f_6 = (-3\kappa/16\Delta\zeta)\,[s^2\zeta^2 t_1 + (1-2s)\,\zeta^2 t - (1-s)^2\,\zeta^2 t_1 t + s(1-s)\,\zeta^3 t] + O(\kappa^3) \tag{5.14d}$$

and

$$\rho'^2 = x'^2 + y'^2, \quad t = \exp\zeta, \quad t_1 = \exp s\zeta, \quad t_2 = \exp[(1-s)\zeta], \quad \Delta = (t-1)^2 - \zeta^2 t,$$

$W = \frac{1}{2}\zeta\rho'$ and the $J_n(W)$ are Bessel functions of the first kind of order n.

Second, $\mathbf{v}^{(0)}$ is given by $\mathbf{v}^{(0)} = \mathbf{v}_1^{(0)} + \mathbf{v}_2^{(0)}$, with

$$\mathbf{v}_1^{(0)} = (u_1^{(0)}, v_1^{(0)}, w_1^{(0)}),$$

$$u_1^{(0)} = \frac{3\kappa^2 D_1}{2}\left(\frac{z'x'^2}{r'^5}\right) - \frac{\kappa A_1}{2}\left(1+\frac{x'^2}{r'^2}\right)\frac{1}{r'} - \frac{\kappa^2 C_1 z'}{r'^3}, \tag{5.15a}$$

$$v_1^{(0)} = \frac{3\kappa^2 D_1}{2}\left(\frac{x'y'z'}{r'^5}\right) - \frac{\kappa A_1}{2}\left(\frac{x'y'}{r'^3}\right), \tag{5.15b}$$

$$w_1^{(0)} = \frac{3\kappa^2 D_1}{2}\left(\frac{z'^2x'}{r'^5}\right) - \frac{\kappa A_1}{2}\left(\frac{z'x'}{r'^3}\right) + \frac{\kappa^2 C_1 x'}{r'^3}, \tag{5.15c}$$

with $D_1 = -\frac{5}{3}\beta'\kappa$, $A_1 = -\frac{3}{2}(U_{sx}^{(0)} - \alpha - \frac{1}{3}\gamma'\kappa^2)$ and $C_1 = -(\Omega_{sy}^{(0)} - \frac{1}{2}\beta'\kappa)$. Hence, from (3.18), it follows, for a freely suspended neutrally buoyant sphere, that

$$A_1 = \tfrac{5}{3}\beta'\kappa^3 K_D \quad \text{and} \quad C_1 = \tfrac{5}{3}\beta'\kappa^4 L_D,$$

so that, in (5.15), the term involving D_1 is $O(\kappa^3)$, the term involving A_1 is $O(\kappa^4)$ and the term involving C_1 is $O(\kappa^6)$:

$$u_1^{(0)} = -\frac{5\kappa^3\beta'}{2}\left(\frac{z'x'^2}{r'^5}\right) - \frac{5\kappa^4\beta' K_D}{6}\left(1+\frac{x'^2}{r'^2}\right)\frac{1}{r'} - \frac{5\kappa^6\beta' L_D z'}{3r'^3}, \tag{5.16a}$$

$$v_1^{(0)} = -\frac{5\kappa^3\beta'}{2}\left(\frac{x'y'z'}{r'^5}\right) - \frac{5\kappa^4\beta' K_D}{6}\left(\frac{x'y'}{r'^3}\right), \tag{5.16b}$$

$$w_1^{(0)} = -\frac{5\kappa^3\beta'}{2}\left(\frac{z'^2x'}{r'^5}\right) - \frac{5\kappa^4\beta' K_D}{6}\left(\frac{z'x'}{r'^3}\right) + \frac{5\kappa^6\beta' L_D x'}{3r'^3}. \tag{5.16c}$$

The velocity field $\mathbf{v}_2^{(0)}$ is given by

$$\mathbf{v}_2^{(0)} = (u_2^{(0)}, v_2^{(0)}, w_2^{(0)}),$$

$$u_2^{(0)} = \int_0^\infty \Big\{\tfrac{1}{2}J_0(W)[\exp(-\Lambda)(2g_4+g_5+\Lambda g_6)+\exp(\Lambda)(2g_7+g_8-\Lambda g_9)]$$
$$-\frac{1}{2}\frac{x'^2-y'^2}{\rho'^2}J_2(W)[\exp(-\Lambda)(g_5+\Lambda g_6)+\exp(\Lambda)(g_8-\Lambda g_9)]\Big\}\zeta\,d\zeta, \tag{5.17a}$$

$$v_2^{(0)} = -\int_0^\infty \frac{x'y'}{\rho'^2}J_2(W)[\exp(-\Lambda)(g_5+\Lambda g_6)+\exp(\Lambda)(g_8-\Lambda g_9)]\zeta\,d\zeta, \tag{5.17b}$$

$$w_2^{(0)} = -\int_0^\infty \frac{x'}{\rho'}J_1(W)[\exp(-\Lambda)(g_4+g_5+g_6+\Lambda g_6)-\exp(\Lambda)(g_7+g_8+g_9-\Lambda g_9)]\zeta\,d\zeta. \tag{5.17c}$$

Here, $g_4(\zeta), g_5(\zeta), \ldots, g_9(\zeta)$ are expressible in terms of g_1, g_2 and g_3, which are given by,

$$g_1 = -\frac{\kappa A_1}{2\zeta} + \frac{\kappa^2 D_1 z'}{8|z'|} - \frac{\kappa^2 C_1 z'}{4|z'|} + \ldots, \tag{5.18a}$$

$$g_2 = \frac{\kappa A_1}{4\zeta} + \ldots, \quad g_3 = \frac{\kappa A_1}{4\zeta} - \frac{\kappa^2 D_1 z'}{8|z'|} + \ldots. \tag{5.18b, c}$$

For a neutrally buoyant particle, the term involving D_1 is $O(\kappa^3)$, the term involving A_1 is $O(\kappa^4)$ and the term involving C_1 is $O(\kappa^6)$; then it can be shown that to the lowest order in κ

$$g_4 = -\frac{5\kappa^3\beta'}{24}\left(\frac{t_2+1}{t-1}\right)+O(\kappa^4), \tag{5.19a}$$

$$g_5 = \frac{5\kappa^3\beta'}{48}\left\{\frac{t_2+1+(1-s)\zeta}{t-1}-\frac{1}{\Delta}\right.$$
$$\times[(t_2+1)(t-1)-2(1-s)\zeta t_2-(1+s)\zeta t-2s\zeta t_2 t-(1-s)\zeta]$$
$$\left.-\frac{\zeta^2}{\Delta(t-1)}[(1-s)^2 t_2+2s(1-s)t_2 t+t^2+s^2 t_2 t^2-(1-s)^2\zeta t-s(1-s)\zeta t^2]\right\}+O(\kappa^4), \tag{5.19b}$$

$$g_6 = (5\kappa^3\beta'/24\Delta)[(t_2+1)(t-1)-(1-s)\zeta t_2-\zeta t-s\zeta t_2 t+(1-s)\zeta^2 t]+O(\kappa^4), \tag{5.19c}$$

$$g_7 = \frac{5\kappa^3\beta'}{24}\left(\frac{t_1+1}{t-1}\right)+O(\kappa^4), \tag{5.19d}$$

$$g_8 = -\frac{5\kappa^3\beta'}{48}\left\{\frac{t_1+1+s\zeta}{t-1}-\frac{1}{\Delta}[(t_1+1)(t-1)-2s\zeta t_1-(2-s)\zeta t-2(1-s)\zeta t_1 t-s\zeta]\right.$$
$$\left.-\frac{\zeta^2}{\Delta(t-1)}[s^2 t_1+2s(1-s)t_1 t+t^2+(1-s)^2 t_1 t^2-s^2\zeta t-s(1-s)\zeta t^2]\right\}+O(\kappa^4), \tag{5.19e}$$

$$g_9 = (-5\kappa^3\beta'/24\Delta)[(t_1+1)(t-1)-s\zeta t_1-\zeta t-(1-s)\zeta t_1 t+s\zeta^2 t]+O(\kappa^4). \tag{5.19f}$$

Finally, the undisturbed velocity field $\mathbf{V}$ is

$$\mathbf{V} = (\beta' z'+\gamma' z'^2)\,\mathbf{e}_x+O(\kappa^2). \tag{5.20}$$

It may now be seen from (5.15) and (5.16) that the dominant term in the expression (5.10) for *neutrally buoyant particles* is due to the stresslet (D_1, determined by the bulk rate of strain) and its reflexion off the walls. The *Stokeslet* contribution (A_1, originating from the lag velocity) and the *couplet* contribution (C_1, originating from the rotation slip) are of one and three orders of magnitude smaller in κ, and hence may be neglected for this case. From this, one can conclude that the lateral force originates from the shear field acting on the sphere rather than the presence of a wall-induced lag velocity or slip–spin. On the other hand, it should be pointed out that for the special case of a non-rotating sphere, where $C_1 = \frac{1}{2}\kappa\beta'$, the stresslet and couplet terms are of same order of magnitude. Similarly, if the lag velocity were significantly larger, as might be the case for a non-neutrally buoyant sphere, the contribution of the Stokeslet term might generate a lateral force of comparable or even larger magnitude than that determined here. Indeed, it is clear from (5.15) and (5.16) that a suitable criterion for neglect of the contribution to the lateral force induced by the body force (for a vertical flow channel) is

$$|\kappa^2 D_1| \gg |\kappa A_1| \quad \text{or} \quad |A_1| \ll \kappa^2\beta'. \tag{5.21}$$

An explicit requirement for the case where $T_y = 0$ follows immediately from (3.17a) and (3.17b), which yield

$$A_1 = (F_x/4\pi + \tfrac{5}{3}\kappa^3\beta' K_D)\,(1+O(\kappa)).$$

That is, we require $$|F_x/4\pi| \ll \kappa^2\beta'. \tag{5.22}$$

When the body force is gravity, (5.22) becomes (in dimensional quantities)

$$a^2|\rho_s - \rho_0|\, g \ll \mu_0\, V_m^* \kappa^2, \tag{5.23}$$

in which g is the gravitational acceleration, ρ_s is the density of the particle, ρ_0 is the density of the suspending fluid and V_m^* is the dimensional mean flow rate, being equal to $\frac{1}{2}V_w^*$ for simple shear flow and $\frac{2}{3}V_{\max}^*$ for two-dimensional Poiseuille flow.

We have used the various estimates (5.12)–(5.20) to evaluate the expression (5.10), leading to the lateral force F_L. As indicated previously, the lower limit for the radial variable r' in V_2 was 0 and the contribution from V_1 was neglected completely. The volume integrations over V_2 were carried out analytically, however the various integrations with respect to ζ were determined numerically for various values of s. The general form found for F_L is

$$F_L = \kappa^2\, Re\,[\beta'^2 G_1(s) + \beta'\gamma' G_2(s)], \tag{5.24}$$

with the convention that a positive force is in the direction of increasing s while a negative force is in the opposite direction. The functions $G_1(s)$ and $G_2(s)$, which are independent of the detailed undisturbed flow, were evaluated numerically for various values of s and are listed in table 4. It is found that

$$G_1(s) = -G_1(1-s), \quad G_2(s) = G_2(1-s), \tag{5.25}$$

and $G_1(s)$ is positive for $0 < s < 0{\cdot}5$ whereas $G_2(s)$ is always positive. The general expression (5.24) for the lateral force is applicable to all undisturbed flow fields of the form $\alpha + \beta' z' + \gamma' z'^2$.

A careful examination of (5.24) indicates the following general behaviour of the individual terms. The first term, which is the interaction of the disturbance stresslet and its wall correction with the bulk shear (hence proportional to β^2), in all cases produces an inward force which tends to cause migration toward the centre-line $s = 0{\cdot}5$. The second term, which is the interaction between the Stresslet and the curvature of the bulk velocity profile (hence proportional to $\beta\gamma$), tends to cause migration in the direction of increasing (absolute) shear rate. For every example of two-dimensional shear flow $\alpha + \beta' z' + \gamma' z'^2$ involving either moving walls, an imposed pressure gradient or a combination of these, the region of largest shear is near one (or both) of the walls.

Reverting to dimensional variables and substituting for $\beta' = V_w = 2V_m$ and $\gamma' = 0$ in (5.24), the lateral force for simple shear flow is thus

$$F_L^* = \rho_0\, V_m^{*2} a^2 \kappa^2 [4G_1(s)], \tag{5.26}$$

which is plotted in figure 2. Hence, for this case, the lateral force is in the positive-z direction for $0 < s < 0{\cdot}5$ and in the negative-z direction for $0{\cdot}5 < s < 1{\cdot}0$. Thus, a stable equilibrium position for the sphere in a simple shear flow between two

s	G_1	G_2	s	G_1	G_2
0·50	0·0	1·072	0·25	0·885	0·711
0·49	0·0419	1·070	0·24	0·907	0·683
0·48	0·0837	1·068	0·23	0·927	0·654
0·47	0·1254	1·066	0·22	0·945	0·625
0·46	0·1669	1·062	0·21	0·960	0·596
0·45	0·2080	1·056	0·20	0·973	0·566
0·44	0·2489	1·050	0·19	0·982	0·536
0·43	0·2894	1·042	0·18	0·988	0·506
0·42	0·3293	1·033	0·17	0·990	0·477
0·41	0·3688	1·023	0·16	0·988	0·448
0·40	0·4077	1·012	0·15	0·981	0·420
0·39	0·4459	1·000	0·14	0·971	0·393
0·38	0·4834	0·987	0·13	0·957	0·368
0·37	0·520	0·972	0·12	0·943	0·345
0·36	0·556	0·956	0·11	0·931	0·324
0·35	0·591	0·940	0·10	0·927	0·306
0·34	0·626	0·922	0·09	0·940	0·292
0·33	0·659	0·902	0·08	0·982	0·282
0·32	0·691	0·882	0·07	1·07	0·278
0·31	0·723	0·861	0·06	1·23	0·280
0·30	0·753	0·838	0·05	1·50	0·291
0·29	0·782	0·815	0·04	1·93	0·315
0·28	0·810	0·790	0·03	2·58	0·354
0·27	0·836	0·765	0·02	3·59	0·414
0·26	0·861	0·738	0·01	5·33	0·505

TABLE 4. Values of G_1 and G_2; $G_1(s) = -G_1(1-s)$, $G_2(s) = G_2(1-s)$.

plane walls is the centre-line $s = 0{\cdot}5$, where $G_1(s) = 0$. This value agrees reasonably well with the experimental observations of Halow & Wills (1970*a*, *b*), who found a stable equilibrium position between $s = 0{\cdot}5$ and $0{\cdot}55$ in a concentric-cylinder Couette flow. In the next section, we shall show that the slight apparent discrepancy in these two results is due to the curvature of the Couette flow streamlines.

For the case of two-dimensional Poiseuille flow, where $\beta' = 4V_{\max}(1-2s)$ and $\gamma' = -4V_{\max}$, the dimensional expression for the lateral force is

$$F_L^* = \rho_0 V_m^{*2} a^2 \kappa^2 [36(1-2s)^2 G_1(s) - 36(1-2s) G_2(s)], \tag{5.27}$$

which is also plotted in figure 2. Clearly the portion $\beta'^2 G_1(s)$ of the force which involves the square of the shear rate tends to push the sphere to the centre, while the term $\beta'\gamma' G_2(s)$, which involves the product of the shear rate and its rate of change, is negative for $0 < s < 0{\cdot}5$ and the positive for $0{\cdot}5 < s < 1$, thus opposing the effect of the first term. There are three positions where the force F_L is zero: the centre-line ($s = 0{\cdot}5$), which is unstable to slight perturbations, and $s = 0{\cdot}2$ and $0{\cdot}8$, which are stable equilibrium points. Unfortunately, the only available experiments for two-dimensional Poiseuille flow, those of Repetti & Leonard (1966) and of Tachibana (1973), are somewhat inconclusive with regard

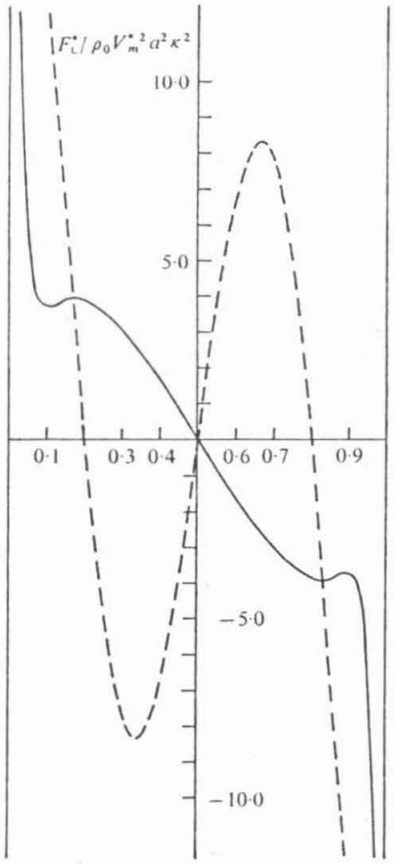

FIGURE 2. Lateral force $F_L^*/\rho_0 V_m^* a^2 \kappa^2$ as a function of lateral position. ——, simple shear flow; – – –, two-dimensional Poiseuillo flow.

to the equilibrium position. In Repetti & Leonard's experiments, the particles were never quite neutrally buoyant. Rewriting the criterion (5.23), we require

$$|\rho_s - \rho_0| \ll \mu_0 V_m^*/d^2 g.$$

Using the maximum viscosity and velocity estimates of 10 cP and 2 cm/s, $\mu_0 V_m^*/d^2 g \sim 10^{-5}$ for Repetti & Leonard's experimental set-up. On the other hand, the density differences were never measured more accurately than to within $\pm 10^{-4}$. The fact that the particles were never really neutrally buoyant may explain why Repetti & Leonard were unable to obtain reliable and conclusive results for the equilibrium position with their 'neutrally buoyant' spheres. The equilibrium positions reported by Tachibana (1973) also exhibit a great deal of scatter. However, Tachibana presented sphere trajectories only for two cases with equilibrium positions of $s = 0{\cdot}2$ and $0{\cdot}8$, which, for reasons that are not clear from his paper, he apparently felt to be the most reliable.

These equilibrium values agree perfectly with the present theoretical predictions.

Finally, it is interesting to note that the predicted equilibrium positions for two-dimensional Poiseuille flow are precisely equivalent to the value measured in a *circular* tube by Segré & Silberberg (1962*a*, *b*). In addition, the form (5.27) for F_L^* in this case is essentially the same as Segré & Silberberg's empirical estimate (cf. the discussion by Brenner 1966, p. 381).

6. Particle trajectories

It is of interest to use the result for the force to calculate the trajectories of the sphere. In particular, the calculated sphere trajectories can be compared with available experimental results reported in the literature. The lateral velocity has been found to be given in dimensional form by

$$Re\, U_{sz}^{(1)*} = \frac{F_L^*}{6\pi\mu_0 a} = \frac{\rho_0 V_m^{2*} d}{6\pi\mu_0}\kappa^3 G(s), \tag{6.1}$$

in which $G(s)$ is given by $G(s) = 4G_1(s)$ (6.2*a*)

for simple shear flow and by

$$G(s) = 36[(1-2s)^2 G_1(s) - (1-2s)\, G_2(s)] \tag{6.2b}$$

for two-dimensional Poiseuille flow. The sphere trajectories can be expressed in terms of the lateral position of the particle either as a function of time or as a function of axial position in the flow channel. Since the lateral velocity $U_{sz}^{(1)*}$ can be expressed as

$$Re\, U_{sz}^{(1)*} = d\frac{ds}{dt^*} = \frac{\rho_0 V_m^{*2} d}{6\pi\mu_0}\kappa^3 G(s) \tag{6.3}$$

and the axial velocity as

$$U_{sx}^{(0)*} = d\, dx'/dt^* = \alpha + O(\kappa^2), \tag{6.4}$$

the trajectory equation may be expressed either as

$$dt^* = \frac{6\pi\mu_0}{\rho_0 V_m^{*2}\kappa^3 G(s)}\, ds \tag{6.5}$$

or equivalently

$$dx' = \frac{6\pi\mu_0\alpha}{\rho_0 V_m^{*2} d\kappa^3 G(s)}\, ds. \tag{6.6}$$

For the time trajectory, we have for both simple shear and two-dimensional Poiseuille flow

$$t^* - t_0^* = \frac{6\pi\mu_0}{\rho_0 V_m^{*2}\kappa^3}\int_{s_0}^{s}\frac{ds'}{G(s')}, \tag{6.7}$$

and for the axial-position trajectory in the simple shear flow case

$$(\alpha = V_w^* s = 2V_m^* s),$$

we have

$$x' - x_0' = \frac{12\pi\mu_0}{\rho_0 V_m^* d\kappa^3}\int_{s_0}^{s}\frac{s'\, ds'}{G(s')}, \tag{6.8}$$

while in the two-dimensional Poiseuille flow case

$$(\alpha = 4V_{\max}^* s(1-s) = 6V_m^* s(1-s)),$$

$$x' - x_0' = \frac{36\pi\mu_0}{\rho_0 V_m^* d\kappa^3}\int_{s_0}^{s}\frac{s'(1-s')}{G(s')}\, ds'. \tag{6.9}$$

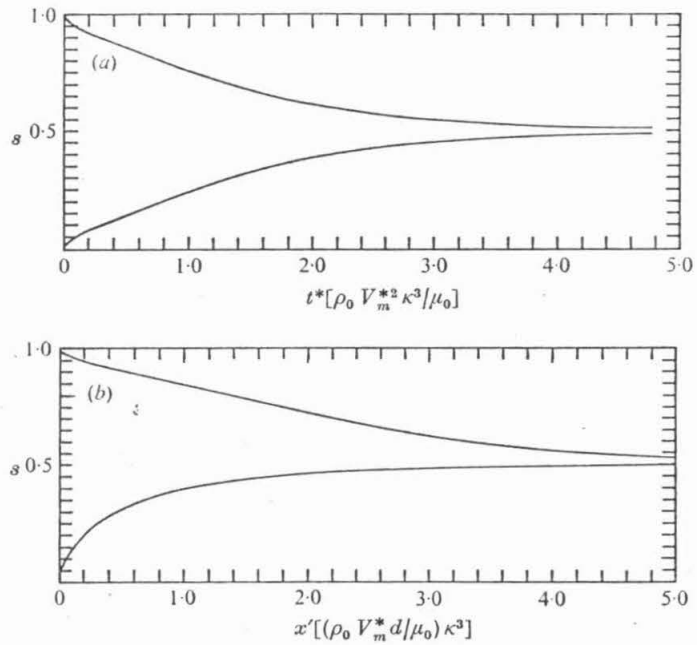

FIGURE 3. Particle trajectory for simple shear flow: lateral position *vs.* (*a*) time and (*b*) axial position.

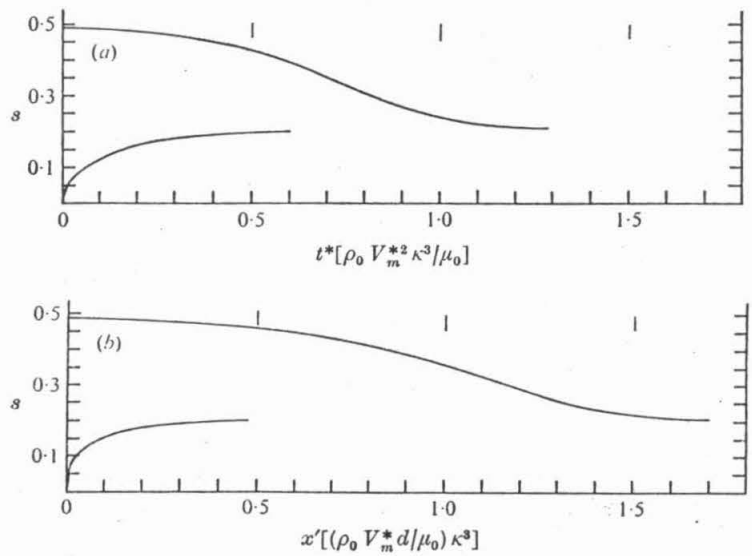

FIGURE 4. Particle trajectory for two-dimensional Poiseuille flow: lateral position *vs.* (*a*) time and (*b*) axial position.

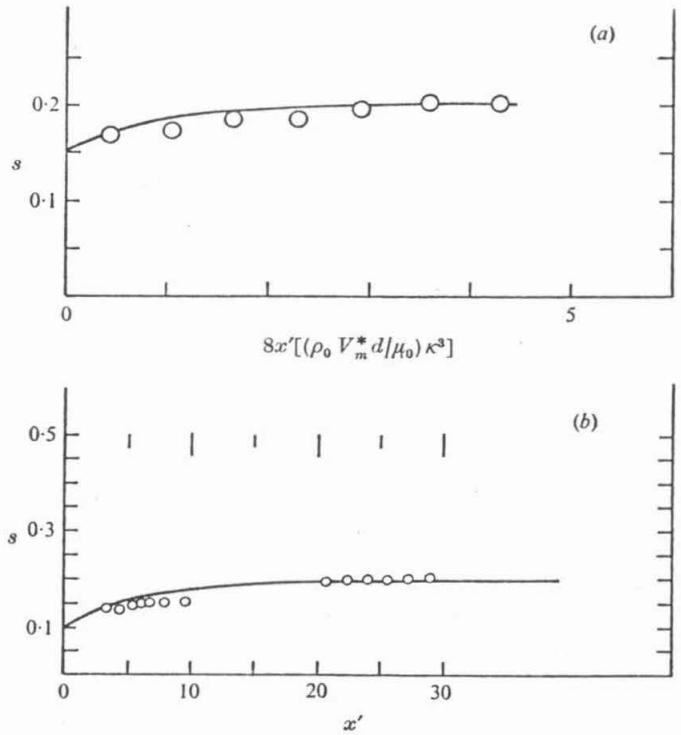

FIGURE 5. A comparison of experimental particle trajectories (Tachibana) in two-dimensional Poiseuille flow with the present theory: ○, experimental (Tachibana); ——, present theory. In (*a*), the lateral position s is plotted *vs.* $8x'[(\rho_0 V_m^* d/\mu_0)\kappa^3]$; and in (*b*) the lateral position s is plotted *vs.* x' with $\rho_0 V_m d/\mu_0 = 32{\cdot}1$ and $\kappa = 0{\cdot}0795$.

For simple shear flow, the particle trajectories (6.7) and (6.8) are plotted in figures 3(*a*) and (*b*) with s_0 taken to be 0·01 and 0·99. The time trajectory is symmetric about $s = 0{\cdot}5$ while the axial-position trajectory is not. For two-dimensional Poiseuille flow, (6.7) and (6.9) are plotted in figures 4(*a*) and (*b*). Since in this case both time and axial-position trajectories are symmetric about $s = 0{\cdot}5$, only $s_0 = 0{\cdot}01$ and 0·49 are considered. The main feature of interest for Poiseuille flow, which we shall discuss at greater length in the following section, is the skewness of the trajectories in the sense that spheres near the wall clearly migrate more rapidly than those near the centre for a given average flow rate V_m^* in a given fluid. This feature reflects the larger lateral force associated with the region nearest the wall.

For the reasons discussed in the previous section, the trajectories of Repetti & Leonard (1966) cannot be compared with our present theory. The only available experimental results are those of Tachibana (1973) and Halow & Wills (1970*a*, *b*).

Tachibana (1973) studied the migration of neutrally buoyant rigid spheres in two- and three-dimensional Poiseuille flow. Particle trajectories giving lateral *vs.* axial position were measured for the two cases cited earlier in which the equilibrium positions were $s = 0{\cdot}2$ and $s = 0{\cdot}8$. These trajectories are reproduced in

figures 5(*a*) and (*b*) together with corresponding trajectories predicted by the present theory. The agreement between observation and theory is remarkably good.

Halow & Wills' experimental investigation of sphere migration was carried out in a Couette flow system in which the inner cylinder was rotated and the outer cylinder was held fixed. For gap widths small compared with the cylinder radius the flow may be approximated as a simple shear flow. Extensive results are given in the thesis of Halow (1968) and our comparison is drawn from this source. As we have indicated earlier, Halow (1968) found the equilibrium position to be close to the centre-line between the two walls, but also somewhat closer to the inner moving wall, corresponding to a value of s between 0·5 and 0·55 in our present nomenclature. We believe that the slight discrepancy between these values and the predicted value of 0·5 is due to the fact that the Couette flow in Halow's apparatus corresponds only approximately to a simple shear flow. In fact, the ratio $2d/(r_1+r_2)$ has values of 0·1, 0·17, 0·22 and 0·3 in his experiments, where r_1 and r_2 are the inner and outer cylinder radii. The case corresponding to the value 0·1 is the nearest to simple shear flow, however, in this case the shear rates are too large to be compared with the present small-inertia expansion. The case 0·17 has sufficiently small shear rates; however, the flow is slightly different from a simple shearing flow.

In order to provide a detailed comparison with the data of Halow (1968), we therefore modify the analysis which is presented in the previous sections for simple shear flow to include the effects of curvature in the velocity distribution. Hence, instead of assuming simple shear flow, let us write an exact expression for the tangential undisturbed velocity field with co-ordinate axes fixed at the centre of the particle:

$$V^* = V_w^* \left(s+\frac{z^*}{d}\right)\left[\frac{r_1(r_2+r)}{r(r_2+r_1)}\right]. \tag{6.10}$$

Here, V_w^* is the tangential velocity of the inner wall, s is the non-dimensional lateral position of the sphere measured from the outer wall, z^* is the lateral position measured from the sphere centre and r (dimensional) is the radial position measured from the centre of the coaxial cylinders. Thus, the factor $r_1(r_2+r)/r(r_2+r_1)$ provides a correction of the simple shear flow profile for the Couette geometry. Provided that $2d/(r_1+r_2)$ is small, we can write

$$\frac{r_1(r_2+r)}{r(r_2+r_1)} = 1-\frac{r_2(r_2-r_1)}{r_1(r_2+r_1)}\left(1-s-\frac{z^*}{d}\right) \tag{6.11}$$

or

$$\begin{aligned} V^* &= V_w^*\left(s+\frac{z^*}{d}\right)\left[1-\frac{r_2(r_2-r_1)}{r_1(r_2+r_1)}(1-s)+\frac{r_2(r_2-r_1)\,z^*}{r_1(r_2+r_1)\,d}\right] \\ &= V_m^* s\left[1-\frac{r_2(r_2-r_1)}{r_1(r_2+r_1)}(1-s)\right]+V_w^*\left[1-\frac{r_2(r_2-r_1)}{r_1(r_2+r_1)}(1-2s)\right]\frac{z^*}{d} \\ &\qquad + V_w^*\left[\frac{r_2(r_2-r_1)}{r_1(r_2+r_1)}\right]\left(\frac{z^*}{d}\right)^2. \end{aligned} \tag{6.12}$$

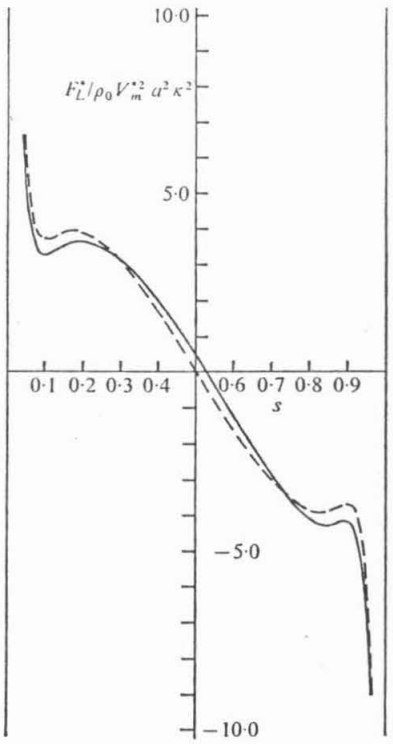

FIGURE 6. A comparison of the lateral force for simple shear flow with that for Couette flow. – – –, simple shear flow; ——, Couette flow with $R = 0{\cdot}1$.

The deviation of the Couette flow profile from simple shear flow depends on the parameter $R = r_2(r_2 - r_1)/r_1(r_2 + r_1)$. We can express the tangential velocity in dimensionless form as

$$V = \alpha + \beta' z' + \gamma' z'^2,$$

where

$$\alpha = V_w s[1 - R(1-s)], \quad \beta' = V_w[1 - R(1-2s)], \quad \gamma' = V_w R. \quad (6.13a, b, c)$$

Hence, our general result (5.24) can be used to calculate the force

$$F_L = Re\,\kappa^2[\beta'^2 G_1(s) + \beta'\gamma' G_2(s)].$$

We have plotted the result for the force with the parameter $R = 0{\cdot}1$ (corresponding to the case of $2d/(r_1 + r_2) = 0{\cdot}17$) in figure 6. Also shown is the force for simple shearing flow. The equilibrium position is seen to be shifted to $s = 0{\cdot}53$. The corresponding sphere trajectory, in the form of lateral position *vs.* time, is plotted in figure 7. On the same figure are the experimental results of Halow (1968) for the corresponding case in which the gap width d is 9·48 mm and $R = 0{\cdot}101$. Again reasonable agreement between theory and experiment is found.

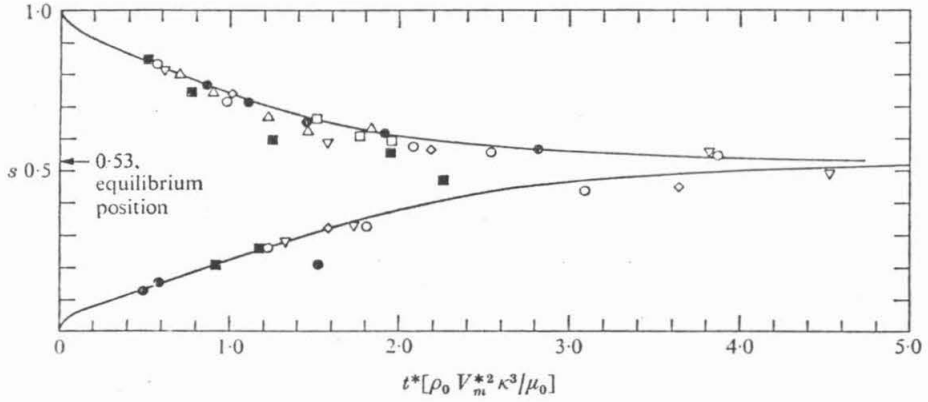

FIGURE 7. A comparison of experimental particle trajectories (Halow) in Couette flow with the present theory (solid line). In the results of Halow, $d = 9{\cdot}48$ mm, $r_2 = 60$ mm, $r_1 = 51$ mm and $R = 0{\cdot}101$. The following points and numbers correspond to different sphere radii reported in the thesis of Halow: ◇, 5, 6 ($a = 0{\cdot}8495$ mm); ○, 11, 12 ($a = 0{\cdot}8495$ mm); ▪, 15, 16 ($a = 0{\cdot}636$ mm); △, 19 ($a = 0{\cdot}735$ mm); □, 20 ($a = 0{\cdot}537$ mm); ▽, 25, 26 ($a = 0{\cdot}296$ mm); ●, 27, 28 ($a = 0{\cdot}296$ mm).

7. Flow of a suspension of rigid spherical particles which undergo translational Brownian motion

As a specific application of the results of the preceding sections, we consider the motion of a dilute suspension of rigid spheres which are simultaneously undergoing inertia-induced lateral migration and translational Brownian motion.

Of course, the preceding results have been derived for a *single* sphere in a given bulk flow, and it is necessary to investigate the circumstances in which the lateral force calculated for that case is applicable to a particle in a suspension of many particles. We have seen that the role of the walls is critical in the migration phenomenon and acts essentially by modifying the inertial behaviour of the flow. In addition, the walls also cause the sphere to have translational and rotational velocities different from those of the surrounding fluid, but the lateral force induced by this difference is smaller by $O(\kappa)$. If we now consider *two* spheres present in the bulk flow, it is clear that the modification of the inertial behaviour of the fluid would not be changed significantly from the single-sphere case because the second sphere constitutes the addition, in effect, of a boundary infinitesimally small compared with the infinitely unbounded walls. In addition, each sphere would also translate and rotate in creeping motion at different velocities as compared with a single sphere. This difference is of order $(a/d)\,(a/l)^2$ for translational motion and $(a/d)\,(a/l)^3$ for rotational motion, l being the inter-particle distance (see Wakiya, Darabaner & Mason 1967; Batchelor & Green 1972). However, we have previously shown that the lateral force will not be affected unless the translational and angular velocities of the sphere are changed to order $(a/d)^2$ and a/d respectively [cf. (5.15)]. Hence, the conditions for neglecting two-particle *inertial* migration compared with the single-particle/wall migration are

$$(a/l)^2 \ll a/d, \quad (a/l)^3 \ll 1. \tag{7.1a, b}$$

For a dilute suspension of concentration Φ ($\sim a^3/l^3$), the condition (7.1*b*) is automatically satisfied and (7.1*a*) becomes

$$\Phi^2 \ll \kappa^3. \tag{7.2}$$

In addition to two-particle inertial migration, it is *possible* that three-particle interactions may cause migration even at *zero* Reynolds number since the collision process is not reversible. Since three-particle interactions have a probability of occurrence $O(\Phi^2)$, a *conservative* condition for the neglect of this effect relative to wall-induced single-particle inertial migration is $\Phi^2 \ll \kappa^2 Re$, or since $Re \ll \kappa^2$,

$$\Phi^2 \ll \kappa^4. \tag{7.3}$$

Hence, if the conditions (7.2) and/or (7.3) are satisfied, it may be assumed that the lateral force on a particle in a suspension is equal to that on a single sphere immersed in the fluid.

Here, we consider the concentration distributions, flow behaviour and effective viscosity of a suspension of uniformly sized rigid spheres undergoing lateral migration with simultaneous Brownian translation in simple shear flow and two-dimensional Poiseuille flow. The concentration distribution is established as the result of a competition between the lateral migration force, which tends to cause the particles to crowd to a preferred position, and Brownian motion, which tends to cause a uniform dispersion across the channel. For our present purposes, we consider only the simple situation of *steady* bulk flow in which the concentration distribution has achieved its final, steady-state configuration.

The governing equation for the steady-state probability density function $\Phi(s)$ for concentration can be written as

$$d[\Phi(U^*_{\mathrm{Br}} + Re\, U^*_{sz})]/ds = 0. \tag{7.4}$$

Here U^*_{Br} represents the effective lateral velocity due to the action of Brownian diffusion in the presence of a concentration gradient, i.e.

$$\Phi U^*_{\mathrm{Br}} = -\left(\frac{kT}{6\pi\mu_0 a}\right)\frac{1}{d}\frac{d\Phi}{ds}, \tag{7.5}$$

where $kT/6\pi\mu_0 a$ is the translational Brownian diffusion coefficient, with k as the Boltzmann constant and T the absolute temperature. The velocity in the z direction induced by inertia is

$$Re\, U^*_{sz} = F^*_L(s)/6\pi\mu_0 a. \tag{7.6}$$

It should be noted that each of (7.5) and (7.6) is only a first approximation in κ. The solution of (7.4) with (7.5) and (7.6) is simply

$$\Phi(s) = \Phi_m \exp\left[\frac{d}{kT}\int_{\frac{1}{2}}^{s} F^*_L(s')\,ds'\right] \Big/ \int_{s''=0}^{1} \exp\left[\frac{d}{kT}\int_{\frac{1}{2}}^{s''} F^*_L(s')\,ds'\right] ds'', \tag{7.7}$$

where Φ_m is the mean concentration

$$\Phi_m \equiv \int_0^1 \Phi(s')\,ds'$$

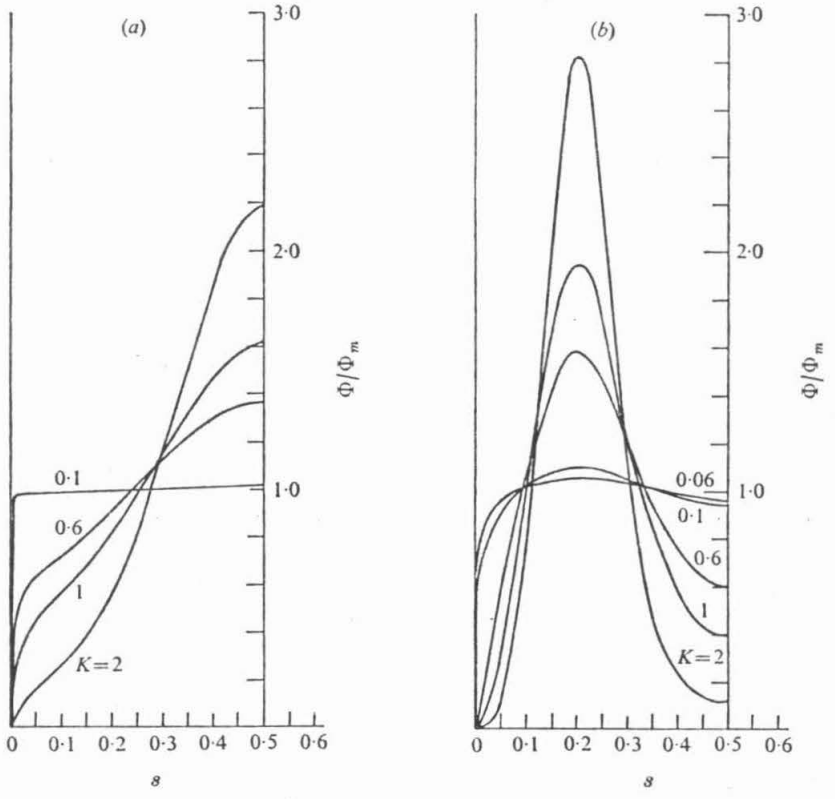

FIGURE 8. Concentration distribution $\Phi(s)/\Phi_m$ for various K in (a) simple shear flow and (b) two-dimensional Poiseuille flow.

and the lower limit of the integral of $F_L^*(s')$ is taken to be $\frac{1}{2}$ for convenience. Substituting the general form for F_L^*, i.e.

$$F_L^*(s) = \rho_0 V_m^{*2} a^2 \kappa^2 G(s),$$

and defining the parameter $K = \rho_0 V_m^{*2} a^4/dkT$, the concentration distribution function may thus be expressed as

$$\Phi(s) = \Phi_m \exp\left[K\int_{\frac{1}{2}}^{s} G(s')\,ds'\right] \Big/ \int_{s''=0}^{1} \exp\left[K\int_{\frac{1}{2}}^{s''} G(s')\,ds'\right] ds''. \tag{7.8}$$

The function $\Phi(s)$ is plotted with K as a parameter in figures 8(a) and (b). Since the distributions are symmetric about $s = 0{\cdot}5$, only half of the channel width is considered. Clearly $K \sim 10$ is inertia controlled whereas $K \sim 0{\cdot}01$ is diffusion controlled, these cases corresponding, respectively, to sharply peaked and nearly uniform concentration distributions.

Provided that (7.2) and/or (7.3) are satisfied *even at the most concentrated region*, the local effective viscosity at any position s may be calculated using the classical formula of Einstein

$$\mu(s) = \mu_0[1 + \tfrac{5}{2}\Phi(s)]. \tag{7.9}$$

There is an additional correction term due to the presence of inertia. For example, in an unbounded system, Lin, Peery & Schowalter (1970) have shown that the correction is $O(Re^{\frac{3}{2}})$. For small Reynolds number, we can neglect this correction and consider only the correction due to a non-uniform particle distribution. Since Φ depends upon s, so does μ, and the velocity profiles for the suspension as a whole will differ slightly (by $O(\Phi_m)$) from their simple form for a fluid of constant viscosity. This change may then be reflected in the relationship between the pressure drop and flow rate ($\Delta P/L$ versus Q) for the Poiseuille flow, and in the relationship between the applied force F_w^* and wall velocity V_w^* for simple shear flow. Hence, an investigator measuring $\Delta P/L$ and Q, or F_L^* and V_w^* as a viscometric measurement for an assumed purely viscous fluid of uniform viscosity would be led to conclude the existence of non-Newtonian behaviour since $\Phi(s)$ changes as a function of the flow rate. The equations for a steady-state unidirectional velocity field in the case of spatially varying local viscosity are simply

$$\frac{d}{ds}\left[\mu(s)\frac{du}{ds}\right] = 0; \quad u = 0 \quad \text{at} \quad s = 0; \quad u = V_w^* \quad \text{at} \quad s = 1, \tag{7.10}$$

for simple shear flow, and

$$\frac{d}{ds}\left[\mu(s)\frac{du}{ds}\right] = \left(\frac{\Delta P}{L}\right)d^2; \quad u = 0 \quad \text{on} \quad \text{the walls}, \tag{7.11}$$

for two-dimensional Poiseuille flow. By solving these equations, the modified velocity profiles can be shown to be

$$\frac{u(s)}{V_w^*} = s + \frac{5}{2}\left[s\Phi_m - \int_0^s \Phi(s')\,ds'\right] \tag{7.12}$$

for simple shear flow and

$$\frac{u(s)}{\frac{3}{2}V_m^*} = [1-(1-2s)^2] + \frac{5}{2}\left\{3[1-(1-2s)^2]\int_0^1 (1-2s')^2\,\Phi(s')\,ds' - 4\int_0^s (1-2s')\,\Phi(s')\,ds'\right\} \tag{7.13}$$

for two-dimensional Poiseuille flow. If $\Phi(s) = \Phi_m$, these expressions reduce to

$$u(s)/V_w^* = s, \tag{7.14}$$

$$u(s)/\tfrac{3}{2}V_m^* = 1-(1-2s)^2, \tag{7.15}$$

which are the appropriate velocity profiles for a fluid of constant viscosity. For simple shear flow, the correction term, (7.14) subtracted from (7.12),

$$\frac{5}{2}\left[s\Phi_m - \int_0^s \Phi(s')\,ds'\right] \tag{7.16}$$

is positive for $0 < s < 0{\cdot}5$ and negative for $0{\cdot}5 < s < 1$, and it is odd about $s = 0{\cdot}5$. Thus, from (7.12), the suspension moves more rapidly near the fixed wall and more slowly near the moving wall as compared with (7.14). For two-dimensional Poiseuille flow, the correction term, (7.15) subtracted from (7.13),

$$\frac{5}{2}\left\{3[1-(1-2s)^2]\int_0^1 (1-2s')^2\,\Phi(s')\,ds' - 4\int_0^s (1-2s')\,\Phi(s')\,ds'\right\} \tag{7.17}$$

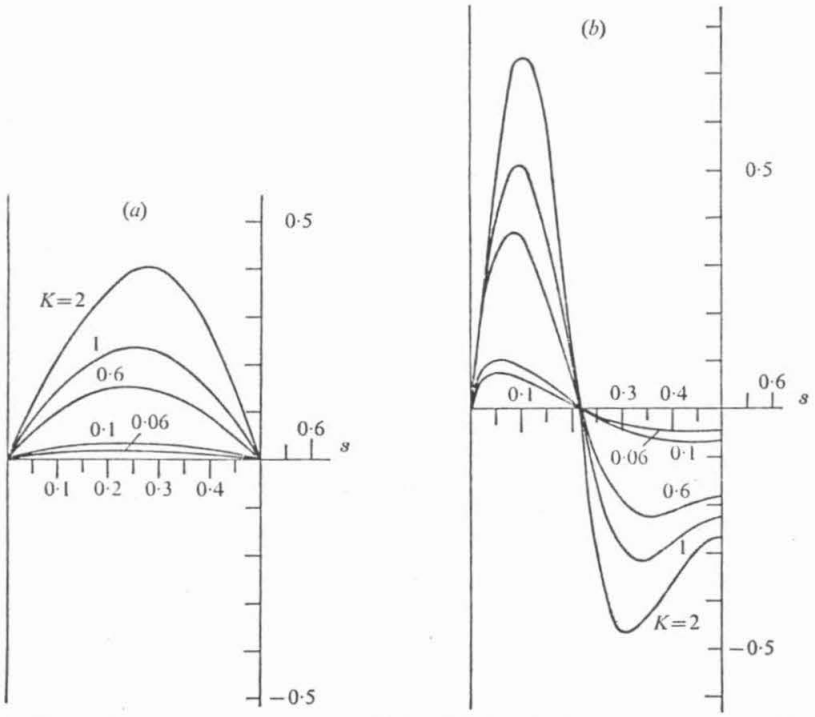

FIGURE 9. Correction term in velocity profile for (*a*) simple shear flow, equation (7.16), and (*b*) two-dimensional Poiseuille flow, equation (7.17).

is negative for $0{\cdot}22 < s < 0{\cdot}78$ and positive for $0 < s < 0{\cdot}22$ and $0{\cdot}78 < s < 1$, and is even about $s = 0{\cdot}5$. Thus, the resulting motion (7.13) is more rapid near the walls and slower near the centre as compared with (7.15). These correction terms (7.16) and (7.17) are plotted in figures 9(*a*) and (*b*) for various values of K. We have also plotted the resulting velocity profiles corresponding to (7.12) and (7.13) in figures 10(*a*) and (*b*) for $K = 2$ and $\Phi_m = 0{\cdot}1$. Although the present small-Φ theory is not expected to hold at a value of Φ_m as large as this, this value does allow the predicted corrections to be discernible on the scale of the bulk flow field. The most interesting feature evident in this figure is the flattening of the velocity profile for the case of two-dimensional Poiseuille flow.

It is of greatest interest to calculate the apparent viscosity μ_{app}, which would be measured by interpretating force/wall velocity or pressure drop/flow rate data as though the particle concentration was uniform, and the suspension therefore Newtonian with a constant viscosity. For simple shear flow, this apparent viscosity may be expressed as

$$\mu_{\text{app}} = F_w^* d / V_w^*, \tag{7.18}$$

where F_w^* is the applied force (equal also to the force required to keep the stationary wall fixed) and V_w^* the velocity of the moving wall. Similarly, for a two-dimensional Poiseuille flow, the apparent viscosity is

$$\mu_{\text{app}} = -\tfrac{1}{12}(\Delta P/L)\, d^3/Q, \tag{7.19}$$

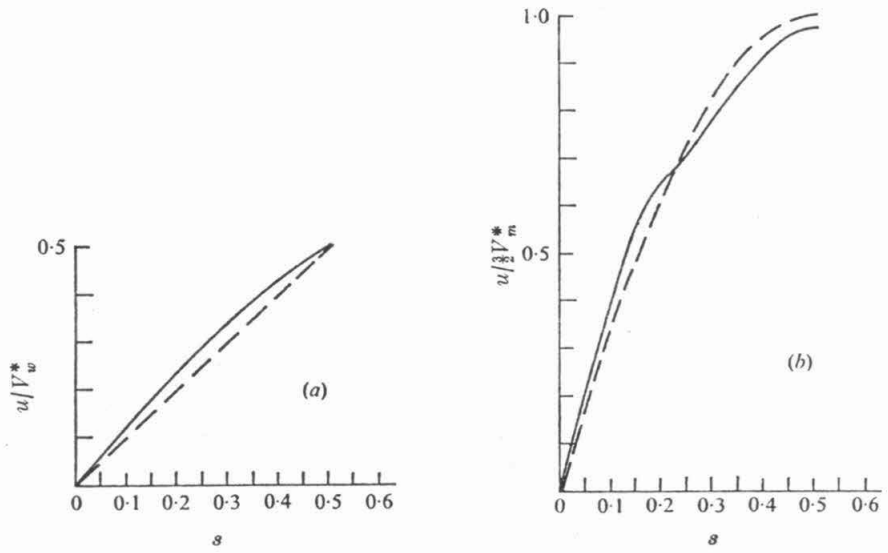

FIGURE 10. Velocity profile for (*a*) simple shear flow and (*b*) two-dimensional Poiseuille flow. – – –, uniform particle distribution; ——, non-uniform particle distribution with $K = 2$, $\Phi = 0{\cdot}1$.

where $\Delta P/L$ and Q are the measured pressure gradient and volumetric flow rate. Using the velocity profiles (7.12) and (7.13), plus the expression (7.9) for the effective *local* viscosity, we evaluate (7.18) and (7.19) to obtain the results

$$\mu_{\text{app}} = \mu_0[1 + \tfrac{5}{2}\Phi_m + O(\Phi_m^2)] \tag{7.20}$$

for simple shear flow and

$$\mu_{\text{app}} = \mu_0\left[1 + \frac{5}{2}\int_0^1 3\Phi(s')\,(1-2s')^2\,ds' + O(\Phi_m^2)\right] \tag{7.21}$$

for two-dimensional Poiseuille flow. Thus the apparent effective viscosity will be independent of the flow rate (shear rate) and equal to the Einstein value with Φ replaced by Φ_m for simple shear flow, but distinctly flow-rate dependent ('non-Newtonian') for two-dimensional Poiseuille flow. We have plotted the expression (7.21) for μ_{app} as a function of the flow-rate parameter K in figure 11. The deviation from the simple Newtonian value corresponding to a uniform concentration distribution ($K = 0$) first decreases with K but then for $K > \sim 0{\cdot}5$ increases monotonically towards the approximate asymptotic value

$$(\mu_{\text{app}} - \mu_0)/\mu_0 = \tfrac{5}{2}\Phi_m(1{\cdot}06).$$

Although this behaviour may appear unusual and at variance with the available data of Segré & Silberberg (1963), it is easily understood on the basis of the present theory. In a non-uniform shear flow, the contribution which a given particle makes to the dissipation of energy (and hence to the effective viscosity) depends on the square of the local velocity gradient. A particle near the wall, for example, contributes a greater fraction of the overall rate of dissipation

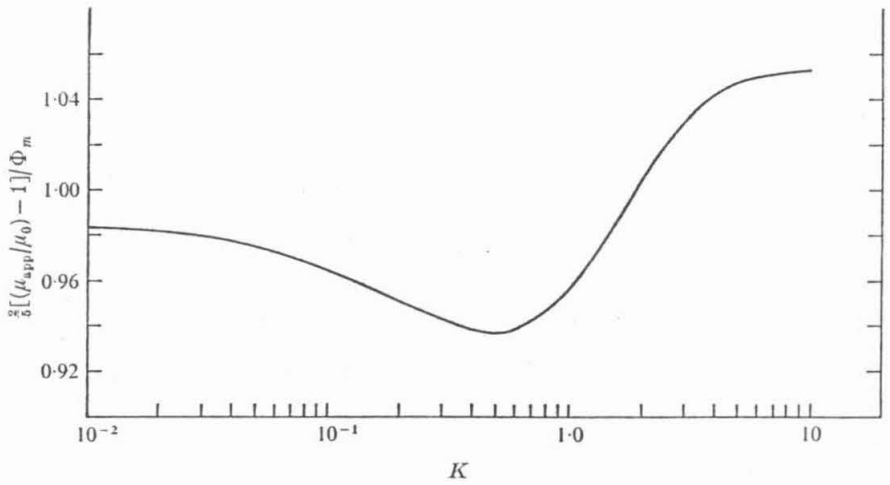

FIGURE 11. Reduced viscosity $\frac{2}{5}(\mu_{app}/\mu_0 - 1)/\Phi_m$ *vs.* K for two-dimensional Poiseuille flow.

than does a particle which is near to the centre-line, where the local shear rate is small. In addition, we have seen (cf. figure 2) that the lateral force is greatest near the wall and least near the centre-line. Hence, as K is increased, the migration of particles from the wall towards the 'equilibrium' position is more effective than the migration from the region nearer the centre-line, and the steady-state concentration distribution becomes skewed in favour of more particles in the centre and less near the walls (cf. figure 8*b*). Thus, initially the change in μ_{app} is towards lower values as the decrease in dissipation due to migration away from the walls dominates the increase caused by outward migration from the vicinity of the centre-line. For some intermediate value of K, the effective viscosity begins to increase as the outward migration from the centre becomes comparable with the inward migration from the walls. The data of Segré & Silberberg (1963) show only a decrease in viscosity with increasing flow rate. However, owing to the large particles used (a = 0·6 mm), the values of K ($\sim 10^8$) are well into the migration-dominated regime where Φ is not small near the equilibrium position and particle–particle interactions are important.

This work was supported, in part, by grant 6489-AC7 from the Petroleum Research Fund, administered by the American Chemical Society, and, in part, by NSF grant GK-35468.

REFERENCES

BATCHELOR, G. K. & GREEN, J. T. 1972 *J. Fluid Mech.* **56**, 375.
BRENNER, H. 1966 *Advances in Chemical Engineering*, vol. 4. Academic.
BRETHERTON, F. P. 1962 *J. Fluid Mech.* **14**, 284.
COX, R. G. & BRENNER, H. 1968 *Chem. Engng Sci.* **23**, 147.

Goldsmith, H. L. & Mason, S. G. 1966 *Rheology: Theory and Applications* (ed. F. R. Eirich), vol. 4. Academic.

Halow, J. S. 1968 Ph.D. thesis, Virginia Polytechnic Institute.

Halow, J. S. & Wills, G. B. 1970*a* *A.I.Ch.E. J.* **16**, 281.

Halow, J. S. & Wills, G. B. 1970*b* *Ind. Eng. Chem. Fund.* **9**, 603.

Happel, J. & Brenner, H. 1973 *Low Reynolds Number Hydrodynamics*. Noordhoff.

Ho, B. P. 1974 Ph.D. thesis, California Institute of Technology.

Lin, C. J., Peery, J. H. & Schowalter, W. R. 1970 *J. Fluid Mech.* **44**, 1.

Repetti, R. V. & Leonard, E. F. 1966 *Chem. Engng Prog. Symp. Ser.* **62**, 80.

Rubinow, S. I. & Keller, J. B. 1961 *J. Fluid Mech.* **11**, 447.

Saffman, P. G. 1965 *J. Fluid Mech.* **22**, 385.

Segré, G. & Silberberg, A. 1962*a* *J. Fluid Mech.* **14**, 115.

Segré, G. & Silberberg, A. 1962*b* *J. Fluid Mech.* **14**, 136.

Segré, G. & Silberberg, A. 1963 *J. Colloid Sci.* **18**, 312.

Starkey, T. V. 1956 *Brit. J. Appl. Phys.* **7**, 52.

Tachibana, M. 1973 *Rheol. Acta*, **12**, 58.

Wakiya, S. J. 1956 *Res. Rep. Fac. Engng, Niigata University (Japan)*, **5**, 1.

Wakiya, S., Darabaner, C. L. & Mason, S. G. 1967 *Rheol. Acta*, **6**, 264.

APPENDIX A

In sections 3 and 4, the required solutions $(\vec{v}^{(0)}, q^{(0)})$ and $(\vec{u}, p)$ were obtained by the method of reflexions. In this appendix, we provide the detailed expressions which were omitted from sections 3 and 4 in the interest of brevity.

To obtain the solution to equation (3.3) for $(\vec{v}_2^{(0)}, q_2^{(0)})$, the velocity field was expressed in terms of six unknown functions g_4, g_5, g_6, g_7, g_8 and g_9 (see equation (3.11)) which were found by satisfying the boundary conditions on the walls, namely $(\vec{v}_1^{(0)}+\vec{v}_2^{(0)})=0$ at $z'=-s$ and $z'=(1-s)$. The resulting expressions for $g_4, \ldots g_9$ are

$$g_4 = -\frac{t_2 g_1^- - g_1^+}{t-1}, \qquad \text{(A-1a)}$$

$$g_5 = \frac{1}{t-1}\left\{(t_2 g_1^- + g_2^+)+\tfrac{1}{2}(t_2 g_3^- + g_3^+) + \tfrac{1}{2}(1-s)\zeta g_3 + \tfrac{1}{2}[(1-s)\zeta + s\zeta t - (t-1)]g_6\right\}, \qquad \text{(A-1b)}$$

$$g_6 = \frac{1}{\Delta}\left\{2t_2(t-1)(g_1^- + g_2^-)+2\zeta t(g_1^+ + g_2^+) + (t-1)(t_2 g_3^- + g_3^+)+s\zeta t(t_2 g_3^- + g_3^+) + (1-s)\zeta t_2(t_1 g_3^+ + g_3^-)+(1-s)\zeta^2 t g_3^+\right\}, \qquad \text{(A-1c)}$$

$$g_7 = -\frac{t_1 g_1^{+} - g_1^{-}}{t-1}\,, \tag{A-1d}$$

$$g_8 = \frac{1}{t-1}\Big\{(t_1 g_1^{+} + g_2^{-}) + \tfrac{1}{2}(t_1 g_3^{+} + g_3^{-}) + \tfrac{1}{2}s\zeta g_3^{-} + \tfrac{1}{2}[s\zeta + (1-s)\zeta t - (t-1)]g_9\Big\}\,, \tag{A-1e}$$

$$g_9 = \frac{1}{\Delta}\Big\{2t_1(t-1)(g_1^{+} + g_2^{+}) + 2\zeta t(g_1^{-} + g_2^{-}) + (t-1)(t_1 g_3^{+} + g_3^{-}) + (1-s)\zeta t(t_1 g_3^{+} + g_3^{-}) + s\zeta t_1(t_2 g_3^{-} + g_3^{+}) + s\zeta^2 t g_3^{-}\Big\}\,, \tag{A-1f}$$

where $t=\exp\zeta$, $t_1=\exp s\zeta$, $t_2=\exp(1-s)\zeta$,

$$\Delta=(t-1)^2-\zeta^2 t. \tag{A-1g}$$

The superscripts + and - on g_1, g_2 and g_3 imply evaluation at $z'=(1-s)$ and $z'=-s$ respectively. These expressions for g_4, ...g_9 are exact to all orders of κ (of course provided $\kappa<<1$ as required by the method by reflexions). In the evaluation of the lateral force on a neutrally buoyant rigid sphere, only terms to $O(\kappa^3)$ in g_4, ...g_9 are required. These expressions to $O(\kappa^3)$ have been given in (5.19) already.

The solutions for $(\vec{v}_3^{(0)}, q_3^{(0)})$ are expressed in terms of the functions of A_3, B_3, C_3, D_3, ...H_3 which are defined in (3.14). As evident in this equation, A_3, B_3, ...H_3 are definite integrals in the variable ζ of the

expressions g_4, g_5, ...g_9. For convenience, we have also expressed A_3 and C_3 in terms of A_1, C_1 and D_1 (cf. equation (3.16)), and the six definite integrals (in the variable ζ) K_A, K_C, K_D, L_A, L_C, L_D. By direct substitution of equations (A-1) and the definitions (3.14) and (3.13), we find the following expressions for these integrals:

$$
\begin{aligned}
K_A = & -\frac{3}{32}[10\Psi(s)+5\pi\cot(\pi s)+10\gamma_E-\zeta_{RZ}(2)] \\
& +\frac{3}{32}\int_0^\infty \Big\{\frac{1}{\Delta}[(t_1+t_2-2)(t-1) \\
& +\zeta\{1-2st_1-2(1-s)t_2+3t-2(1-s)t_1t \\
& -2st_2t\}-\zeta^2\{(1-s)^2t_2+s^2t_1+t-s^2t_2t \\
& -(1-s)^2t_1t\}+\zeta^3 2s(1-s)t]+\frac{\zeta^2}{\Delta(t-1)} \\
& [(t_2+t_1)t-t(t+1)+\zeta t]\Big\}\,d\zeta \quad , \qquad \text{(A-2a)}
\end{aligned}
$$

$$
\begin{aligned}
K_C = & -\frac{3}{16}[2\Psi'(s)-\pi^2\operatorname{cosec}^2(\pi s)] \\
& -\frac{3}{16}\int_0^\infty \frac{\zeta}{\Delta}\Big\{(t_2-t_1)(t-1)-s\zeta t_2(t-1) \\
& +(1-s)\zeta t_1(t-1)-\zeta(t_2-t_1) \\
& -(1-2s)\zeta^2 t\Big\}\,d\zeta \quad , \qquad \text{(A-2b)}
\end{aligned}
$$

$$
\begin{aligned}
K_D = & \frac{3}{64}[6\Psi'(s)-3\pi^2\operatorname{cosec}^2(\pi s)-2(1-2s)\zeta_{RZ}(3)] \\
& +\frac{3}{64}\int_0^\infty \Big\{\frac{\zeta}{\Delta}[(t_2-t_1)(t-1) \\
& +\zeta\{(1-2s)(t_1+t_2+1)(t-1)+(t_1-t_2)(t+1)\}
\end{aligned}
$$

$$+\zeta^2\{s^2t_1-(1-s)^2t_2-(1-s)^2t_1t+s^2t_2t\}]$$
$$+\frac{\zeta^3}{\Delta(t-1)}[(t_2-t_1)t-(1-2s)\zeta t]\Big\}\,d\zeta \quad , \qquad \text{(A-2c)}$$

$$L_A = -\frac{1}{16}[2\Psi'(s)-\pi^2\mathrm{cosec}^2(\pi s)]$$
$$+\frac{1}{16}\int_0^\infty \frac{\zeta}{\Delta}\Big\{(t_1-t_2)(t-1)+\zeta\{(t_2-t_1)t$$
$$+st_1(t-1)-(1-s)t_2(t-1)\}$$
$$+\zeta^2(1-2s)t\Big\}\,d\zeta \quad , \qquad \text{(A-2d)}$$

$$L_C = -\frac{1}{16}[\Psi''(s)+\pi^3\mathrm{cosec}^2(\pi s)\ \cot(\pi s)$$
$$-2\zeta_{RZ}(3)]+\frac{1}{8}\int_0^\infty \frac{\zeta^2}{\Delta}\Big\{(t_2+t_1)(t-1)$$
$$-2\zeta t\Big\}\,d\zeta \quad , \qquad \text{(A-2e)}$$

$$L_D = \frac{1}{32}[\Psi''(s)+\pi^3\mathrm{cosec}^2(\pi s)\ \cot(\pi s)$$
$$-2\zeta_{RZ}(3)]-\frac{1}{32}\int_0^\infty \frac{\zeta^2}{\Delta}\Big\{(t_1+t_2+2)(t-1)$$
$$-\zeta\{st_1+(1-s)t_2+2t+st_2t+(1-s)t_1t\}$$
$$+\zeta^2t\Big\}\,d\zeta \quad . \qquad \text{(A-2f)}$$

Here, $\Psi(s)$ is the Psi (or digamma) function and $\Psi'(s)$, $\Psi''(s)$ are the polygamma functions; $\gamma_E=0.5772$ is the Euler's constant; and $\zeta_{RZ}(2)=1.6449$, $\zeta_{RZ}(3)=1.2021$ are the Riemann Zeta functions*. Notice that some of the integrals that

* For definition and tabulation of these functions, see Abramowitz, M. & Stegun, I.A., Handbook of Mathematical Functions, Dover 1968.

appear in K_A, K_C, ...L_D are integrated analytically and some, which are left in their definite integral form, have to be integrated numerically. Values for K_D, K_A and L_A are tabulated in tables that appear in section 3.

Similarly, in section 4, $\vec{u}_2$ was expressed in terms of four unknown functions f_3, f_4, f_5, and f_6. Upon application of the boundary condition $\vec{u}_1+\vec{u}_2=0$ on the walls $z'=-s$ and $z'=1-s$, these are found to be

$$f_3 = -\frac{1}{\Delta}[(t_2-1)(t-1)+\zeta\{(1-s)t_2-t+st_2t\} - (1-s)\zeta^2 t]f_1-\frac{2}{\Delta}[t_2(t-1)-\zeta t]f_2 \quad , \qquad \text{(A-3a)}$$

$$f_4 = \frac{\zeta^2}{2\Delta}[(1-s)^2t_2-(1-2s)t-s^2t_2t+s(1-s)\zeta t]f_1 +\frac{1}{\Delta}[(t_2+1)(t-1)-\zeta\{(1-s)t_2+t+st_2t\} +s\zeta^2 t]f_2 \quad , \qquad \text{(A-3b)}$$

$$f_5 = -\frac{1}{\Delta}[(t_1-1)(t-1)+\zeta\{st_1-t+(1-s)t_1t\} - s\zeta^2 t]f_1-\frac{2}{\Delta}[t_1(t-1)-\zeta t]f_2 \quad , \qquad \text{(A-3c)}$$

$$f_6 = \frac{\zeta^2}{2\Delta}[s^2t_1+(1-2s)t-(1-s)^2t_1t+s(1-s)\zeta t]f_1 +\frac{1}{\Delta}[(t_1+1)(t-1)-\zeta\{st_1+t+(1-s)t_1t\} +(1-s)\zeta^2 t]f_2 \quad . \qquad \text{(A-3d)}$$

The expressions for f_3, f_4, f_5 and f_6 to $O(\kappa)$ have been

given in equation (5.14). Finally, the solutions for $(\vec{u}_3, p_3)$ were obtained in terms of A_3 and B_3. For convenience, we have expressed A_3 in terms of A_1 and B_1 and two integrals K_A and K_B (cf. (4.11)). The expressions for K_A and K_B are

$$K_A = -\frac{3}{16}\int_0^\infty \frac{\zeta^2}{\Delta}\left\{s^2t_1+(1-s)^2t_2-(1-s)^2t_1t -s^2t_2t+2s(1-s)\zeta t\right\}d\zeta+\frac{3}{8}\int_0^\infty \frac{1}{\Delta}\left\{(t_1+t_2-2)(t-1)+\zeta\{st_1+(1-s)t_2-2t+(1-s)t_1t +st_2t\}-\zeta^2t\right\}d\zeta \quad , \tag{A-4a}$$

$$K_B = \frac{3}{16}\int_0^\infty \frac{\zeta^2}{\Delta}\left\{(t_1+t_2+2)(t-1)-\zeta\{st_1 +(1-s)t_2+2t+(1-s)t_1t+st_2t\}+\zeta^2t\right\}d\zeta -\frac{3}{8}\int_0^\infty \frac{\zeta^2}{\Delta}\left\{(t_1+t_2)(t-1)-2\zeta t\right\}d\zeta \; . \tag{A-4b}$$

Values of K_A are tabulated in table 3 of section 4.

CHAPTER III

MIGRATION OF RIGID SPHERES IN A TWO-DIMENSIONAL UNIDIRECTIONAL FLOW OF A SECOND-ORDER FLUID

The lateral migration of a neutrally buoyant rigid sphere suspended in a second-order fluid is studied theoretically for unidirectional two-dimensional flows. The results demonstrate the existence of normal stress induced migration whenever there is a lateral variation of shear rate in the undisturbed flow. The migration occurs in the direction of decreasing absolute shear rate, which corresponds to the centerline for a plane Poiseuille flow and to the outer cylinder wall for Couette flow. The direction of migration agrees with existing experimental data for a viscoelastic suspending fluid, and qualitative agreement is found between the theoretically predicted and experimentally measured sphere trajectories.

The text of Chapter III comprises an article (coauthor, Dr. L. G. Leal) which is submitted to Journal of Fluid Mechanics for publication. To provide a technological application to the result of this chapter, the migration of particles inside a screw extruder is considered in Appendix B.

1. Introduction

Experimental and theoretical studies of suspensions have revealed two distinct mechanisms by which suspended particles can produce flow-rate dependent macroscopic behavior. First, when the concentration of particles is spatially uniform, nonlinear macroscopic behavior can result if the individual particles deform or preferentially orient in a manner which depends on the magnitude of the bulk velocity field. Macroscopic effects of this first type represent an intrinsic property of the suspension, and are thus reflected in the characteristic non-Newtonian form of the particle contribution to the bulk stress. Even when the particle contributions to the bulk stress are linear, however, the measured macroscopic variables in a particular viscometric experiment may still exhibit a nonlinear (flow-rate dependent) relationship. An example is the experimental measurements of flow-rate versus pressure drop for a dilute suspension of rigid spheres in a capillary viscometer by Segré and Silberberg (1963). One cause for such behavior is the presence, under appropriate conditions, of flow-induced lateral motion of the suspended particles. This motion tends to produce a non-uniform concentration distribution that depends both on the macroscopic flow rate and on the detailed geometry of the viscometer. In a recent theoretical investigation, Ho & Leal (1974), we have considered the problem of inertia-induced migration of rigid spherical particles in a two-dimensional, quadratic, unidirectional shear flow (simple shear and plane Poiseuille flow are two examples) of a Newtonian fluid. The present communication is concerned with migration induced in similar circumstances as a result of non-Newtonian properties in the ambient suspending fluid.

The phenomenon of lateral migration in non-Newtonian liquids has been studied experimentally by Mason and co-workers (Karnis & Mason, 1966; Gauthier,

Goldsmith & Mason, 1971a,b) and by Highgate & Whorlow (1968, 1969). Mason's studies have demonstrated that the magnitude and even the direction of migration depends critically on the detailed rheological characteristics of the suspending fluid. Two distinct sets of results were obtained, one for purely viscous fluids (labelled pseudoplastic by Mason) which show a strong shear thinning of viscosity, but only very weak normal stress or relaxation (recoil) phenomena, and the other for fully viscoelastic fluids (labelled elasticoviscous by Mason). In the latter case, which was studied by Karnis & Mason (1966) for Poiseuille and Couette flows, rigid spherical particles were found to migrate in the direction of minimum shear rate, i.e. toward the centerline in Poiseuille flow and toward the outer cylinder wall in Couette flow. On the other hand, when the suspending fluid is purely viscous, Gauthier, Goldsmith & Mason (1971a, 1971b) have shown that migration of rigid spheres occurs in the opposite sense, i.e. toward the wall in Poiseuille flow and toward the inner cylinder in Couette flow. Detailed particle trajectories were measured in each case. Unfortunately, however, the available rheological data are both incomplete and of questionable accuracy (cf. Bartram, 1973), so that the main value of these studies is qualitative. Related migration phenomena in viscoelastic fluids were also reported by Highgate & Whorlow (1968, 1969) who studied Couette flow and the viscometrically interesting cone and plate geometry. In the latter case, relatively rapid radial migration was observed which completely depleted the gap of the viscometer of suspended spheres after several minutes. The case of Couette flow was found, in the experiment of Highgate & Whorlow (1968, 1969), to exhibit an axially directed migration (i.e. at right angles to the cross-gap migration of Mason, et. al.) which again eventually depleted the gap of particles (although on a

relatively longer time scale compared with the cone and plate case).

To date, no proper theoretical analysis has been reported for any of these phenomena, though it was suggested both by Highgate & Whorlow (1968, 1969) and Karnis & Mason (1966) that a qualitatively relevant explanation could be obtained in the viscoelastic case by simply taking account of the net force produced on a sphere by the gradients of normal stress in the undisturbed flow. It is, however, clear that such an "explanation" is entirely irrelevant to the observed phenomena. First of all, in the unidirectional flows under consideration, any gradients in the deviatoric normal stress components must be balanced by gradients in the pressure so that the net lateral force on any fluid element (and hence on the sphere) in the undisturbed flow is precisely zero. Second, no account has been taken of the disturbance flow (and associated normal stresses) which is induced by the particle and is of at least comparable magnitude to the undisturbed motions in its vicinity.

We consider here a complete theoretical analysis for the cases of plane Poiseuille and Couette flow of a second-order fluid. It is, of course, well-known that the second-order fluid model is only relevant for very slow and thus nearly Newtonian flows. In particular, deviations of the stress components from their Newtonian values are of only infinitesimal magnitude, and are confined in unidirectional shear flows of the type we consider here to the first and second normal stress differences. In spite of these limitations, we feel that the analysis is of fundamental interest and at least qualitatively applicable to problems of practical interest. Our reasons for this optimism are several-fold. First is the fact that the n^{th} order fluid expansion, of which the second-order fluid includes the first two terms, is

the common slow-flow limit of most other models of viscoelastic fluid behavior. Thus, in spite of uncertainties which persist in the formulation of general viscoelastic fluid models, the n^{th} order fluid "models" are almost certainly relevant for flows which have a characteristic time scale which exceeds the intrinsic relaxation time of the material. Secondly, since the shear-dependence of the viscosity only comes into the n^{th} order fluid expansion at third order, the second-order model provides a rational basis for separating the effects of normal stress induced particle migration, from that induced in the purely-viscous case by gradients of the shear viscosity. In spite of the fact that the normal stress induced migration is necessarily restricted in magnitude by the nature of the second-order fluid model, there is no contribution at all from the dominant first-order (Newtonian) terms. Hence, under appropriate circumstances the small instantaneous effect can produce a major accumulative change in the particle motion. Finally, we would call attention to the recent calculation by one of us (Leal, 1974) of orbit drift for long slender particles in simple shear flow of a second-order fluid. This work has provided one example, which is closely related to the present work, of a case where the second-order fluid model gives quantitative comparison with experimental data, even outside the range of bulk shear rates where the model is strictly applicable. Good comparison was accomplished in the orbit drift case by simply using measured values of the rheological parameters at the relevant bulk shear rate rather than the zero-shear values for which the model is strictly relevant. We suggest, therefore, that the qualitative physics of the normal stress effects

may not be too badly represented by the second-order fluid approximation over a reasonably wide range of shear rates.

The detailed analysis required for the present problem follows rather closely that reported in our earlier study, Ho & Leal (1974), of inertia-induced migration in a Newtonian fluid. Thus, we concentrate our discussion primarily on those features which are unique to the non-Newtonian problem, and refer the reader to our earlier paper for other details of the calculation.

2. The Basic Equations

We consider a neutrally buoyant rigid sphere of radius a freely suspended in an incompressible second-order fluid which is confined between two parallel plane walls separated by a distance d. The suspending fluid is assumed to be undergoing a steady unidirectional, two-dimensional bulk flow which we denote as V_i. The fluid density will be denoted by ρ_o, and the zero-shear viscosity by μ_o. All quantities will be nondimensionalized by the characteristic length a, and a characteristic velocity $\bar{\beta}a$ where $\bar{\beta}$ is an average shear rate for the bulk flow. Later, in order to make the calculation tractable, we will restrict our analysis to small particles for which $a \ll d$. Finally, for convenience, we will use convected cartesian coordinates with an origin which is coincident with the center of the sphere. The equations of motion may thus be expressed in the form

$$\mathrm{Re}\left[\frac{\partial U_i}{\partial t} + U_j U_{i,j}\right] = T_{ij,j}, \qquad U_{j,j} = 0, \tag{2.1a,b}$$

where the stress tensor T_{ij}, for a second order fluid is

$$T_{ij} = -P\delta_{ij} + A_{(1)ij} + \lambda A_{(1)ik}A_{(1)kj} + \lambda\varepsilon_1 A_{(2)ij}, \tag{2.1c}$$

where

$$A_{(1)ij} = U_{i,j} + U_{j,i}, \tag{2.1d}$$

$$A_{(2)ij} = \frac{\partial A_{(1)ij}}{\partial t} + U_k A_{(1)ij,k} + A_{(1)ik} U_{k,j} + A_{(1)kj} U_{k,i}. \tag{2.1e}$$

$A_{(1)ij}$ is the rate of strain tensor and $A_{(2)ij}$ is the second Rivlin-Ericksen tensor. The relevant dimensionless parameters are the Reynolds number $Re \equiv \rho_o \bar{\beta} a^2/\mu_o$, and the non-Newtonian parameters $\lambda = \phi_3 \bar{\beta}/\mu_o$ and $\varepsilon_1 = \phi_2/\phi_3$ in which ϕ_2 and ϕ_3 are related to the magnitude of the normal stress components in shear flow (see (2.7)). Available experimental evidence indicates that $\lambda > 0$ and $\varepsilon_1 \leq -0.5$ in most polymeric solutions and melts, these values corresponding to a positive first normal stress difference and a negative second normal stress difference in simple shear flow. The case $\varepsilon_1 = -0.5$ corresponds to the so-called Weissenberg fluid in which the second normal stress difference is exactly zero.

The dimensionless parameter λ is a measure of the intrinsic relaxation time for the suspending fluid relative to the dynamic scale $\bar{\beta}^{-1}$. In the present work we consider λ to be small so that the constitutive relationship (2.1c) differs only slightly from that of a Newtonian fluid. In addition, we assume that the fluid motion is also dynamically slow so that inertial effects may be neglected. More precisely, we require

$$Re \ll \lambda \ll 1, \tag{2.2a}$$

so that the Newtonian creeping motion velocity and pressure fields are modified by nonlinear effects associated with nonzero values of λ rather than dynamic inertial effects associated with nonzero values of the Reynolds number. The first inequality (i.e. $Re \ll \lambda$) is satisfied provided

$$\phi_3 >> \rho_o a^2. \tag{2.2b}$$

Thus, for a given fluid, the neglect of dynamic inertia compared to non-Newtonian effects is justified for sufficiently small particles.

We consider the undisturbed bulk flow to be steady, unidirectional and two-dimensional. Special cases of this general type include plane Poiseuille flow, simple shear flow, or any combination of these. Since $V_j V_{i,j} \equiv 0$, the equations of motion for the undisturbed flow are simply

$$\Pi_{ij,j} = 0, \quad V_{j,j} = 0, \tag{2.3a,b}$$

in which

$$\Pi_{ij} = -Q\delta_{ij} + E_{(1)ij} + \lambda E_{(1)ik}E_{(1)kj} + \lambda\varepsilon_1 E_{(2)ij}, \tag{2.3c}$$

and

$$E_{(1)ij} = V_{i,j} + V_{j,i}, \tag{2.3d}$$

$$E_{(2)ij} = V_k E_{(1)ij,k} + E_{(1)ik}V_{k,j} + E_{(1)kj}V_{k,i}. \tag{2.3e}$$

A solution to these equations, which encompasses both two-dimensional Poiseuille and simple shear flow, is

$$V_i = V\delta_{xi},$$

$$V = \alpha + \beta z + \gamma z^2 - (U_s)_x, \tag{2.4}$$

$$Q = 2\gamma x + 4\gamma(\beta z + \gamma z^2)(1 + 2\varepsilon_1)\lambda + \text{constant},$$

where $(U_s)_x$ is the velocity of the sphere in the x direction. For a simple

shear flow, as depicted in Figure (1a), the constants α, β and γ are

$$\alpha = V_w s, \qquad \beta = V_w \kappa, \qquad \gamma = 0 , \tag{2.5}$$

where V_w is velocity of the moving wall, s is the non-dimensionalized distance across the gap width from the fixed wall, d is the gap width, and $\kappa = a/d$. For a two-dimensional Poiseuille flow, as depicted in Figure (1b),

$$\begin{aligned} \alpha &= 4\, V_{max}\, s(1 - s), \\ \beta &= 4\, V_{max}\, (1 - 2s)\kappa , \\ \gamma &= -4\, V_{max}\, \kappa^2 , \end{aligned} \tag{2.6}$$

where V_{max} is the maximum velocity at the mid-point between the walls. It may be noted that, for a second order fluid, the undisturbed velocity field is unchanged from that of a Newtonian fluid having the same viscosity μ_o, but does produce a contribution to the isotropic pressure at order λ. The first and second normal stress differences are respectively given by

$$\begin{aligned} \Pi_{xx} - \Pi_{zz} &= -2 \left(\frac{dV}{dz}\right)^2 \varepsilon_1 \lambda , \\ \Pi_{zz} - \Pi_{yy} &= \left(\frac{dV}{dz}\right)^2 (1 + 2\varepsilon_1)\lambda \quad . \end{aligned} \tag{2.7}$$

For the analysis of equations (2.1), it is convenient to define a disturbance velocity $v_i = U_i - V_i$, and pressure $q = P - Q$. Then assuming (2.2) to hold, the steady state equations of motion satisfied by v_i and q are

$$\pi_{ij,j} = 0, \quad v_{j,j} = 0, \tag{2.8a}$$

in which

$$\pi_{ij} = -q\delta_{ij} + e_{(1)ij} + \lambda\left[e_{(1)ik}e_{(1)kj} + W_{(1)ij}\right] + \lambda\varepsilon_1\left[e_{(2)ij} + W_{(2)ij}\right], \tag{2.8b}$$

and

$$e_{(1)ij} = v_{i,j} + v_{j,i},$$

$$e_{(2)ij} = v_k e_{(1)ij,k} + e_{(1)ik}v_{k,j} + e_{(1)kj}v_{k,i}, \tag{2.8c}$$

$$W_{(1)ij} = E_{(1)ik}e_{(1)kj} + e_{(1)ik}E_{(1)kj},$$

$$W_{(2)ij} = V_k e_{(1)ij,k} + e_{(1)ik}V_{k,j} + e_{(1)kj}V_{k,i} + v_k E_{(1)ij,k} + E_{(1)ik}v_{k,j} + E_{(1)kj}v_{k,i}.$$

Here $e_{(1)ij}$ and $e_{(2)ij}$ are respectively, the rate of strain tensor and the second Rivlin-Ericksen tensor for acceleration of the disturbance flow v_i; while $W_{(1)ij}$ and $W_{(2)ij}$ are tensors arising from the interaction of the disturbance flow v_i and the bulk flow V_i. We seek solutions of (2.8) plus associated boundary conditions, subject to the asymptotic restriction, $\lambda << 1$. Thus, we assume

$$v_i = v_i^{(0)} + \lambda v_i^{(1)} + \ldots$$

$$q = q^{(0)} + \lambda q^{(1)} + \ldots \tag{2.9}$$

Substituting (2.9) into (2.8) and equating equal powers of λ, we obtain governing equations for $v_i^{(0)}$ and $v_i^{(1)}$. For $(v_i^{(0)}, q^{(0)})$, we obtain

$$\begin{aligned} &\pi_{ij,j}^{(0)} = 0, \quad v_{j,j}^{(0)} = 0, \\ &\pi_{ij}^{(0)} = -q^{(0)}\delta_{ij} + e_{(1)ij}^{(0)}, \end{aligned} \tag{2.10}$$

which is the equation of motion of a Newtonian fluid and can be written in the more familiar form:

$$-q_{,i}^{(0)} + v_{i,kk}^{(0)} = 0, \qquad v_{j,j}^{(0)} = 0 , \tag{2.11}$$

with the appropriate boundary conditions:

$$\begin{aligned} &v_i^{(0)} = \varepsilon_{ijk}(\Omega_s^{(0)})_j x_k - V_i \quad \text{on } r = 1, \\ &v_i^{(0)} = 0 \qquad\qquad\qquad \text{on the walls}, \\ &v_i^{(0)} \to 0 \qquad\qquad\qquad \text{as } \vec{r} \to \infty. \end{aligned} \tag{2.12}$$

Here $(\Omega_s^{(0)})_j$ is the angular velocity of the sphere to 0(1). For $(v_1^{(1)}, q^{(1)})$, we obtain

$$\begin{aligned} &\pi_{ij,j}^{(1)} = 0, \quad v_{j,j}^{(1)} = 0, \\ &\pi_{ij}^{(1)} = -q^{(1)}\delta_{ij} + e_{(1)ij}^{(1)} + \Sigma_{ij}^{(0)} \\ &\Sigma_{ij}^{(0)} = e_{(1)ik}^{(0)} e_{(1)kj}^{(0)} + W_{(1)ij}^{(0)} + \varepsilon_1 \left[e_{(2)ij}^{(0)} + W_{(2)ij}^{(0)} \right], \end{aligned} \tag{2.13}$$

where $\Sigma_{ij}^{(0)}$ contains only terms from V_i and $v_i^{(0)}$. We can also write (2.13) as

$$-q_{,i}^{(1)} + v_{i,kk}^{(1)} = -\Sigma_{ik,k}^{(0)} \ , \ v_{j,j}^{(1)} = 0 \ . \tag{2.14}$$

The appropriate boundary conditions are

$$\begin{aligned} v_i^{(1)} &= \varepsilon_{ijk}\left(\Omega_s^{(1)}\right)_j x_k + \left(U_s^{(1)}\right)_i && \text{on } r = 1 \ , \\ v_i^{(1)} &= 0 && \text{on the walls} \ , \\ v_i^{(1)} &\to 0 && \text{as } \vec{r} \to \infty \ . \end{aligned} \tag{2.15}$$

Here $\left(\Omega_s^{(1)}\right)_i$ and $\left(U_s^{(1)}\right)_i$ are the angular and translational velocities of the sphere at $O(\lambda)$. All of the variables $\left(\Omega_s^{(0)}\right)_i$, $\left(\Omega_s^{(1)}\right)_i$, $\left(U_s^{(0)}\right)_i$, and $\left(U_s^{(1)}\right)_i$ are unknown, in general, and must be obtained as part of the solution to the problem. Our present objective is to find the z component of $\left(U_s^{(1)}\right)_i$ which is the lateral velocity of the sphere induced by the non-Newtonian behavior of the suspending fluid.

The method employed is analogous to that developed in our earlier evaluation of the inertia-induced lateral velocity in a Newtonian fluid (Ho & Leal, 1974). That is, by using the reciprocal theorem, we show that the lateral velocity $\left(U_s^{(1)}\right)_z$ can be calculated without the explicit solution of $v_i^{(1)}$. A new velocity field (u_i, p) is defined by

$$\begin{aligned} t_{ij,j} &= 0, \qquad u_{j,j} = 0, \\ t_{ij} &= -p\delta_{ij} + a_{(1)ij}, \end{aligned} \tag{2.16}$$

$$a_{(1)ij} = u_{i,j} + u_{j,i},$$

or in its more familiar form

$$\begin{aligned} &-p_{,i} + u_{i,kk} = 0, \qquad u_{j,j} = 0, \\ &u_i = \delta_{zi} \qquad\qquad \text{on } r = 1, \\ &u_i = 0 \qquad\qquad \text{on the walls,} \\ &u_i \to 0 \qquad\qquad \text{as } \vec{r} \to \infty. \end{aligned} \tag{2.17}$$

Combining (2.13a) and (2.16a) and integrating over the entire fluid volume, we obtain

$$\int_{V_t} \left(\pi^{(1)}_{ij,j} u_i - t_{ij,j} v^{(1)}_i \right) dV = 0, \tag{2.18}$$

which can be rearranged to give

$$\int_{V_f} \frac{\partial}{\partial x_j}\left(\pi^{(1)}_{ij} u_i - t_{ij} v^{(1)}_i \right) dV - \int_{V_f} \left(\pi^{(1)}_{ij} u_{i,j} - t_{ij} v^{(1)}_{i,j} \right) dV = 0. \tag{2.19}$$

Upon applying the divergence theorem to the first integral, and using the definition of $\pi^{(1)}_{ij}$ and t_{ij} in the second integral, (2.19) becomes

$$\begin{aligned} -\int_A n_j \left(\pi^{(1)}_{ij} u_i - t_{ij} v^{(1)}_i \right) dA - \int_{V_f} \Big[\Big(-q^{(1)} \delta_{ij} + e^{(1)}_{(1)ij} \Big) u_{i,j} \\ - \left(-p\delta_{ij} + a_{(1)ij} \right) v^{(1)}_{i,j} \Big] dV = \int_{V_f} \Sigma^{(0)}_{ij} u_{i,j} dV, \end{aligned} \tag{2.20}$$

where n_j is the outer unit normal for the surfaces. It is easily shown that the integrand of the second integral is identically zero. Thus application of boundary conditions on the first integral gives the simplified form

$$-\int_A n_j \pi_{zj}^{(1)} dA + \left(U_s^{(1)}\right)_i \int_A n_j t_{ij}\, dA + \varepsilon_{imk}\left(\Omega_s^{(1)}\right)_m \int_A x_k n_j t_{ij} dA = \int_{V_f} \Sigma_{ij}^{(0)} u_{i,j} dV \quad . \tag{2.21}$$

The first integral is the force on the sphere in the z direction due to $v_i^{(1)}$ and is assumed to be zero for a neutrally buoyant sphere since the acceleration of the sphere yields a term of order $Re\kappa(U_s)_z^2$. The second integral is the force on the sphere due to u_i and is equal to $-6\pi[1 + O(\kappa) + O(\lambda^2)]\delta_{zi}$. The third integral is the torque on the sphere due to u_i and is identically zero due to the symmetry of the problem (2.17). Since $\Sigma_{ij}^{(0)}$ is symmetric, the integrand of the fourth integral can be written as $\Sigma_{ij}^{(0)} u_{i,j} = \frac{1}{2}\Sigma_{ij}^{(0)} a_{ij}$ where $a_{ij} = a_{(1)ij} = u_{i,j} + u_{j,i}$ is the rate of strain tensor for the velocity field u_i. Therefore (2.21) becomes

$$6\pi\left(U_s^{(1)}\right)_z = -\frac{1}{2}\int_{V_f} \Sigma_{ij}^{(0)} a_{ij} dV \quad . \tag{2.22}$$

We have shown, in the inertial migration case (Ho & Leal, 1974), that an equivalent result may also be obtained for the O(Re) contribution to the lateral migration velocity, if one first calculates the force which would be necessary to keep the sphere from migrating and then calculates the migration velocity by equating this force to the Stokes' drag for uniform translation with velocity $\left(U_s^{(1)}\right)_z$ through a quiescent fluid. Using identical arguments, the equivalence of these two approaches may also be proven in the present case. Thus the force on the sphere in the z direction which is equivalent to (2.22) is simply

$$F_L = -\frac{1}{2}\lambda\int_{V_f} \Sigma_{ij}^{(0)} a_{ij} dV \quad . \tag{2.23}$$

It may be noted that the integrand in (2.23) has a different form from its counterpart in the inertial migration problem:

$$F_L = - Re\int_{V_f} u_i f_i dV \tag{2.24}$$

where $$f_i = v_j^{(0)} v_{i,j} + v_j v_{i,j}^{(0)} + v_j^{(0)} v_{i,j}^{(0)}$$

and from the more cumbersome force expression which was used by Leal (1974) in a recent calculation of the motion of slender rod-like particles in a second order fluid (see equation 29, Leal, 1974). In particular, (2.24) has the nonhomogeneous term f_i of the O(Re) equations of motion dotted directly with u_i, whereas the present form (2.23) involves the double dot product of the nonhomogeneous part of the stress tensor at $O(\lambda)$ (see (2.13)) with the rate of strain tensor corresponding to u_i. Leal (1974) has shown that if a_{ij} were replaced in (2.23) by u_i and $\Sigma_{ij}^{(0)}$ with $\Sigma_{ij,j}^{(0)}$ in analogy with (2.24), an additional integral of $\left(e_{(1)}^{(0)}\right)^2 + \epsilon_1 e_{(2)}^{(0)}$ over the sphere surface would be required to obtain F_L. The difference between the forms (2.23) and (2.24) is thus introduced primarily as a matter of computational convenience. The forms (2.23) and (2.24) may also be seen to arise as equivalent natural choices if we consider the overall rate of work done on a fluid volume. In dimensional terms, this quantity can be expressed as the sum of two terms (see Batchelor, 1967, p. 152):

$$\int_{V_f} \left(\rho v_i g_i + \frac{1}{2}\pi_{ij} e_{(1)ij}\right) dV \tag{2.25}$$

where $g_i = \dfrac{\partial v_i}{\partial t} + v_j v_{i,j}$ and all other quantities have their usual meanings.

If the rate of work is nondimensionalized by $\mu V^2 L$ (V and L are the characteristic velocity and length respectively), the first integral of (2.25) becomes (in dimensionless form)

$$Re\int_{V_f} v_i g_i dV \tag{2.26}$$

which is similar to (2.24). For a second order fluid (in which the dimensionless stress is given by $\pi_{ij} = e_{(1)ij} + \lambda\sigma_{ij}$), the second integral of (2.25) has a non-Newtonian contribution given by (in dimensionless form)

$$\frac{1}{2}\lambda\int_{V_f} \sigma_{ij} e_{(1)ij} dV \tag{2.27}$$

which is similar to (2.23).

3. Evaluation of the Lateral Force

In order to evaluate the lateral force F_L using (2.23), the product $\Sigma^{(0)}_{ij} a_{ij}$ must be integrated over the complete volume of fluid which is outside the sphere and bounded between the two walls. Thus, in general, solutions of (2.11), (2.12) and (2.17) for $v_i^{(0)}$ and u_i are required throughout the complete fluid domain. Although the derivation of these solutions would be extremely difficult in the general case, approximate analytical results can be obtained for small particles, i.e. $\kappa \equiv \frac{a}{d} << 1$, via the well-known method of reflections. Thus, we shall limit our subsequent analysis to $\kappa << 1$, in addition to the condition (2.2a) which was adopted earlier. The solutions for $v_i^{(0)}$ and u_i were derived in our earlier analysis of the inertial migration problem, Ho & Leal (1974), and in view of their length, we shall not repeat them here, but rather

concentrate our attention on the evaluation of the volume integral in (2.23).

It is convenient, as in the case of inertial migration, to divide the volume of integration, V_f, into two parts, V_1 and V_2, where

$$V_1 = \{\vec{r} | 1 \leqslant r < \lambda\kappa^{\chi-1}\},$$
$$V_2 = \{\vec{r} | \lambda\kappa^{\chi-1} \leqslant r < \infty, -s\kappa^{-1} \leqslant z \leqslant (1-s)\kappa^{-1}\}. \tag{3.1}$$

Here λ is a constant of order κ^0 and $0<\chi<1$. Hence

$$\begin{aligned} F_L &= -\frac{1}{2}\lambda\left\{\int\int_{V_1} \Sigma_{ij}^{(0)} a_{ij} dV + \int_{V_2} \Sigma_{ij}^{(0)} a_{ij} dV\right\} \\ &= -\frac{1}{2}\lambda\ (F_{L1} + F_{L2}). \end{aligned} \tag{3.2}$$

In contrast to the previous case, Ho & Leal (1974), the dominant contribution to (3.2) will be shown to arise from the integration over V_1, i.e. from the region near the sphere. In order to demonstrate this fact we consider the order of magnitude of each of the two integrals in (3.2).

Let us first examine the integral over V_1, i.e. F_{L1}. In this region, it can be shown by using the solutions for $v_i^{(0)}$ and u_i from Ho & Leal (1974) that the integrand behaves like

$$\begin{aligned} \Sigma_{ij}^{(0)} a_{ij} = \beta^2 &\left[X_1\left(\frac{x}{r^6}, \ldots\right) + \varepsilon_1 X_2\left(\frac{x}{r^6}, \ldots\right)\right] \\ &+ \beta\gamma\left[Y_1\left(\frac{1}{r^4}, \frac{1}{r^6}, \frac{1}{r^8}, \ldots\right) + \varepsilon_1 Y_2\left(\frac{1}{r^4}, \frac{1}{r^6}, \frac{1}{r^8}, \ldots\right)\right] + O(\kappa^4). \end{aligned} \tag{3.3}$$

The functions Y_1 and Y_2 depend on the undisturbed flow V and on $v_i^{(0)}$ and u_i for the motion of a sphere in an unbounded fluid domain. That is, the reflection of this solution off the walls, and the subsequent higher order corrections at the walls and at the sphere surface contribute to X_1 and X_2 and the $O(\kappa^4)$ terms. Since $\beta^2 \sim \kappa^2$ and $\beta\gamma \sim \kappa^3$, the $O(\kappa^4)$ terms may be neglected for $\kappa << 1$. Furthermore, the integral of X_1 and X_2 over the spherical shell $1 \leq r < \lambda\kappa^{\chi-1}$ is identically zero. Thus,

$$F_{L1} = \int_{r=1}^{r\leq\lambda\kappa^{\chi-1}} \Sigma_{ij}^{(0)} a_{ij} dV$$

$$= \int_{r=1}^{r<\lambda\kappa^{\chi-1}} \beta\gamma \left[Y_1\left(\frac{1}{r^4}, \frac{1}{r^6}, \frac{1}{r^8} \ldots\right) + \varepsilon_1 Y_2\left(\frac{1}{r^4}, \frac{1}{r^6}, \frac{1}{r^8} \ldots\right) \right] dV + O(\kappa^4). \quad (3.4)$$

Finally, denoting the indefinite integral of $Y_1 + \varepsilon_1 Y_2$ as $\Psi\left(\frac{1}{r}, \frac{1}{r^3}, \frac{1}{r^5}, \ldots; \varepsilon_1\right)$ and noting that the upper limit of (3.4) can be replaced by ∞ with an error of $o(\kappa^3)$, we obtain

$$F_{L1} = \beta\gamma \Psi\left(\frac{1}{r}, \frac{1}{r^3}, \frac{1}{r^5}, \ldots; \varepsilon_1\right)\Bigg|_{r=1}^{r=\infty} + o(\kappa^3) \quad (3.5)$$

$$= \beta\gamma\left(\Psi_1 + \varepsilon_1 \Psi_2\right) + o(\kappa^3).$$

Let us now turn to F_{L2}. In the region V_2, it is appropriate to use the "outer" variable r' defined by $r' = \kappa r$. Thus, transforming the integral expression for F_{L2} into this outer coordinate system, we obtain

$$F_{L2} = \kappa^{-3} \int_{r'=\lambda\kappa^{\chi}}^{r'=O(1)} \Sigma_{ij}^{(0)'} a'_{ij} dV', \quad (3.6)$$

where the superscript ' signifies the use of outer variables. Again using the solutions of Ho & Leal (1974) it may be shown that $\Sigma_{ij}^{(0)'} a_{ij}' = O(\kappa^7)$. It thus follows from (3.6) that $F_{L2} = o(\kappa^3)$.

We thus see that the dominant $O(\kappa^3)$ contribution to the lateral force is due entirely to F_{L1} which is itself dominated, for small κ, by the disturbance velocity fields for the sphere in an infinite fluid domain, i.e.

$$F_L \sim -\frac{1}{2}\lambda\beta\gamma\left(\Psi_1 + \epsilon_1\Psi_2\right) + o(\kappa^3). \tag{3.7}$$

Unlike the inertial case, the reflection of the infinite domain solution off the walls yields only higher order corrections to F_L. Thus in calculating the lateral force to $O(\kappa^3)$ for a sphere not too close to a wall, the only role played by the walls is in the establishment of the undisturbed profile, V. In addition, it should be noted from (3.7) that the lateral force F_L is proportional to $\beta\gamma$. Hence in the case of simple shear ($\gamma = 0$) no lateral migration should occur to $O(\kappa^3)$.

In order to obtain more quantitative results, the coefficients Ψ_1 and Ψ_2 must be evaluated. From the definition of $\Sigma_{ij}^{(0)}$, these are simply

$$\Psi_1 = \int_{r=1}^{\infty}\left[W_{(1)ij}^{(0)} + e_{(1)ik}^{(0)} e_{(1)kj}^{(0)}\right] a_{ij}\,dV,$$

$$\Psi_2 = \int_{r=1}^{\infty}\left[W_{(2)ij}^{(0)} + e_{(2)ij}^{(0)}\right] a_{ij}\,dV.$$

Straightforward, though tedious, evaluation of these terms gives

$$\Psi_1 = \left(\frac{118}{25} - \frac{1}{6}\right)\pi, \tag{3.8a}$$

$$\Psi_2 = -\left(\frac{612}{35} + \frac{9}{56}\right)\pi, \tag{3.8b}$$

and the lateral force is

$$F_L = -\pi\beta\gamma\lambda\left\{\frac{683}{300} - \varepsilon_1 \frac{4941}{560}\right\} + o(\kappa^3) \tag{3.9}$$

$$= -\pi\beta\gamma\lambda N(\varepsilon_1) + o(\kappa^3).$$

In (3.8a), the first term is the contribution from $W^{(0)}_{(1)ij}$ and the second term is from $e^{(0)}_{(1)ik}e^{(0)}_{(1)kj}$; while in (3.8b), the first term is the contribution from $W^{(0)}_{(2)ij}$ and the second term is from $e^{(0)}_{(2)ij}$. It is of interest to note that the contributions to F_L of the extra non-Newtonian stress $\Sigma^{(0)}_{ij}$ associated with the interaction of the bulk flow and the disturbance flow (i.e. $W^{(0)}_{(1)ij}$ and $W^{(0)}_{(2)ij}$) are numerically dominant over the contributions associated with the disturbance velocity alone (i.e. $e^{(0)}_{(1)ik}e^{(0)}_{(1)kj}$ and $e^{(0)}_{(2)ij}$). Also, we may recall that the lateral force for a neutrally buoyant sphere with no external torque in the inertial case stems from the stresslet contribution to the far-field behavior of the disturbance flow. Here in the non-Newtonian case, the lateral force depends on the disturbance velocity field close to the sphere, and all of the velocity terms coming from D_1, E_1, F_1, G_1, H_1 and B_1 in the disturbance velocity $v^{(0)}_i$ (see Section 3 of Ho & Leal, 1974) contribute to the same order of magnitude. The contributions from the Stokeslet term A_1 and the couplet term C_1 are asymptotically small and thus neglected for a neutrally buoyant freely rotating particle. However, closer examination of these terms is useful since it leads to criteria for neglect of external body forces and couples. In order to neglect the contribution from A_1, it can be shown from $v^{(0)}_i$ that we require

$$\gamma >> A_1 \,. \tag{3.10a}$$

For a neutrally buoyant sphere $A_1 \sim \kappa^3$ while $\gamma \sim \kappa^2$. However, with an external body force F_x acting on the sphere in the x direction, $A_1 \sim |F_x|$, and thus the contribution from A_1, can only be neglected if

$$\gamma >> |F_x| \,. \tag{3.10b}$$

If the body force is gravitational, then in dimensional quantities, (3.10b) becomes

$$\gamma^* >> |\rho_s - \rho_o| g/\mu_o, \tag{3.11a}$$

which for the case of Poiseuille flow is

$$V^*_{max} >> d^2 |\rho_s - \rho_o| g/\mu_o. \tag{3.11b}$$

It is coincidental that the same criteria for neglect of body force contributions was also obtained for the inertial migration case (see (5.23) of Ho & Leal, 1974). It can also be shown that in order to neglect the couplet term C_1, we require

$$\beta >> C_1. \tag{3.12}$$

For a freely rotating sphere, $C_1 \sim \kappa^4$, and the condition is satisfied. On the other hand, for a non-rotating sphere with $\Omega_{sy} = 0$, C_1 is $\beta/2$ and hence contributes to F_L at the same order of magnitude as the rest of the terms D_1, E_1, F_1,.... Again, this is true in the inertial migration case. It thus also follows that the present single particle migration result is applicable for a suspension of spheres provided conditions (7.2) and (7.3) of Ho & Leal (1974) are satisfied.

Finally, it may be noted that the approximate condition (2.2a) for neglect of the inertial contribution to the lateral force compared to the non-Newtonian contribution may now be improved by direct comparison of the magnitudes of the predicted lateral force in each case. In the present theory, we have shown that the lateral force due to the non-Newtonian effect is of order $\lambda\kappa^3$, while the analysis of Ho & Leal (1974) produced an inertial contribution of order $\bar{R}e\kappa^2$. Thus, a more accurate form of the condition (2.2a) is

$$\lambda\kappa >> Re \ , \tag{3.13a}$$

or, in dimensional terms

$$\phi_3 >> \rho_o a d. \tag{3.13b}$$

The expression (3.9) for F_L is the main result of the present analysis, and is valid whenever the conditions (3.11), (3.12) and (3.13) are satisfied. It shows that the direction and magnitude of the lateral migration depend on the magnitude and sign of the normal stress parameters λ and ε_1. The majority of available viscometric and theoretical studies (summarized in Leal, 1974) support the conclusion that the first normal stress difference in simple shear flow is positive, while the second normal stress difference is negative and approximately 10 - 20% of the first normal stress difference in magnitude. Thus, referring to Eqs. (2.7), it may be seen that

$$\lambda > 0 \quad \text{and} \quad -0.6 \leq \varepsilon_1 \leq -0.5.$$

Expressing the lateral force as

$$F_L = -\beta\gamma G(\lambda, \varepsilon_1)$$

it follows that $G(\lambda,\varepsilon_1)$ is strictly positive, so that particle migration is always in the direction of least (absolute) shear rate. Thus the equilibrium position of particles in Poiseuille flow is midway between the walls, and in Couette flow is the outer cylinder (irrespective of which cylinders are rotating or the direction of rotation). Although none of the available experimental studies were carried out in a regime for which the second-order fluid model is strictly applicable, these theoretical results are at least in qualitative agreement with the observations of Karnis & Mason (1966) which were made in strongly viscoelastic solutions. Since the only relevant non-Newtonian characteristic of the second-order fluid is the existance of nonzero normal-stress components, it may perhaps be inferred that the migration phenomenon in a fully viscoelastic fluid which exhibits both a shear-thinning viscosity and nonzero normal stresses is dominated by the normal stress contributions. A stronger statement could only be made after a more quantitative comparison of particle trajectories with measurements in a fully characterized fluid. In the following section, we provide the necessary theoretical results for the trajectories, and show that they agree qualitatively with the available trajectory measurements of Karnis & Mason (1966). Unfortunately, however, the desired quantitative comparison could not be made with any certainty because of a lack of quantitative rheological data for the test fluid.

Finally, an alternative, but completely equivalent expression, for F_L may be obtained which separates the contributions of the first and second normal stress differences, $-2\varepsilon_1\lambda$ and $(1+2\varepsilon_1)\lambda$ (cf. (2.7)),

$$F_L = -\pi\beta\gamma\left[\frac{683}{300}(1+2\varepsilon_1)\lambda + \left(\frac{4941}{1120}+\frac{683}{300}\right)(-2\varepsilon_1\lambda)\right] + o(\kappa^3). \qquad (3.14)$$

The two terms are of opposite sign since $(1+2\varepsilon_1)\lambda \leq 0$ and $-2\varepsilon_1\lambda > 0$, meaning that

the two normal stress contributions are in opposite directions. However, the term in square brackets is dominated by the first normal stress difference provided only $\varepsilon_1 < 0$.

4. Particle Trajectories

In order to facilitate a more quantitative comparison between the present theory and experiments, it is necessary to calculate the particle trajectories. To achieve this, we use the (dimensional) equations for the lateral velocity

$$(U_s)_z^* = d\frac{ds}{dt^*} = -\phi_3 \beta^* \gamma^* a^2 N(\varepsilon_1)/6\mu_o, \tag{4.1}$$

and for the axial velocity

$$(U_s)_x^* = d\frac{dx'}{dt^*} = \alpha^*, \tag{4.2}$$

to obtain the differential trajectory equations

$$dt^* = -\frac{6d\mu_o ds}{\phi_3 \beta^* \gamma^* a^2 N(\varepsilon_1)}, \tag{4.3a}$$

$$dx' = -\frac{6\alpha^* \mu_o ds}{\phi_3 \beta^* \gamma^* a^2 N(\varepsilon_1)}. \tag{4.3b}$$

Here $x' = \kappa x$, t^* is the dimensional time, and α^*, β^*, γ^* are the dimensional forms of α, β and γ, respectively. Upon integration, (4.3a) and (4.3b) become

$$t^* - t_o^* = -\frac{6\mu_o d}{\phi_3 a^2 N(\varepsilon_1)} \int_{s'=s_o}^{s} \frac{ds'}{\beta^*(s')\gamma^*(s')}, \tag{4.4a}$$

and

$$x'-x'_o = -\frac{6\mu_o}{\phi_3 a^2 N(\varepsilon_1)} \int_{s=s_o}^{s} \frac{\alpha^*(s')ds'}{\beta^*(s')\gamma^*(s')} \quad . \tag{4.4b}$$

Equation (4.4a) gives the lateral position s as a function of time, while (4.4b) gives lateral position as a function of axial position in the flow domain. Let us first consider the case of plane Poiseuille flow for which

$$\begin{aligned} \alpha^* &= 4V^*_{max} s(1-s), \\ \beta^* &= 4V^*_{max}(1-2s)/d, \\ \gamma^* &= -4V^*_{max}/d^2. \end{aligned} \tag{4.5}$$

In this case, (4.4a) and (4.4b) give

$$-\ell n\left(\frac{1-2s}{1-2s_o}\right) = \frac{16\ V^{*2}_{max} K^3 \phi_3 N(\varepsilon_1)}{3\mu_o a d}\ (t^*-t^*_o) \tag{4.6a}$$

$$(s^2-s_o^2) - (s-s_o) - \frac{1}{2}\ell n\left(\frac{1-2s}{1-2s_o}\right) = \frac{8\ V^*_{max} K^3 \phi_3 N(\varepsilon_1)}{3\mu_o a}\ (x'-x'_o). \tag{4.6b}$$

These trajectory equations are plotted in Figures (2a) and (2b). So far as we are aware, no experiments have been reported on migration in two-dimensional Poiseuille flow of a non-Newtonian fluid. However, the predicted results do agree qualitatively with the trajectories measured in three-dimensional Poiseuille flow by Karnis & Mason (1966) as may be seen by comparing their Figure (4a) with our Figure (2b). Although quantitative agreement would not be expected, it is encouraging that substitution of the experimental parameters into

Equation (4.6b) with the assumption $\varepsilon_1 = -0.55$, does yield reasonable agreement with the experiments for the order of magnitude of the axial distance traveled between an initial lateral position, $s_o = 0.24$, and a final position $s_f = 0.43$. It should, however, be emphasized that no measurements were made of the second normal stress coefficient (requiring us to assume $\varepsilon_1 = -0.55$; see the estimate of ε_1 in Section 3), that the other rheological data was not measured by Karnis & Mason (1966), but rather adapted from Brodnyan, Gaskins & Philippoff (1957), and that the fluid used in the experiments was sufficiently non-Newtonian that the bulk velocity profile differed substantially from the assumed parabolic shape. For these reasons, we have not attempted any more detailed comparison, nor have we carried out the theory for the three-dimensional case in spite of the fact that the analysis is an obvious and straightforward extension of the present work.

The only other experimental observations which are relevant to the present theory are for Couette flow, also reported by Karnis & Mason (1966). The present theory shows that in simple shear flow, where $\gamma = 0$, there is no lateral migration to $O(\kappa^3)$. However, in Couette flow, the small curvature of the velocity profile causes γ to be nonzero and thus yields lateral migration. It can be shown that in all cases, where one or both cylinders are rotating either in the same or opposite sense, the shear rate always has a minimum absolute value at the outer cylinder wall, which is thus the expected direction of migration according to the present theory. However, due to detailed differences in the bulk velocity profiles for different combinations of cylinder rotation, the magnitude of the migration velocity will differ from case to case. Both of these features (i.e. outward migration and a dependence of the magnitude on the sense and magnitude of rotation of the individual cylinders) were observed by Karnis & Mason (1966) who studied the two simplest cases in

which (1) the inner cylinder was rotated holding the outer stationary, and (2) the outer cylinder was rotated holding the inner stationary. For simplicity, we shall confine our present discussion to these two limiting cases, which we shall refer to as case I and case 2, respectively. We denote the radii of the inner and outer cylinders as r_1 and r_2, and the gap width as $d = (r_2 - r_1)$. A dimensionless measure of the degree of profile curvature is (case 1)

$$R_1 = \frac{r_2(r_2-r_1)}{r_1(r_1+r_2)} \quad ,$$

and (case 2)

$$R_2 = \frac{r_1(r_2-r_1)}{r_2(r_1+r_2)} \quad .$$

Provided $R_1 << 1$ and $R_2 << 1$, we can approximate the (dimensional) undisturbed velocity profile in the general form (2.4)

$$V^*(z^*) = \alpha^* + \beta^* z^* + \gamma^* z^{*2} \tag{4.7}$$

in which z^* is the axis perpendicular to the walls and directed towards the rotating cylinder. For case 1, the outer stationary cylinder is thus represented by $s = 0$ and the inner rotating cylinder by $s = 1$. For case 2, the outer cylinder is $s = 1$ and the inner cylinder, $s = 0$. The coefficients α^*, β^*, and γ^* in each case are given in Table (1). The approximation inherent in (4.7) takes into account the changing shear rate across the gap but neglects the curvature of walls. Given (4.7), the migration velocities and time trajectories are easily obtained by substituting β^* and γ^* into the general expressions (4.1) and (4.4a). The results are (case 1)

$$(U_s)_z^* = -\frac{\kappa^3 V_w^{*2} \phi_3 N(\varepsilon_1)}{6\mu_o a} R_1 \, [1-R_1(1-2s)], \tag{4.8a}$$

$$\frac{1}{3}\left(\frac{V_w^*}{d}\right)^2 \frac{\kappa^2 \phi_3 N(\varepsilon_1)}{\mu_o} (t^*-t_o^*) = -\frac{1}{R_1^2} \ln\left[\frac{1-R_1(1-2s)}{1-R_1(1-2s_o)}\right] ; \tag{4.8b}$$

and (case 2)

$$(U_s)_z^* = -\frac{\kappa^3 V_w^{*2} \phi_3 N(\varepsilon_1)}{6\mu_o a} R_2 \, [1 + R_2(1-2s)], \tag{4.9a}$$

$$\frac{1}{3}\left(\frac{V_w^*}{d}\right)^2 \frac{\kappa^2 \phi_3 N(\varepsilon_1)}{\mu_o} (t^*-t_o^*) = -\frac{1}{R_2^2} \ln\left[\frac{1+ R_2(1-2s)}{1+R_2(1-2s_o)}\right] . \tag{4.9b}$$

The trajectories, (4.8b) and (4.9b) are plotted in Figure (3) for $R_1 = 0.138$ and $R_2 = 0.0884$, the values used in Karnis & Mason's experiments. Again, qualitative agreement is found between the theory and experiment for $\kappa = 0.012$, the smallest value used by Karnis and Mason. However, the rate of migration which was measured seems to increase too slowly with κ when compared to the present theoretical result. One possible explanation for this is that the larger value used, $\kappa = 0.056$, is simply too large for the present theory to be applicable. This speculation is, in fact, supported by the trajectory data (Figure(8)of Karnis & Mason, 1966) which shows a definite wall effect over almost the whole span in the latter case. It may also be noted that the experimental values of R_1 and R_2 are fairly large for the approximate linearization of the flow geometry to be accurate. Finally, all of the same difficulties with regard to the existence of reliable rheological data are present here that were previously noted in the Poiseuille flow case.

References:

Bartram, E., 1973, M.Sc. Thesis, McGill University.

Batchelor, G. K., 1967, An Introduction to Fluid Mechanics, Cambridge University Press.

Brodnyan, J. G., F. H. Gaskins and W. Philippoff, 1957, Trans. Soc. Rheol., 1, 109.

Gauthier, F., H. L. Goldsmith and S. G. Mason, 1971a, Rheol. Acta, 10, 344.

Gauthier, F., H. L. Goldsmith and S. G. Mason, 1971b, Trans. Soc. Rheol., 15, 297.

Highgate, D. J. and R. W. Whorlow, 1968, in Polymer Systems: Deformation and Flow, R. E. Wetton and R. W. Whorlow, Ed., MacMillan, London, 251-261.

Highgate, D. J. and R. W. Whorlow, 1969, Rheol. Acta, 8, 142.

Ho, B. P. and L. G. Leal, 1974, J. Fluid Mech., 65, 365.

Karnis, A. and S. G. Mason, 1966, Trans. Soc. Rheol., 10, 571.

Leal, L. G., 1974, "The Slow Motion of Slender Rod-Like Particles in a Second-Order Fluid", submitted to J. Fluid Mech.

Segré, G. and A. Silberberg, 1963, J. Colloid Sci., 18, 312.

Table Captions:

Table 1. The coefficients α^*, β^* and γ^* for Couette flow. Case 1: Outer cylinder stationary and inner cylinder rotating; Case 2: Outer cylinder rotating and inner cylinder stationary.

Figure Captions:

Figure 1: The physical system for (a) simple shear flow and (b) two-dimensional Poiseuille flow.

Figure 2: Particle trajectory for two-dimensional Poiseuille flow: lateral position vs. (a) time and (b) axial position.

Figure 3: Particle trajectory for Couette flow with $R_1 = 0.138$ and $R_2 = 0.0884$. Case 1: Outer cylinder stationary and inner cylinder rotating; Case 2: Outer cylinder rotating and inner cylinder stationary.

	Case 1	Case 2
α^*	$V_w^* s\ [\ 1-R_1\ (1-s)\ ]$	$V_w^* s\ [\ 1+R_2\ (1-s)\ ]$
β^*	$V_w^*\ [\ 1-R_1\ (1-2s)\ ]/d$	$V_w^*\ [\ 1+R_2\ (1-2s)\ ]/d$
γ^*	$V_w^*\ \kappa_1/d^2$	$-V_w^*\ R_2/d^2$

Table 1

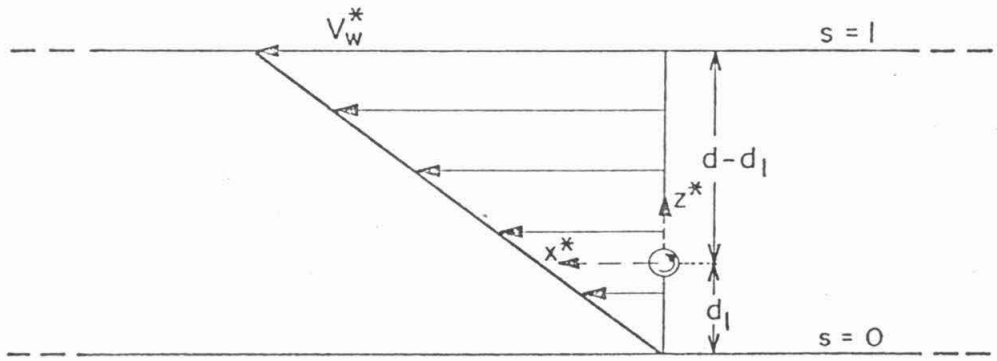

FIGURE 1(a)

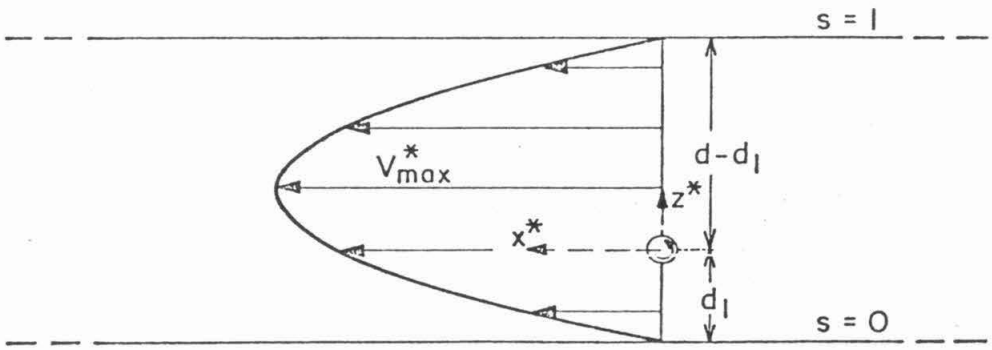

FIGURE 1(b)

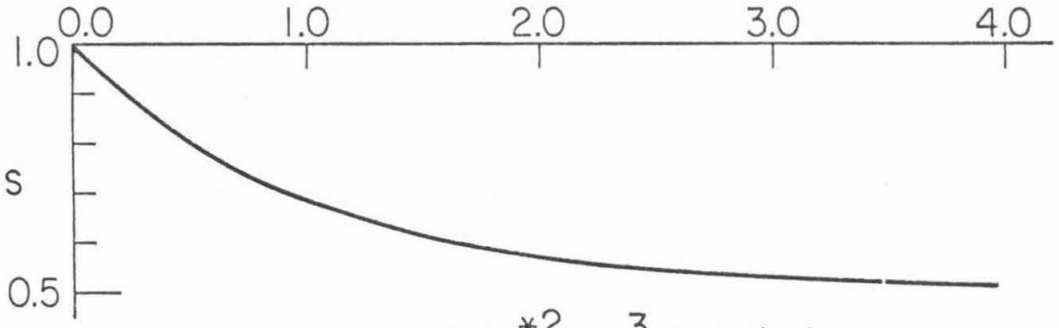

FIGURE 2(a) $t^* \left[\frac{16\, V_{max}^{*2}\, \kappa^3 \phi_3 N(\epsilon_1)}{3\mu_0\, a\, d} \right]$

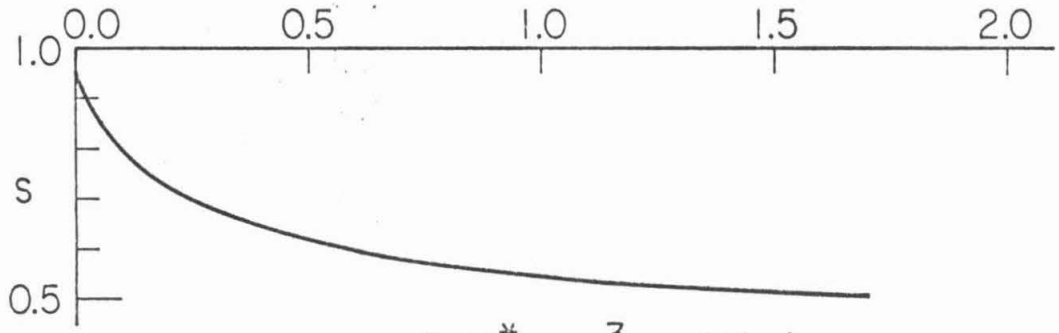

FIGURE 2(b) $x' \left[\frac{8\, V_{max}^{*}\, \kappa^3 \phi_3 N(\epsilon_1)}{3\mu_0\, a} \right]$

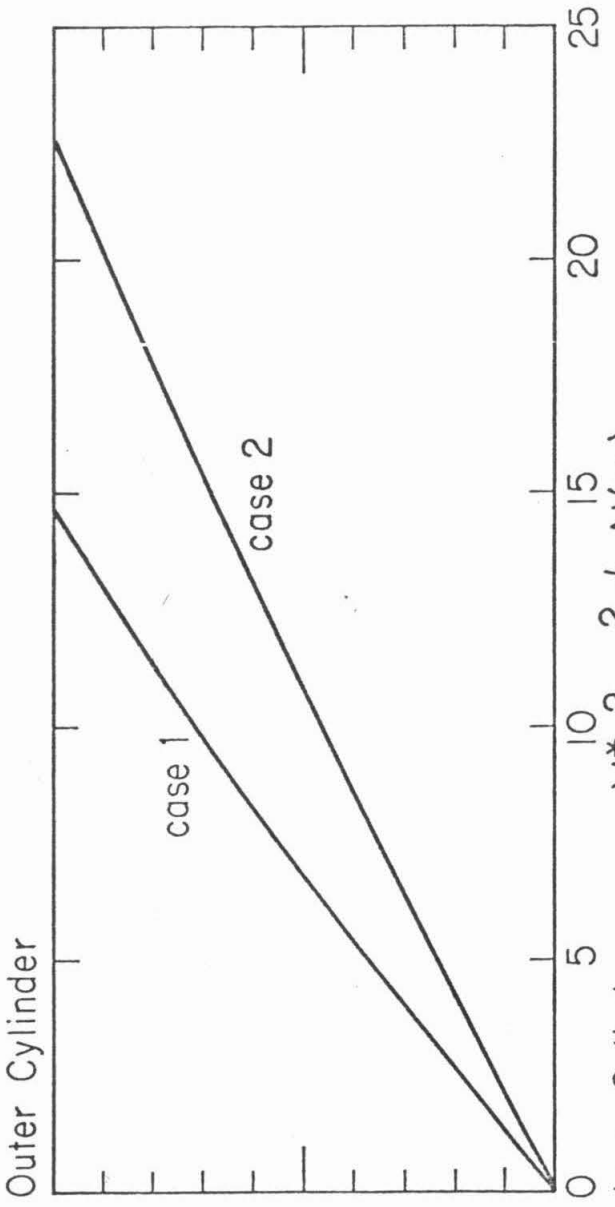
Outer Cylinder
case 1
case 2
0
5
10
15
20
25
Inner Cylinder
$t^*\left(\frac{V_w^*}{d}\right)^2\left[\frac{\kappa^2\,\phi_3 N(\epsilon_1)}{3\mu_0}\right]$

FIGURE 3

APPENDIX B

1. Introduction

In a recent study (Ho & Leal, 1974), hereafter denoted as I, we have theoretically calculated trajectories and final equilibrium positions for neutrally buoyant rigid spheres which migrate laterally across a unidirectional flow of a second-order fluid. The result of lateral migration in a suspension of such particles is a spatially non-uniform concentration distribution. For most technological applications involving composite materials made up of particles (e.g. filler) suspended in polymeric solutions or melts, such concentration anomalies will have an adverse effect on the bulk properties of the finished product. In the present note, we adapt the analysis of I to consider migration of neutrally buoyant rigid, spherical particles in a second-order fluid which is flowing through a screw extruder.

We recognize, of course, that the second-order fluid limit of the general simple-fluid constitutive model does not provide a full description of the rheological properties of polymeric solutions or melts. Indeed, for a simple steady shear flow the only viscoelastic characteristics exhibited by the second-order fluid are nonzero normal stress differences whose magnitude varies quadrati-

cally with shear rate. The shear-thinning of viscosity is only partially included at the third-order fluid level. Nevertheless, we are hopeful that the analysis presented here will produce at least qualitative insight into the behavior to be expected in a real extrusion process involving particles in a polymer melt. Support for this optimism is based, in part, on the fact that our theoretical results in I were shown to agree qualitatively, and even semi-quantitatively with available experimental results for polymer solutions up to 4% by weight which exhibit both large normal stresses and strong shear-thinning phenomena.

The analysis is similar in many respects to that in I, and we shall use much of the same nomenclature as well as the main results for the lateral migration velocity in our present work.

2. The basic undisturbed flow in the extruder

A longitudinal cross-section of a typical screw extruder is shown in figure 1. As indicated, the barrel of the extruder is a stationary cylindrical tube, inside which the screw rotates at a rate which we shall characterize by U_c, the tangential velocity at the screw base in the azimuthal direction. Thus, choosing the x and y axes (rectangular coordinates) to be parallel and perpendicular, respectively, to the screw flight, the velocity of the screw base in the x direction (down-channel) is $U_c\cos\phi$, while that in

the y direction (cross-channel) is simply $U_c \sin\phi$. Here, ϕ is the flight angle, as defined in figure 1. In the following analysis, which is relevant for a single suspended particle whose radius a is much less than the channel depth d, the origin for the z coordinate direction is taken coincident with the center of the particle (i.e. z=0 is the normal center-plane for the particle) and z is positive in the direction of the screw base. The distance across the gap measured from the barrel and nondimensionalized with respect to d will be denoted by s; s=0 at the barrel and s=1 at the screw base. All other distances are nondimensionalized with respect to the particle radius a, while velocities are nondimensionalized with respect to the characteristic velocity βa, where β is some average shear rate.

In order to analyze the basic, undisturbed flow in the extruder, we use the usual simplifying assumptions as outlined, for example, by Bernhardt (1959, Chapter 4). These are: (i) a small depth-to-width ratio (d/w) in the flow channel, (ii) negligible channel edge effects, i.e. neglecting the presence of the screw flights, (iii) no leakage flow through the clearance between the barrel surface and the screw flights, and finally (iv) isothermal conditions. Among these assumptions, the last is the most restrictive in practice. If (i) is satisfied, the curvature of the channel around the screw axis can be ignored and the screw channel can figuratively be unrolled and laid out flat for

purposes of the present discussion. The bulk undisturbed velocity profile (relative to a coordinate system fixed with respect to the screw barrel) inside the channel and away from the flight surfaces can be written approximately as the sum of down-channel and cross-channel components,

$$V_i = \overline{V}(z)\delta_{xi} + \overline{\overline{V}}(z)\delta_{yi} . \qquad \text{(B-1)}$$

We will identify quantities related to the down-channel flow with a single overbar, and those related to the cross-channel flow by double overbars.

The down-channel component $\overline{V}(z)$ is composed of two distinct parts: first, the motion induced by the x component of the velocity of the screw base, $U_c\cos\phi$, and second, that induced by the imposed pressure gradient in the x direction. If the pressure is denoted by Q, the pressure gradient is given by $\partial Q/\partial x$ $(=2\gamma)$, which is a positive quantity for a reverse pressure drop as is usually observed in screw extruders, and

$$\overline{V}(z) = U_c(\cos\phi)s + U_c(\cos\phi)\kappa z - \gamma\kappa^{-2}s(1-s) - \gamma\kappa^{-1}(1-2s)z + \gamma z^2 . \qquad \text{(B-2)}$$

Here κ denotes that ratio a/d of particle radius to channel depth d, and is assumed to be small. The volume flow rate in the x direction due to the flow induced by the motion

of the screw is $1/2U_c\cos\phi$, while that due to the reverse pressure gradient is $-1/6\kappa^{-2}\gamma$. The minus sign in the last term indicates backflow for $\gamma>0$. It is usual practice to define a quantity A as the absolute value of the ratio of volume flow rates,

$$A \equiv \kappa^{-2}\gamma/3U_c\cos\phi. \qquad \text{(B-3)}$$

The form of the velocity profile in the x direction depends upon A. When A=0 there is no pressure gradient and the flow reduces to a simple shear flow as shown in figure 2a. For $0<A\leq 1/3$, there is a reverse pressure gradient, but it is not sufficiently strong to produce any backflow. A typical velocity profile in this case is shown in figure 2b. Finally, for $1/3<A\leq 1$, backflow occurs between s=0 and s=(3A-1)/3A (see figure 2c), with the limit A=1 corresponding to the case of zero net flow in the x direction. An alternative form for $\bar{V}(z)$, which incorporates A is

$$\bar{V}(z) = U_c\cos\phi[s+\kappa z-3As(1-s)-3A(1-2s)\kappa z + 3A\kappa^2 z^2] . \qquad \text{(B-4)}$$

The undisturbed down-channel flow is of the general type analyzed by us in I, namely

$$\bar{V}(z) = \bar{\alpha}+\bar{\beta}z+\bar{\gamma}z^2 \tag{B-5}$$

with
$$\begin{aligned} \bar{\alpha} &= U_c\cos\phi[s-3As(1-s)] \\ \bar{\beta} &= \kappa U_c\cos\phi[1-3A(1-2s)] \\ \bar{\gamma} &= \kappa^2 U_c\cos\phi[3A] = \gamma. \end{aligned} \tag{B-6}$$

For the cross-channel flow, the undisturbed velocity profile depends only on the velocity of the screw (independent of A), and is given by the general form

$$\begin{aligned} \bar{\bar{V}}(z) = U_c\sin\phi[&s+\kappa z-3s(1-s)-3(1-2s)\kappa z \\ &+3\kappa^2 z^2] \end{aligned} \tag{B-7}$$

A typical profile is plotted in figure 3. Again, the undisturbed bulk flow is of the general quadratic type analyzed in I,

$$\bar{\bar{V}}(z) = \bar{\bar{\alpha}}+\bar{\bar{\beta}}z+\bar{\bar{\gamma}}z^2 \ , \tag{B-8}$$

where
$$\begin{aligned} \bar{\bar{\alpha}} &= U_c\sin\phi[s-3s(1-s)] \\ \bar{\bar{\beta}} &= \kappa U_c\sin\phi[1-3(1-2s)] \\ \bar{\bar{\gamma}} &= 3\kappa^2 U_c\sin\phi \ . \end{aligned} \tag{B-9}$$

3. The lateral force on the sphere

We have shown in I that the lateral force on the sphere can be calculated for a quadratic unidirectional flow knowing only the disturbance creeping motion induced by the sphere in a Newtonian suspending fluid, plus a second, 'complementary' Stokes solution. We consider a neutrally buoyant rigid sphere of radius a freely suspended between the screw barrel and the screw base at a distance s from the barrel. We denote the disturbance flow to zeroth order in $\lambda(=\phi_3\beta/\mu_o$, see I for the definition of these quantities) as $v_i^{(0)}$, which is the Newtonian solution. In view of the linearity of the governing Stoke's problem, it is permissable and convenient to denote the individual disturbance motions induced by a sphere in $\bar{V}(z)\delta_{xi}$ alone as $\bar{v}_i^{(0)}$, while that corresponding to $\bar{\bar{V}}(z)\delta_{yi}$ is denoted as $\bar{\bar{v}}_i^{(0)}$. The overall solution is simply the sum of the two parts,

$$v_i^{(0)} = \bar{v}_i^{(0)} + \bar{\bar{v}}_i^{(0)}. \qquad \text{(B-10)}$$

Let us now recall, from equation (2.13) of I, the expression for the 'extra stress' to order λ due to the viscoelastic property of the suspending second-order fluid, i.e.

$$\Sigma_{ij}^{(0)} = e_{(1)ik}^{(0)} e_{(1)kj}^{(0)} + W_{(1)ij}^{(0)} + \varepsilon_1[e_{(2)ij}^{(0)} + W_{(2)ij}^{(0)}]. \qquad \text{(B-11)}$$

Since the expression for $\Sigma_{ij}^{(0)}$ is not linear in $v_i^{(0)}$, we obviously cannot write $\Sigma_{ij}^{(0)}$ as the sum of the 'extra stresses' generated by the down channel and cross channel flows separately. Indeed, substitution of (B-10) and the definitions of $e_{(1)}^{(0)}$, $W_{(1)}^{(0)}$, $e_{(2)}^{(0)}$ and $W_{(2)}^{(0)}$ (see equation (2.8c) of I) into equation (B-11) yields

$$\Sigma_{ij}^{(0)} = \bar{\Sigma}_{ij}^{(0)} + \bar{\bar{\Sigma}}_{ij}^{(0)} + \hat{\Sigma}_{ij}^{(0)}, \qquad \text{(B-12)}$$

where the first two terms on the right hand side are simply the 'extra stresses' associated with the sphere suspended in $\bar{V}\delta_{xi}$ and $\bar{\bar{V}}\delta_{yi}$ separately (see I). The last term in (B-12), $\hat{\Sigma}_{ij}^{(0)}$, arises due to the nonlinearity of equation (B-11) and is given (after suppressing superscripts (0)), by

$$\hat{\Sigma}_{ij} = \bar{e}_{(1)ik}\bar{\bar{e}}_{(1)kj} + \bar{\bar{e}}_{(1)ik}\bar{e}_{(1)kj} + \hat{W}_{(1)ij} + \varepsilon_1[\hat{e}_{(2)ij} + \hat{W}_{(2)ij}], \qquad \text{(B-13)}$$

where $$\hat{W}_{(1)ij} = \bar{E}_{(1)ik}\bar{\bar{e}}_{(1)kj} + \bar{\bar{e}}_{(1)ik}\bar{E}_{(1)kj} + \bar{\bar{E}}_{(1)ik}\bar{e}_{(1)kj} + \bar{e}_{(1)ik}\bar{\bar{E}}_{(1)kj},$$

$$
\begin{aligned}
\hat{W}_{(2)ij} = {} & \bar{V}_k \bar{\bar{e}}_{(1)ij,k} + \bar{\bar{e}}_{(1)ik} \bar{V}_{k,j} \\
& + \bar{\bar{e}}_{(1)kj} \bar{V}_{k,i} + \bar{\bar{V}}_k \bar{e}_{(1)ij,k} \\
& + \bar{e}_{(1)ik} \bar{\bar{V}}_{k,j} + \bar{e}_{(1)kj} \bar{\bar{V}}_{k,i} \\
& + \bar{v}_k \bar{\bar{E}}_{(1)ij,k} + \bar{\bar{E}}_{(1)ik} \bar{v}_{k,j} \\
& + \bar{\bar{E}}_{(1)kj} \bar{v}_{k,i} + \bar{\bar{v}}_k \bar{E}_{(1)ij,k} \\
& + \bar{E}_{(1)ik} \bar{\bar{v}}_{k,j} + \bar{E}_{(1)kj} \bar{\bar{v}}_{k,i},
\end{aligned}
$$

$$
\begin{aligned}
\hat{e}_{(2)ij} = {} & \bar{v}_k \bar{\bar{e}}_{(1)ij,k} + \bar{\bar{e}}_{(1)ik} \bar{v}_{k,j} \\
& + \bar{\bar{e}}_{(1)kj} \bar{v}_{k,i} + \bar{\bar{v}}_k \bar{e}_{(1)ij,k} \\
& + \bar{e}_{(1)ik} \bar{\bar{v}}_{k,j} + \bar{e}_{(1)kj} \bar{\bar{v}}_{k,i}.
\end{aligned}
\tag{B-14}
$$

Now, we have shown in I, by use of the reciprocal theorem, that the lateral force on a sphere to $O(\lambda)$ is (cf. equation (2.23) of I)

$$
\begin{aligned}
F_L &= -\tfrac{1}{2}\lambda \int_{V_f} \Sigma^{(0)}_{ij} a_{ij} \, dV \\
&= -\tfrac{1}{2}\lambda \int_{V_f} [\bar{\Sigma}^{(0)}_{ij} + \bar{\bar{\Sigma}}^{(0)}_{ij} + \hat{\Sigma}^{(0)}_{ij}] a_{ij} \, dV.
\end{aligned}
\tag{B-15}
$$

The integral of the first two terms is identical to that in (2.23) of I, with the appropriate velocity fields $\bar{v}_i^{(0)}$, $\bar{V}_i$ and $\bar{\bar{v}}_i^{(0)}$, $\bar{\bar{V}}_i$. Thus, upon integration we obtain (cf. (3.9) of I)

$$-\frac{1}{2}\lambda \int_{V_f} \bar{\bar{\Sigma}}^{(0)}_{ij} a_{ij} \, dV = -\pi \bar{\bar{\beta}} \bar{\bar{\gamma}} \lambda N(\varepsilon_1),$$

$$-\frac{1}{2}\lambda \int_{V_f} \bar{\bar{\bar{\Sigma}}}^{(0)}_{ij} a_{ij} \, dV = -\pi \bar{\bar{\bar{\beta}}} \bar{\bar{\bar{\gamma}}} \lambda N(\varepsilon_1). \qquad \text{(B-16)}$$

A little effort, using the definitions of $\hat{\Sigma}^{(0)}_{ij}$ in equations (B-13) and (B-14), shows that the last integral of (B-15) is identically zero. Thus, the total lateral force on a sphere suspended in a screw extruder is simply

$$\begin{aligned} F_L &= -\pi\lambda(\bar{\bar{\beta}}\bar{\bar{\gamma}} + \bar{\bar{\bar{\beta}}}\bar{\bar{\bar{\gamma}}})N(\varepsilon_1) + O(\kappa^3) \qquad \text{(B-17)} \\ &= -3\pi\lambda\kappa^3 U_c^2 N(\varepsilon_1)\{A\cos^2\phi[1-3A(1-2s)] \\ &\quad + \sin^2\phi[1-3(1-2s)]\} \\ &= 3\pi\lambda\kappa^3 U_c^2 N(\varepsilon_1) G(s), \end{aligned}$$

where $N(\varepsilon_1) \equiv \left(\frac{683}{300} - \varepsilon_1 \frac{4941}{560}\right)$.

The lateral velocity of the sphere can be obtained by using Stokes equation:

$$U_{sz} = \frac{1}{2}\lambda\kappa^3 U_c^2 N(\varepsilon_1) G(s). \qquad \text{(B-18)}$$

Here positive values of the force and velocity represent migration towards the screw base (s=1.0) and negative values represent migration towards the barrel (s=0). Rheological data for polymeric solutions and melts indicate that $\lambda N(\varepsilon_1)$

is positive (see I). The direction of migration thus depends on the function G(s), which is plotted in Figure 4 for various values of A and a typical value for ϕ of 30°.

4. Particle trajectories

In order to see the practical implications of the lateral migration force F_L, it is necessary to consider the resultant trajectories for a typical sphere. The velocity of the sphere is most conveniently written as the sum of x, y and z components:

$$U_s = U_{sx}\hat{i}+U_{sy}\hat{j}+U_{sz}\hat{k} \qquad \text{(B-19)}$$

where

$$U_{sx} = U_c\cos\phi[1-3A(1-s)]s$$
$$U_{sy} = U_c\sin\phi[1-3(1-s)]s$$
$$U_{sz} = \tfrac{1}{2}\lambda\kappa^3 U_c^2 N(\varepsilon_1)G(s).$$

In order to calculate trajectories, it is assumed that the velocity of the sphere in the x and y directions equal to the undisturbed velocity of the fluid. On the other hand, the velocity in the z direction is the lateral migration velocity, equation (B-18). The residence time of a typical sphere inside the extruder can be calculated knowing the mean undisturbed fluid velocity in the x direction. From the values of U_{sy} and U_{sz}, the particle position on a cross-sectional plane of the channel can be obtained. In

this section, we consider only the particle path on the y-z plane of the channel. It will be shown that all particles eventually end up at the position s=2/3.

Let us write the velocities U_{sy} and U_{sz} in dimensional quantities,

$$U^*_{sy} = w\frac{d(\bar{\bar{y}})}{dt^*} = U^*_c(\sin\phi)s(3s-2) \qquad \text{(B-20)}$$

$$U^*_{sz} = d\frac{ds}{dt^*} = \frac{U^*_c}{2}\left(\frac{\phi_3 U^*_c}{\mu_o d}\right)N(\varepsilon_1)\kappa^2 G(s). \qquad \text{(B-21)}$$

Here $\bar{\bar{y}}$ (=y*/w) is the channel position in the y direction, nondimensionalized by the channel width w. Thus the cross-sectional area of the channel is bounded by walls at s=0 (barrel), s=1 (screw base), and $\bar{\bar{y}}$=0, $\bar{\bar{y}}$=1 (screw flights). From the expression U^*_{sy} (also see figure 3), the sphere is seen to move towards $\bar{\bar{y}}$=1 for 2/3<s<1 and to move towards $\bar{\bar{y}}$=0 for 0<s<2/3. At the walls $\bar{\bar{y}}$=0 and $\bar{\bar{y}}$=1, we simply assume that the particles turn the corner following a streamline which is determined in such a manner that fluid mass is conserved. In another words, if the particle approaches $\bar{\bar{y}}$=0 on a streamline (say s=σ) corresponding to a total mass flux measured across a plane which extends from s=σ to the wall s=0, then we assume that it leaves $\bar{\bar{y}}$=0 traveling in the opposite direction on a streamline (say s=σ*) which bounds a region of equal mass flux

measured across a plane which extends from $s=\sigma^*$ to the other wall $s=1$. The same is true for a particle approaching the wall $\bar{\bar{y}}=1$. Then it is easy to show that (see McKelvey, 1962 p. 320)

$$\sigma^3-\sigma^2 = (\sigma^*)^3-(\sigma^*)^2. \tag{B-22}$$

The sphere trajectory is obtained from equations (B-20) and (B-21), together with the assumption that the spheres turn around at the walls $\bar{\bar{y}}=0$ and $\bar{\bar{y}}=1$ according to equation (B-22). Thus, combining the equations (B-20) and (B-21), we obtain

$$\begin{aligned} d\bar{\bar{y}} &= \frac{(d/w)\sin\phi}{\frac{1}{2}\left(\frac{\phi_3 U_c^*}{\mu_o d}\right)N(\varepsilon_1)\kappa^2}\left(\frac{s(3s-2)}{G(s)}\right)ds \\ &= \frac{(d/w)\sin\phi}{\Xi}\left(\frac{s(3s-2)}{G(s)}\right)ds\ . \end{aligned} \tag{B-23}$$

Upon integration this becomes

$$\bar{\bar{y}}_2-\bar{\bar{y}}_1 = \frac{(d/w)\sin\phi}{\Xi}\int_{s_1}^{s_2}\frac{s(3s-2)}{G(s)}ds\ . \tag{B-24}$$

The quantity $\Xi\left(=\frac{1}{2}\left(\frac{\phi_3 U_c^*}{\mu_o d}\right)N(\varepsilon_1)\kappa^2\right)$ is proportional to the rate of migration. Thus, large values of Ξ correspond to rapid migration, and the particle trajectory will clearly depend on the value of Ξ. We present a typical trajectory in

figure 5 for $\frac{(d/w)\sin\phi}{\Xi} = 100$, $\phi=30°$, and A=0.5. The paths in figure 5 are simply drawn as straight lines to show the trajectory qualitatively. Thus the actual trajectory is slightly different from that given in figure 5 especially at the screw flights $\bar{\bar{y}}=0$ and $\bar{\bar{y}}=1$. As indicated, the trajectory of the particle is a closed spiral, tending toward an equilibrium position s=2/3. The latter occurs because the rate of lateral migration is greater for s>2/3, where the particle travels from left to right in figure 5, than for s<2/3 where the particle travels from right to left. Although the details differ, the same effect is found for all values of $\frac{(d/w)\sin\phi}{\Xi}$, ϕ and A. In the regime from s=0 to the position where the migration velocity is zero, the direction of migration is reversed, but a little thought shows that a particle in this regime will migrate downward as it moves from right to left, thus eventually again ending up on the spiral path leading to equilibrium at s=2/3.

It is worth noting that particles close to barrel and the screw (i.e. s=0 and s=1) have the largest residence time in the extruder. The position s=2/3 corresponds to minimum residence time (see McKelvey 1962, p. 322). Thus we arrive at the conclusion that, due to normal stress induced migration, spheres suspended inside a screw extruder have a tendency to drift towards the position s=2/3 where the residence time in the extruder is minimum.

REFERENCES

Bernhardt, E.C., ed. 1959 Processing of Thermoplastic Materials. Reinhold.

Ho, B.P. & Leal, L.G. 1974 Migration of rigid spheres in a two-dimensional unidirectional flow of a second-order fluid. Submitted to Journal of Fluid Mechanics.

McKelvey, J.M. 1962 Polymer Processing. Wiley.

FIGURE CAPTIONS

Figure 1. Schematic diagram of longitudinal cross-section of a screw extruder.

Figure 2. Velocity profile of down channel flow for various values of A.

Figure 3. Velocity profile of cross channel flow.

Figure 4. Lateral force function G(s) as a function of lateral position for $\phi=30°$ and various values of A.

Figure 5. Sphere trajectory in the y-z plane for $(d/w)\sin\phi/\Xi=100$, A=0.5 and $\phi=30°$.

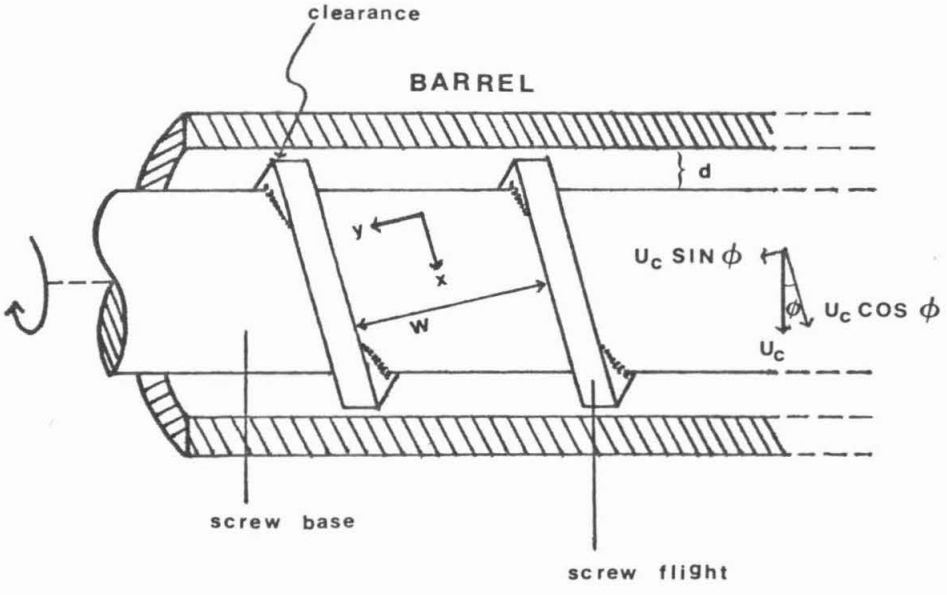
clearance
BARREL
d
y
x
W
U_c SIN ϕ
U_c COS ϕ
ϕ
U_c
screw base
screw flight

FIGURE 1

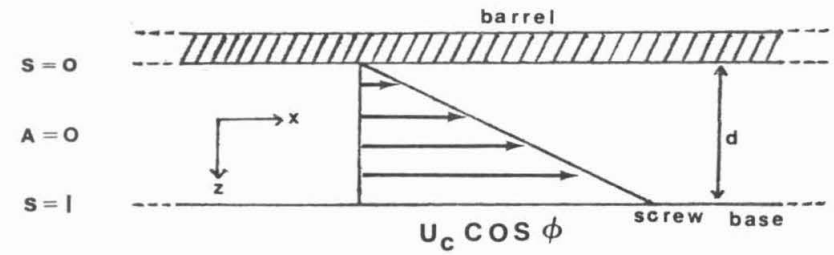

FIGURE 2a

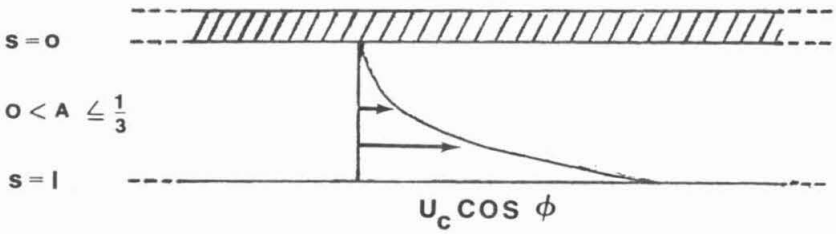

FIGURE 2b

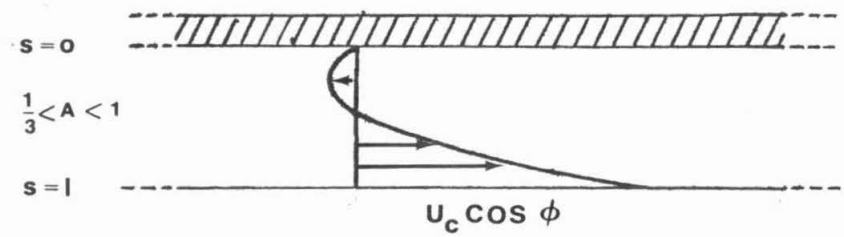

FIGURE 2c

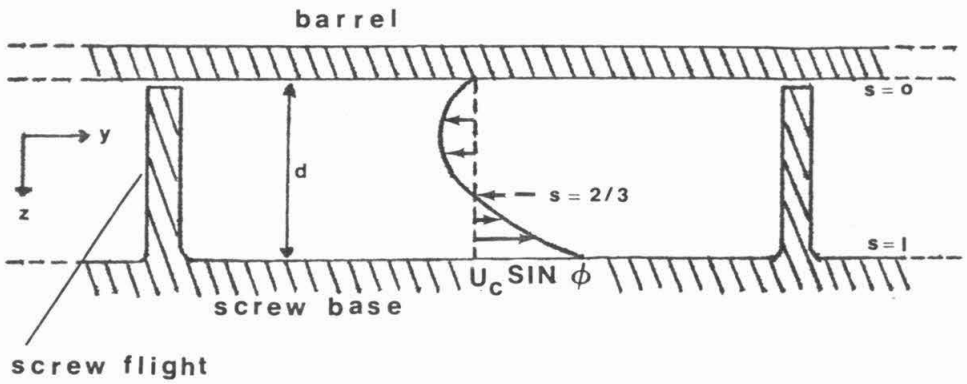

FIGURE 3

FIGURE 4

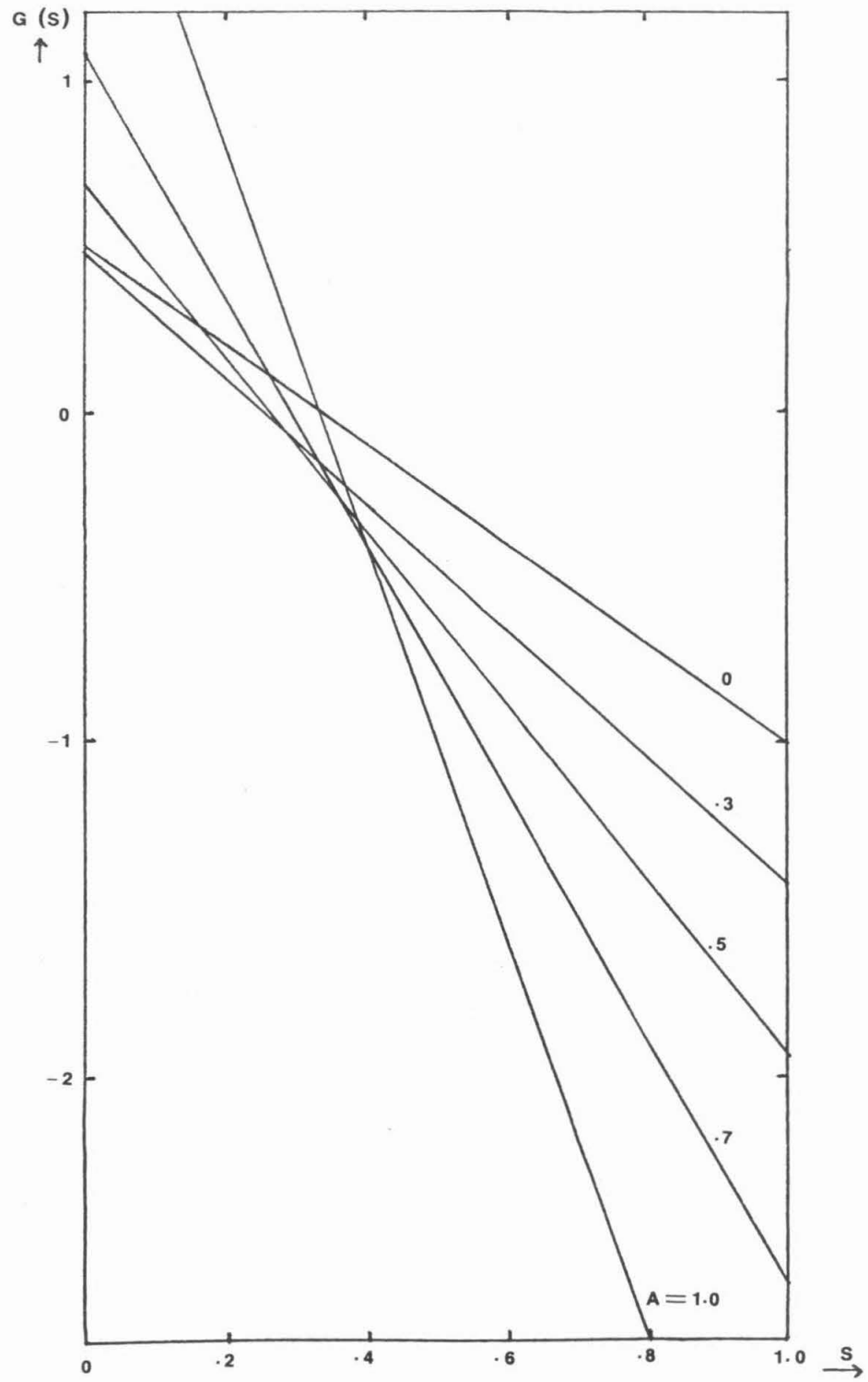

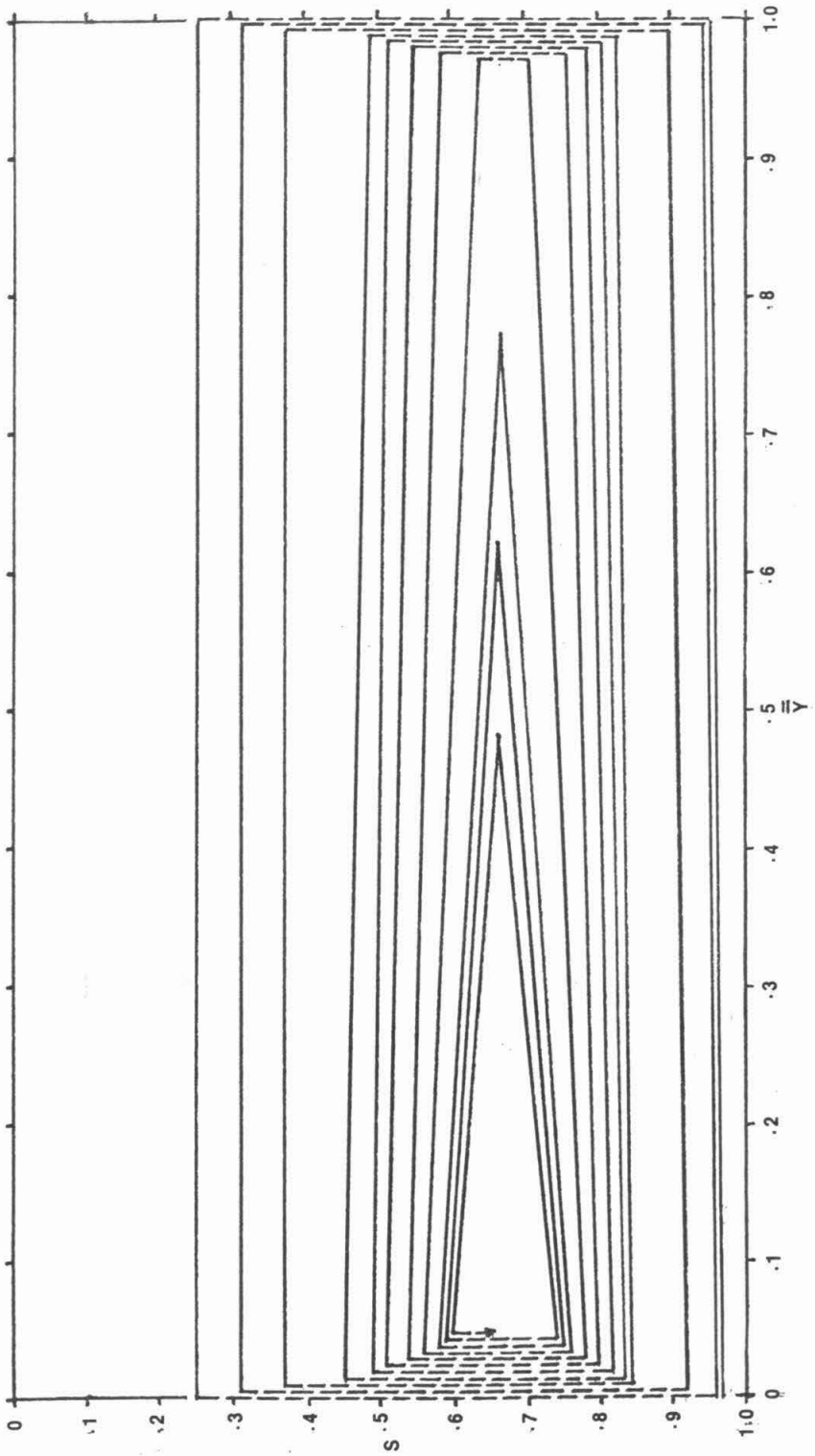

FIGURE 5

CHAPTER IV

THE CREEPING MOTION OF LIQUID DROPS THROUGH A CIRCULAR TUBE OF COMPARABLE DIAMETER

The problems in the previous two chapters are concerned with particles whose dimensions are small compared with the wall dimension, whereas this chapter considers particles of comparable dimension as the containing walls. The creeping motion of neutrally bouyant Newtonian drops through a circular tube is studied experimentally for drops which have an undeformed radius comparable in size to that of the tube. Both a Newtonian and a viscoelastic suspending fluid were used in the experiments to determine the influence of viscoelasticity. The extra pressure drops due to the presence of the suspended drops, the shape and velocity of the drops, and the streamlines of the flow are reported for various viscosity ratios, total flow rates, and drop sizes. The text of Chapter IV is an article prepared for publication (coauthor, Dr. L. G. Leal). The photographs of the drop shapes omitted in the text are given in Appendix C.

1. Introduction

The experimental study reported in this paper is concerned with the creeping motion of neutrally buoyant drops of a Newtonian fluid through a straight, circular tube when the diameters of the undeformed drop and the tube are of similar magnitude. Both Newtonian and viscoelastic suspending fluids have been considered in the present work. Much of the earliest interest in these problems arose because of the suggested analogy in the Newtonian case between the drop motion and the motion of erythrocytes in the capillaries. Although subsequent work on erythrocyte motion has now largely eliminated this motivation for investigation, the motion of a drop or train of drops through tubes of constant or variable cross-sectional area remains of considerable technological importance in its own right. One specific example, where the case of a viscoelastic suspending fluid is of special significance, is the motion of oil droplets in a porous matrix during secondary (oil) recovery processes which use polymeric 'pusher' fluids - e.g. micelle or polymer flooding (see Savins (1969)).

In the present experiments, we have determined the change in the pressure drop, ΔP^{+}, which is required, in the presence of the suspended drops, to produce a given total volumetric flow rate Q; the drop shape; the velocity of

the drops U relative to the average velocity $\bar{V}$ of the two-phase system as a whole; and, finally, the streamline patterns with respect to a frame of reference in which the drops are stationary. The independent variables which were varied for both the Newtonian and viscoelastic suspending fluids are the total volumetric flow rate Q, the volume of the suspended drops v, and the shear viscosity ratio σ of the suspended fluid μ_i compared to that of the suspending fluid, μ_o. For the case of a Newtonian system in the absence of fluid inertia effects, the appropriate characteristic pressure is simply $\mu_o\bar{V}/R_o$, where R_o is the radius of the tube. The extra pressure drop ΔP^+, nondimensionalized by $\mu_o\bar{V}/R_o$, is then a function of (i) the relative size of the drop as measured by the ratio (λ) of undeformed drop radius to tube radius, (ii) the relative viscosity $\sigma=\mu_i/\mu_o$, and (iii) a deformation parameter $\Gamma=\mu_o\bar{V}/\gamma$, where γ is the interfacial tension between the suspending fluid and the drop. When the suspending fluid is viscoelastic, additional parameters are required which measure the degree of elasticity.

So far as we are aware, no previous investigation has considered the case of a viscoelastic suspending fluid. However, there have been several prior experimental and theoretical studies on the creeping motion of both drops and solid particles through a circular tube when the

suspending fluid is Newtonian. On the theoretical side, the investigations which are most relevant to the present work are those of Hetsroni, Haber & Wacholder (1970), Brenner (1971), and Hyman & Skalak (1969, 1970). Hetsroni, et.al. (1970) used the method of reflexions to solve for the flow fields in and around a single undeformed drop suspended in a Poiseuille flow. Their result for the velocity of a neutrally buoyant concentrically located spherical drop, which is valid for small values of λ, is

$$U/\overline{V} = 2-\frac{4\sigma}{3\sigma+2}\lambda^2+O(\lambda^3). \qquad (1)$$

Since the drop is assumed spherical, the boundary condition for the normal component of the stress is not satisfied. However, upon substitution of the velocity fields for an undeformed drop, this boundary condition gives a first approximation to the deformed shape of the drop. The result, obtained by Hetsroni, et.al. (1970), for the case of a neutrally buoyant concentrically located drop is

$$r = r_o[1+\tfrac{1}{2}L_3{}^o(5\cos^3\theta-3\cos\theta)]+O(\lambda^3), \qquad (2)$$

where $L_3{}^o = \frac{10+11\sigma}{10(1+\sigma)}\Gamma\lambda^2$,

which is valid provided $\sigma=O(1)$ and $\Gamma\to 0$. Here r_o is the

radius of the undeformed drop, r is the radial variable measured relative to the center of the drop, and θ is the polar angle measured counterclockwise from the axis of the undisturbed velocity vector. It should be noted, that the deviation from spherical shape is predicted to increase linearly with Γ, and also to increase slightly, for constant Γ, with increase of the viscosity ratio σ. Hetsroni, et.al. (1970) did not obtain results for the extra pressure drop due to the presence of the drop. However, shortly thereafter, Brenner (1971) obtained this result using the reciprocal theorem for low Reynolds number flow. The result for a neutrally buoyant concentrically located spherical drop is

$$\frac{\Delta P^{+} R_o}{\mu_o \overline{V}} = \frac{16[(9\sigma+2)^2-40]}{27(\sigma+1)(3\sigma+2)}\lambda^5 + O(\lambda^{10}). \qquad (3)$$

It is significant, as Brenner has pointed out, that ΔP^{+} may be either positive or negative (i.e. it is predicted that the overall pressure drop can be either increased or decreased by the presence of the drop) depending on the magnitude of σ. In addition, although equation (3) is strictly valid only for $\lambda << 1$, the very small relative error would appear to allow quite reasonable results for values of λ as large as 0.3 - 0.4.

For higher values of λ, Hyman & Skalak (1969, 1970) studied the case of an equally spaced train of neutrally buoyant concentrically located drops including both deformed and undeformed shape. Although exact solutions of the equations of motion were derived, these were in the form of an infinite series of algebraic equations. Hence, in order to obtain quantitative (numerical) results, it was necessary to truncate the series and restrict the parameters σ, Γ and particle spacing to specific values, while keeping $\lambda \leq 0.8$. For $\lambda > 0.8$, the number of the algebraic equations required for convergence became excessive, even with the shape specified. Moreover the actual deformation from a spherical shape became so large for $\lambda > 0.8$ that many trials would have been required to attain the correct equilibrium shape of the drop. Comparison of the results of Hyman & Skalak (1969) on the velocity of a single undeformed drop with equation (1) indicates agreement to three significant figures for $\lambda \leq 0.4$ but increasing deviation for larger values of λ, presumably due to the neglect of higher order terms in λ in equation (1). At $\lambda = 0.7$, the velocities predicted by equation (1) exceed the values calculated by Hyman & Skalak (1969) by 3%. At $\lambda = 0.8$, the difference is 6%. Likewise comparison of ΔP^{+} from Hyman & Skalak (1969) with that predicted by Brenner's theory, equation (3), shows

that the latter increasingly underpredicts the former with increasing λ. At $\lambda=0.5$, the difference is 5%.

On the experimental side, Hochmuth & Sutera (1968, 1970) have investigated the case of solid hemispheres and caps in a Newtonian suspending fluid, as a model for the motion of blood erythrocytes through capillaries. In addition, Prothero & Burton (1961, 1962a, b) have reported a more or less qualitative investigation on a train of gas bubbles in a Newtonian fluid as a model for blood flow through capillaries. However, the only investigations of direct relevance to the present paper are those of Goldsmith & Mason (1963) and Bretherton (1961) who studied the motion of very large ($\lambda>>1$) suspended drops in slow motion ($\Gamma<<1$) where the drop and tube wall are separated by only a thin layer of suspending fluid. The variables measured in these studies were mainly the velocity of the fluid drop relative to the average fluid velocity, and the thickness of the thin layer of fluid separating bubble and wall. The chief result of qualitative interest here was the adoption of an apparent asymptotic behavior for large λ in which the velocity of the drop and thickness of the thin layer of fluid becomes independent of λ. No measurements were made of ΔP^+.

The present investigation covers the range $\lambda \sim 1$, for intermediate values of Γ, and σ varying from approximately

0.2 to 2. Thus, for the Newtonian case, our results lie between the available theory ($\lambda<\sim 0.8$) and experiments ($\lambda>>1$). In addition, we provide an initial study of the additional effects associated with a viscoelastic suspending fluid. The range of λ near unity is of considerable interest since it is here that the maximum variations of drop shape and wall effect on ΔP^+ may be expected.

2. Apparatus and experimental techniques

(i) Experimental set-up

The experimental set-up is shown schematically in figure 1. The test section, where all the data were obtained, consisted of a horizontal, 120 cm. long, precision bore glass tube of 1 cm. internal diameter ($2R_o$). Two pressure taps were located 50 cm. apart, with the furthest upstream tap being approximately 50 cm. from the entrance to the 1 cm. tube. These pressure taps were connected to a manometer which was conventional except for a valve at the bottom which could be closed to allow the pressure difference at the bottom of the two legs to be measured and recorded using a differential pressure transducer. The method of obtaining ΔP^+ with this set-up will be described later in this section. The 50 cm. section of tube upstream of the first pressure tap, and the 20 cm. section downstream of the second were intended to minimize end effects. At its upstream end, the test section was connected to a section of larger (1.4 cm. diameter) glass tube into which the drops were manually injected using a precision micrometer syringe (accurage to ±0.001 ml.) connected to a 17 gauge hypodermic needle. The larger diameter tube was adopted in order to facilitate the injection of the larger drops ($\lambda>1$) after it was found that the injection method inevitably brought the drops into contact with the wall of the smaller 1 cm. tube

where they became permanently affixed due to the wetting properties of the drop liquid. Both the 1 and 1.4 cm. glass tubes were enclosed within a long plexiglass constant temperature bath.

The suspending fluid was pumped at a constant flow rate using a variable speed Harvard Apparatus reciprocal action infusion-withdrawal syringe pump. While one syringe was supplying the suspending fluid into the test section by injection, the other was being filled from a reservoir by withdrawal thus allowing a continuous flow to be maintained. A large storage section was connected to the exit of these syringes and placed inside the constant temperature bath to insure that the suspending fluid was equilibrated at the bath temperature (25.0±0.5°C) before entering the test section. Two thermocouples, one at each pressure tap,were used to monitor the temperature of the suspending fluid in the test section. The drops were injected one by one with the pump completely turned off. After a given volume of the drop fluid was injected, the bulk fluid was pumped slowly so that the drop detached from the hypodermic needle. The drops were found to migrate to the concentric position as long as they were neutrally buoyant, so that no special effort was made to inject them onto the centraline of the tube. When trains of several drops were considered, as was most often the

case, the drops were injected as close as possible to evenly spaced. However, as observed here, and also predicted by Hyman & Skalak (1969, 1970), interactions between the drops were negligible provided the distance between centers was only slightly larger than the tube diameter. As all of our data were taken with the spacing at least this large, the precision of equal spacing was not critical to the results.

(ii) Materials

For the Newtonian case, the suspending fluid was 95.75% by weight glycerine in water. The percent glycerine was monitored during the course of the experiments using a hydrometer to measure the solution density at 25.0°C (1.251 gm./c.c.). The viscosity was measured using a Canon-Fenske capillary viscometer and was consistently found to be within 2% of the published literature value of 417 c.p. at 25°C. It is believed that the small (2%) discrepancies can be attributed to slight variations in the bath temperature for the viscometer which could not be controlled more accurately than ±0.1°C. It is well known that glycerine exhibits a rather strong dependence of the viscosity on temperature. For example, a 0.5°C change from 25°C produces a 5% change in the viscosity. Indeed, when an attempt was made to calibrate the experimental set-up of figure 1, by using

measured flow-rate and pressure drop to determine the viscosity, it was found that only approximately 5% agreement with literature values could be obtained. This discrepancy presumably reflects the accuracy of temperature control which was ±0.5°C in the test section.

The viscoelastic suspending fluid was a 0.5% by weight solution of Dow Separan AP30 (an ionic polyacrylamide) in water. The viscosity and primary normal stress difference for this material have previously been reported as a function of shear rate by Leal, Skoog and Acrivos (1971). Other properties, such as relaxation and retardation times, or elongational viscosity which are required to characterize the material behavior in a time-dependent nonviscometric flow are also available in the literature (Huppler, Ashare & Holmes, 1967a, b). However, since the present experiments encompass only a single polymer concentration, we will not consider the various viscoelastic parameters further, with the exception of the shear viscosity, μ_o, which can be compared directly with Newtonian case. Since the viscosity of 0.5% Separan is strongly shear-rate dependent and the flow through a tube (with or without drops) has a nonuniform shear rate, there is some arbitrariness in the precise value of μ_o to assign for a particular flow rate. However, in view of the fact that one of the major variables of interest is the additional

pressure drop relative to that of the pure suspending fluid, we have used the apparent viscosity of the visco-elastic fluid at the wall shear-rate of the pure suspending fluid which is appropriate for each volume flow rate. Thus, in order to obtain the apparent viscosity as a function of volume flow rate, the pressure drop across the 50 cm. test section (L) was measured for various flow rates Q. For a unidirectional flow of any fluid, a simple force balance shows that the wall shear stress τ_w is related to the pressure drop by

$$\tau_w = \frac{R_o}{2}\left(\frac{\Delta P}{L}\right) . \tag{4}$$

Furthermore, it can be shown (see Coleman, Markovitz and Noll (1966)) that the wall shear rate is given for any fluid by

$$\beta_w = \frac{3n+1}{4n}\left(\frac{4Q}{\pi R_o^3}\right) , \tag{5}$$

where n is the slope of τ_w versus $(4Q/\pi R_o^3)$ on a log-log plot. Although n may generally vary with flow rate, we have found that n=0.450 provides a good approximation of the viscosity (of 0.5% Separan) in the range of shear rates characterizing the present experiments. Thus, for

our present purposes, the relationship between $\mu_o=\tau_w/\beta_w$ and β_w can be represented by a power-law model. The apparent viscosity, $\mu_o=\tau_w/\beta_w$, for various flow rates is tabulated in table 1, together with other pertinent information on the conditions of our experiments. Literature values obtained in a simple shear viscometer are found to be slightly lower than the values obtained by the present method, but the slope of μ_o versus β_w is the same. Although no normal stress measurements were made in the present study, we have also listed values of the first normal stress difference at each β_w from the work of Leal, Skoog and Acrivos (1971) in table 1.

The suspended drops consisted of a well-mixed solution of silicone oil (Dow Corning 200 fluid, a dimethyl silioxane polymer) and carbon tetrachloride which behaves as a Newtonian fluid in the range of shear rates of the present experiments. The two liquids were mixed in such a proportion that the density matched that of the suspending fluid to within 0.001 gm./c.c. For the viscoelastic system, a mixture of about 18 parts silicone oil to 1 part carbon tetrachloride yielded a density of 1.000 gm./c.c. equal to that of the Separan AP 30/water solution. For the Newtonian system, a mixture of about 12 parts silicone oil to 10 parts carbon tetrachloride gave a density of 1.251 gm./c.c. equal to that of the

hydrolyzed glycerine. Four grades of silicone oil having different viscosities but equal density were used for the Newtonian system and will be labeled as systems 1 through 4. Another four grades of silicone oil were used for the viscoelastic system and will be labeled as systems 5 through 8. The viscosity of the silicone oil-carbon tetrachloride mixture was measured by a Canon-Fenske capillary viscometer at 25.0°C. An appropriate dimensionless parameter is the viscosity ratio $\sigma=\mu_i/\mu_o$. The viscosity of the glycerine is constant while that of the Separan in water is flow-rate dependent. Consequently σ is also flow-rate dependent for the viscoelastic system. The viscosity of the silicone oil-carbon tetrachloride mixture (μ_i) and the viscosity ratios for the eight systems are given in table 1 for the various flow rates used in the experiments.

(iii) Conditions of the experiments

The experiments in each of the Newtonian and viscoelastic case were thus carried out for four different combinations of the suspending and drop fluids corresponding to the systems 1 through 8. In addition, for each system of fluids, we used four different volume flow rates, and, at each flow rate, six different volumes v for the suspended drops. The various flow rates are labeled as a, b, c, and d, with a corresponding to the lowest flow

rate. They were chosen so that the bulk Reynolds number ($Re=\rho\bar{V}R_o/\mu_o$) is small in every case. The values actually attained for Re (maximum of 0.1) are listed in table 1. The six different drop volumes v and corresponding λ are

v (ml.)	.2	.3	.4	.5	.6	.7
λ	.726	.831	.914	.985	1.046	1.102

At low Reynolds number, the parameter which characterizes the degree of drop deformation is the ratio $\Gamma=\mu_o\bar{V}/\gamma$ which is a measure of the relative importance of the viscous stresses compared to the interfacial tension, γ. The interfacial tension, measured using a DuNoüy platinum ring tensiometer, was found to be 22 dyne/cm. for the glycerine-silicone oil+carbon tetrachloride interface, while that of the Separan+water-silicone oil+carbon tetrachloride interface was found to be 38 dyne/cm. Although γ was thus fixed by the choice of materials, the parameter Γ was actually varied by the choice of various flow rates $\bar{V}$ (and μ_o for the viscoelastic case). In fact, the primary reason for varying Q in the experiments was to study the effects of the flow rate on drop deformation.

(iv) Methods of measurement

Pressure measurements were made using a combination of a standard U-tube manometer, which was attached to the pressure taps in the test section, and a differential, variable-reluctance pressure transducer and indicator system manufactured by Validyne Engineering Corporation. In order to minimize transients and other anomalies associated with the motion of the drops directly above the pressure taps, they were located 50 cm. apart. This rather large separation was designed not only to allow the drop or train of drops to be completely contained between the two taps, but also to insure adequate time in this 'enclosed' configuration for the measured pressure difference to attain a steady value. The major difficulty associated with the wide separation of pressure taps was that the overall pressure drop was quite large, considerably exceeding the extra pressure drop ΔP^+ which was the main pressure variable of interest. In order to achieve reasonable accuracy for the small change ΔP^+, we used the combination of manometer and transducer as mentioned. The manometer was allowed to come to equilibrium with the suspending fluid alone moving through the test section at the desired flow rate Q, and the valve at the bottom of the manometer was then closed, thus effectively separating the two legs. In this configuration, the

pressure transducer, which had a full scale range of ±1 inch of water at 25°C, could be used to accurately measure the differences in the pressure at the two taps which arose because of the presence of the drops in the test section, (i.e. ΔP^+ directly). Carbon tetrachloride was chosen as the manometer fluid because of its relatively low viscosity which produces a response time for the transducer of less than 6 seconds. In order to enhance the magnitude of the pressure signal, experiments were generally run with 10 to 24 drops in a train. The additional pressure drop ΔP^+ for one drop was then obtained by dividing the total extra pressure drop by the total number of drops. It had previously been predicted by Hyman & Skalak (1969, 1970) for the Newtonian case that the pressure drop per drop should be independent of spacing for separation of centers by at least one tube diameter. This was confirmed experimentally in the present study for both the Newtonian and viscoelastic fluid cases.

Photographs giving the drop shape and streamlines were taken by cameras which were moved parallel to the direction of motion of the drops. Those obtained for determination of drop shape were photographed using a 35 mm. single lens reflex camera with diffused background lighting, and ASA 400 Tri-X film (Kodak). The streamline

pictures were taken using a Graflex camera fitted for high speed Polaroid Type 57 (3000 ASA) film. A 300 watt projector lamp was allowed to shine through a 0.01 inch wide slit in a completely dark room. The slit was aligned lengthwise parallel to the tube so that the cross-sectional plane through the center of the tube was illuminated for the pictures, which were taken in a horizontal direction. The motion of the fluid was traced out by very small suspended particles, which appear as streaks in the pictures for exposure times of approximately 3 seconds. Since the object (the suspended drop) was enclosed by a curved surface(the circular tube), we found that it was necessary to match the refractive index between the suspending fluid and the fluid in the constant temperature bath in order to minimize photographic distortions of the drop shape. The matching was considered adequate when the radii measured from the photograph of a spherical drop were found to differ by less than 1.5% in any direction. Water was used in the bath when the suspending fluid was Separan-water. Aqueous sugar solution, 60% by weight having a refractive index of 1.44,was used in the bath when the suspending fluid was glycerine (refractive index 1.46).

3. Experimental results

In the present study we have measured ΔP^+, U and drop shape for the eight different fluid systems listed in table 1, each at four different flow rates and with six drop sizes ranging from $0.7 \leq \lambda \leq 1.1$. The results are presented and discussed in the following four sections. Although the discussion is primarily focused on the Newtonian case, comparison is also made, where appropriate, between the Newtonian and viscoelastic systems. In order to facilitate this comparison, the values of the internal drop viscosity were chosen to provide similar values of σ for system 1 and 5, 2 and 6, 3 and 7, and 4 and 8. In addition, the values of Γ for the viscoelastic system with volume flow rates b and d are very nearly the same as the values for the flow rates a and b, respectively, in the Newtonian system. The only experimental runs which are directly comparable with any of the available theoretical analyses are those for systems 2b and 2d which have almost the same values of Γ^{-1} (=10 and 4) and σ (=1.0) as were assumed in the analysis of Hyman & Skalak (1970).

(i) Drop shape

Photographs depicting drop shape were taken for the full complement of fluid systems, flow rates and drop volumes. For purposes of the present discussion, we reproduce those for systems 1a, 1b, 4a, 4b, 5b, 5d, 8b,

and 8d in figure 2. The remainder may be found in Ho (1975). The shapes differ with variations in the flow rate $\overline{V}$, the viscosity ratio σ and the drop size as measured by λ.

Let us first consider the variations in shape as λ is changed, holding $\overline{V}$ and σ constant. Obviously, in all cases, the length of the drop (i.e. the maximum dimension measured in the direction of the tube axis) increases with λ since the volume of the drop is increased, and the streamwise extent is unconstrained. As λ increases, the maximum width (measured in the radial direction from the tube axis) first increases, but then, constrained by the wall, tends to become a constant for $\lambda \gtrsim 1$. That is, the width of the layer of suspending fluid between the wall and the drop is essentially independent of the drop volume for $\lambda \gtrsim 1.0$. We will see, in a latter section, that the drop velocity also becomes independent of the drop volume as λ is increased above 0.9. Both of these features were also observed by Goldsmith & Mason (1963) in their investigation of the motion of very large bubbles.

Next we consider variations in shape caused by increase of the flow-rate $\overline{V}$. It is evident, from figure 2, that drops of the same volume and same σ, in both Newtonian and viscoelastic suspending fluids, become more elongated (in the direction of motion) as $\overline{V}$ increases.

This increase in deformation with increased velocity is both intuitively obvious, and in qualitative agreement with the theoretical predictions of Hetsroni, et.al. (1970) and Hyman & Skalak (1970).

Finally, we turn to the dependence of drop shape on the viscosity ratio σ. For the Newtonian system, as σ is increased with λ and $\overline{V}$ held constant, the drops become more elongated - i.e. more viscous drops suffer a larger deformation. Although opposite to the intuitive notion that a more viscous drop should be less easily deformed, this result is in agreement with the perturbation theories of Hetsroni, et.al. (1970) (cf. equation (2)) and of Hyman & Skalak (1970). It should be noted however that both the theories and the present experiments are relevant only for viscosity ratios σ of order unity, and one cannot, therefore, extrapolate to the obvious contradiction that a rigid sphere ($\sigma \to \infty$) is more deformable than a gas bubble (where $\sigma \to 0$). Also, the shape change associated with a change in the viscosity ratio by a factor of ten is comparable in magnitude to that induced by a change in velocity $\overline{V}$ of only 30%. This more pronounced influence of Γ on the shape, compared to σ, is again substantiated qualitatively by equation (2) from Hetsroni, et.al. (1970). For the viscoelastic case, it is also clear from figure 2 that the more viscous drops are more elongated for a given

value of $\bar{V}$ and λ. However, unlike the Newtonian case where the general drop shape is qualitatively similar for all values of σ, the drops in the viscoelastic fluid are not only more elongated with increase of σ, but also become increasingly pointed at the front and flattened at the back when compared to drops of smaller σ which exhibit a maximum girth somewhere near the middle of the drop (see figure 2).

It is also interesting to compare drops of same σ and Γ for the Newtonian and viscoelastic systems. Thus, as shown in figure 2, for the case of high σ, on comparing system 1a (σ=2.04, Γ^{-1}=13.3) with system 5b (σ=3.7,Γ^{-1}=13.3) and 1b (σ=2.04, Γ^{-1}=9.9) with 5d (σ=4.9,Γ^{-1}=10.1), it may be seen that the drops in the viscoelastic systems appear more 'streamlined' than those in the Newtonian systems. On the other hand, for the case of small σ, on comparing system 4a (σ=0.19, Γ^{-1}=13.3) with system 8b (σ=0.13, Γ^{-1}=13.3) and system 4b (σ=0.19, Γ^{-1}=9.9) with system 8d (σ=0.17,Γ^{-1}=10.1), it is apparent that the drops in the viscoelastic systems are bulged and appear <u>less</u> 'streamlined' in shape compared with those in the Newtonian systems. It is also significant, that for all σ, the layers of suspending fluid between the drops and wall are thicker in the viscoelastic systems than in the corresponding Newtonian case.

(ii) Streamlines

In order to obtain a more detailed view of the dynamics of drop motion in tubes, a series of flow visualization studies were made, based upon streamline pictures taken in the manner described in section 2. The camera was mounted on a platform which was moved horizontally at precisely the same speed as the drops, which thus appear motionless in the pictures. Both Newtonian and viscoelastic suspending fluids were used. However, except for obvious changes resulting from the differences in drop shape, no qualitative differences could be detected between these two cases (see figure 3). In both, the fluid inside the drop recirculates with no net motion since the photographs were taken from a frame of reference which moved with the drop velocity. The motion of the suspending fluid has two distinct regimes. A central core of recirculating fluid is found between two drops and centered about the tube axis with a radius approximately the same as the deformed drop radius. Since the entire central core recirculates, there is no net motion of this core of suspending fluid. That is, the average velocity inside this "bolus" is the same as the drop velocity U. For this reason, the stagnation points in this core are located at about the same radial distance from the axis as the stagnation points inside the drop. Since $U/\overline{V}>1$,

fluid in the second regime, which is a shell between the core and the tube wall, flows backwards relative to the drops. These qualitative features are similar to the observations of Goldsmith & Mason (1963) and Prothero & Burton (1961). The work of Prothero & Burton (1961) was intended to show that the bolus flow helps increase the mass transfer from the bulk fluid to the walls. Taylor (1960), who also reported a study on the motion of large bubbles in tubes, predicted the existence of a stagnation ring and stagnation vertex on the leading end of a bubble. This seems to be in agreement with our pictures since no motion of tracer particles is discernable in this region. Finally, a 'recirculating' core of suspending fluid is also found upstream and downstream of the leading and trailing drops of a train, including the case of a single drop.

(iii) Drop velocity

We now turn to the measured values of the drop velocity relative to the average overall fluid velocity for the system. Measurements were made for all combinations of the viscosity ratio, drop size and volume flow-rate in both the Newtonian and viscoelastic systems. The complete set of results are tabulated in table 2. As expected (cf.

equation (1)), the drop velocity exceeds $\overline{V}$ in every case, generally falling between 30 to 60% faster. It is useful to consider the variations in $U/\overline{V}$ with respect to $\overline{V}$, λ, and σ more closely.

We begin with the variation in U with λ, holding $\overline{V}$ and σ fixed. In both the viscoelastic and Newtonian systems, the increasing wall effect causes the drop velocity to decrease with increasing λ, until $\lambda \gtrsim 0.9$ when the velocity becomes practically independent of λ. As we have noted previously, the latter observation is in agreement with the results of Goldsmith & Mason (1963), and is presumably a result of the independence of the drop cross-section on λ which was noted in the section 3(i). In order to compare the present experimental results with the available theory, we have plotted the quantity $(U/\overline{V}-2)$ in figure 4a as a function of λ for the four Newtonian systems at the lowest flow rate (a) where deformation is least important. Also shown are the theoretical predictions from the equation (1) of Hetsroni, et.al. (1970) at the same viscosity ratios, and the numerical results of Hyman & Skalak (1969) for $\sigma=1$ and no shape deformation. The equation (1), which is strictly valid only for $\lambda \ll 1$, predicts too high values for $U/\overline{V}$ at the moderate values of λ which characterize the experiments. On the other hand, agreement with the results of Hyman & Skalak (1969) is quite good. Comparing results

for the Newtonian and viscoelastic systems, it may be noted that the rate of decrease of $U/\bar{V}$ with increase of λ is more rapid for the Newtonian case. As a consequence, for comparable values of σ and Γ, drops in the Newtonian system move faster than in the viscoelastic system for $\lambda \lesssim 0.8$, but slower for $\lambda \gtrsim 0.9$.

The relative drop velocity $U/\bar{V}$ increases with increasing average fluid velocity for both the Newtonian and viscoelastic cases. That is, more rapid relative drop motion is associated with larger deformation. This trend is in qualitative agreement with the available theoretical results of Hyman & Skalak (1970), as may be seen in figure 4b, where we have plotted $(U/\bar{V}-2)$ versus λ for the Newtonian system 2, $\sigma=0.93$, at the four flow rates a - d, together with Hyman & Skalak's (1970) calculated values for $\sigma=1$, $\Gamma^{-1}=4$ and 10, and $\lambda=0.5$ and 0.7.

Finally, we turn to the variation in $U/\bar{V}$ with σ, holding λ and $\bar{V}$ constant. The experimental results in both the Newtonian and viscoelastic systems show that $U/\bar{V}$ increases as σ decreases. Unlike particle deformation, however, in which variations in σ are relatively unimportant compared to variations in $\bar{V}$, the effect of σ on $U/\bar{V}$ is comparable to the effect of $\bar{V}$. As is obvious from figure 4a, theory and experiment are in qualitative agreement with regard to the dependence of $U/\bar{V}$ on σ.

(iv) Extra pressure drop ΔP^+

The quantity of most interest from the technological point of view is the change in the pressure drop ΔP^+ due to the presence of suspended drops, relative to that which would occur at the same volume flow rate with the suspending fluid alone. The various experimental results are summarized in figure 5 (Newtonian systems 1, 3, 4), figure 6 (viscoelastic systems 5, 7, 8), and figure 7 (systems 2 and 6) where we have plotted the dimensionless quantity $(\Delta P^+ R_o/\mu_o \bar{V})$ as a function of λ for various combinations of σ and flow rate. Also shown along with the Newtonian systems are calculated values for $(\Delta P^+ R_o/\mu_o \bar{V})$ taken from the small λ theory for undeformed drops of Brenner (1971) (see equation (3)). Before discussing these results in detail, it is useful to first summarize the various physical phenomena which can affect the magnitude and sign of the extra pressure drop.

These separate logically into three distinct mechanisms: the simple exchange of suspending fluid with drop fluid of different viscosity which, in principle, would be active even if the flow field were unchanged; the alteration of the flow field due to the presence of the drop interface; and the alteration of drop shape, leading to changes in the flow. Brenner's (1971) analysis of an undeformed drop demonstrates the nature of the

interaction of the first two mechanisms for a moderately small drop ($\lambda<<1$). In particular, even when $\sigma=1$ so that the first mechanism is not active, Brenner's solution shows that the extra dissipation associated with modification of the flow fields still gives $\Delta P^{+}>0$. Only when σ is decreased to approximately 0.48 does the replacement of more viscous with less viscous fluid overtake the effect of altered flow to give $\Delta P^{+}=0$. The effect of drop deformation for these moderate values of λ is to decrease ΔP^{+} compared to its value in the undeformed state. Thus, any of the features producing larger deformation (see section 3(i)) will produce also a tendancy toward lower ΔP^{+}. It should be noted that, in many instances, the various effects will be competing so that ΔP^{+} may either increase or decrease depending on the relative importance of each. For example, increase of $\overline{V}$ with constant σ and λ was previously seen to give increased deformation and thus by the present argument, a decrease in ΔP^{+}. However, increase of σ for $\overline{V}$ and λ fixed also increases deformation, but at the same time increases the average μ in the system and causes some alteration of the flow fields in and around the drop. In view of the weak dependence of the shape on σ, it should be expected that the latter effects will dominate, thus producing increased values of ΔP^{+}. Finally, it should be noted that as λ is increased, the increased

wall effect will tend to cause ΔP^+ to increase as λ^5 for small λ (see equation (3)). However, as λ is increased near unity, the drop shape is constrained by the presence of the walls, and, in fact, we have seen that the main effect of increasing volume is to increase the length of the drop with other geometric features remaining reasonably unchanged. Indeed, for $\lambda>1$, it might be expected that the differential change in ΔP^+ with change of λ is approximately the change associated with an increase in length of an annular flow region for two fluids of different viscosity. This suggests, therefore, that for large λ the main effect on ΔP^+ is equivalent to simple replacement of one fluid with another of different viscosity. Furthermore, it can be anticipated that the change in ΔP^+ with λ in this simplified regime will be in the direction of increasing ΔP^+ with increase of λ for $\sigma>1$, and of decreasing ΔP^+ with increase of λ for $\sigma<1$. Thus, for <u>intermediate</u> λ, we may anticipate a transition in the value of σ corresponding to $\Delta P^+=0$, from ~ 0.48 to 1.

Let us now consider the detailed experimental results in the light of these qualitative physical ideas.

a) <u>Newtonian fluid systems</u>

The most straightforward variations are those for different values of σ, holding the flow rate and

drop size λ fixed. The general trend is consistent with theoretical expectations; for the two largest values of σ, the added pressure drop is always positive, while for the smallest value (σ=0.19) it is always negative. The intermediate value (σ=0.58) shows both positive and negative values depending on the flow rate and on λ. These results may be compared qualitatively with the theoretical prediction of Brenner (1971) that $\Delta P^+=0$ for $\sigma\simeq 0.48$, assuming small λ and no deformation. Although the experimental results are complicated by the effects of particle deformability and varying degrees of wall-effect for the larger values of λ, it is nevertheless clear from this comparison that the main influence of varying σ is, as anticipated in the introduction to this section, simply the replacement of fluid with drop fluid of different viscosity, which of course also affects the flow fields. The third mechanism, resulting from increased deformation with increase of σ, would actually tend to cause a smaller ΔP^+ for a more viscous drop. However, it is obvious from the experimental results that this change in deformation is so small that its effect on ΔP^+ is very much dominated by the first two mechanisms.

Like the dependence on σ, the dependence of ΔP^+ on flow rate is relatively straightforward. Indeed, for fixed σ and fixed λ, $(\Delta P^+ R_o/\mu_o \bar{V})$ decreases with increase of flow

rate in every case. That is, the behavior of pressure drop is similar to that of a shear-thinning fluid. This is perhaps more clearly illustrated in figure 8, where we have plotted $(\Delta P^{+} R_o/\mu_o \overline{V})$ as a function of the flow-rate parameter $\Gamma \equiv \mu_o \overline{V}/\gamma$ for $\sigma=2.04$ and various values of λ. As we have suggested in the introduction to this section, the dependence of ΔP^{+} on flow rate (or Γ) is primarily a reflection of the dependence of drop shape on Γ. It is evident from figure 8, which is typical of all four Newtonian fluid systems, that the dependence of the additional pressure drop on $\overline{V}$ (or Γ) is not very significant for small drop volumes (low values of λ), but that the change in ΔP^{+} with flow rate becomes very prominent for larger values of λ(larger drops). This behavior is consistent with the observations which we have reported of drop shape. Thus, for small volumes, especially v=0.2 ml. (λ=0.726), the shape is not significantly altered as the flow rate is changed, while for larger volumes, the change in shape with flow rate is much more prominent.

Compared to the influences of σ and Γ on ΔP^{+}, the dependence on drop size (λ) is more complicated. This is because changes in the drop size are associated with several competing mechanisms for change in ΔP^{+}. Assuming that the drops are either spherical or

only slightly deformed, the two main influences of increasing λ are due to the increased volume of the suspended drop and the increased wall effect (effectively, the decrease of cross-sectional area of the channel which is available for the suspending fluid). This is indeed the case for values of $\lambda \simeq 0.7$ where our results are seen to behave similarly to the predictions of Brenner (1971) which only includes these two mechanisms. The experimental results for system 2 are plotted in figure 7, together with the corresponding theoretical results of Brenner (1971), and the results of Hyman & Skalak (1969, 1970) for an undeformed drop with $\sigma=1.0$ and $\lambda \leq 0.8$ and a deformable drop with $\sigma=1.0$, $\Gamma^{-1}=4$ and $\Gamma^{-1}=10$ at $\lambda=0.5$ and 0.7. Given the slight differences in σ and Γ between experiment and the Hyman-Skalak theory, the comparison is quite satisfactory.

As λ increases towards $\lambda \simeq 1$, the drops are increasingly deformed from the spherical shape, and for cases with $\Delta P^+ > 0$, the rate of increase of ΔP^+ with respect to λ is decreased. Similarly, for the case of $\Delta P^+ < 0$, ΔP^+ decreases more rapidly. This is the 'transition region' in our experiments where the rate of change of ΔP^+ with λ begins to deviate from the behavior predicted by equation (3).

The behavior for $\lambda > 1$ requires more careful consideration. Although the drops are more deformed from a

spherical shape for larger values of λ, the main change, as we have noted earlier, is an increase in length. Specifically, the changes in geometry at the front and back of the drop are relatively small and it is mainly the region of 'constant' cross-sectional area which is increased. Thus, the change is the detailed flow s structure with increase of $\lambda \gtrsim 1$ is almost totally confined to an increase in length of the annular flow-like region at the middle of the drop. For a true annular flow of two immiscible fluids, the pressure drop is increased with increasing $\sigma > 1$ and decreased for $\sigma < 1$. We suggest that the measured increments of ΔP^+ with increase in $\lambda \geq 1$ can be interpreted essentially as being due to an increase in length of an (admittedly complicated) annular flow-like regime. This would imply, as suggested in the introduction of this section, that ΔP^+ should increase with increase of λ for $\lambda \gtrsim 1$ and $\sigma > 1$, but decrease for $\sigma < 1$. This qualitative idea is in complete agreement with the experimental results for $\lambda \gtrsim 1$. Thus for system 2 ($\sigma < 1$), the extra pressure drop increases with respect to λ for $\lambda \lesssim 1$, but does decrease for $\lambda \gtrsim 1$ as expected. Similarly for system 3 ($\sigma = 0.58$), the extra pressure drop, which is initially positive and increasing for $\lambda \lesssim 1$, reaches a maximum at 1, and then decreases to negative values for 1. The same argument can be applied to systems 1 and 4 to

explain the behavior of ΔP^+ for $\lambda \gtrsim 1$. In particular, we have found that ΔP^+ increases at a decreasing rate for system 1 but at an increasing rate for system 4 in the region $\lambda \gtrsim 1$. Surprisingly, it appears that we can actually estimate the increase (or decrease) in extra pressure drop for a change in λ by assuming that the increase in ΔP^+ is due solely to an increase in the length of an annular core of the suspended fluid. This increase (for $\sigma > 1$) or decrease ($\sigma < 1$) of additional pressure drop can be shown to be

$$-8\Delta L\left(\frac{\beta^4}{\beta^4+\frac{\sigma}{1-\sigma}}\right), \tag{6}$$

where ΔL is the increase in the length of the drop and β is the radial distance of the interface measured from the tube axis. Both quantities are nondimensionalized by the tube radius R_o. An example is given for system 4 (see figure 5) where this effect on ΔP^+ is assumed to hold starting from $\lambda = 0.985$ and values of ΔL and β are obtained from the drop shape photographs.

(b) Viscoelastic fluid systems

Let us now consider the role of viscoelasticity in contributing to the extra pressure drop. Qualitatively, a comparison of the results for systems 5 - 8 in figures 5 and 7 with those for systems 1 - 4 in figures 6 and 7 shows surprisingly little difference when ΔP^+ is

nondimensionalized with respect to the characteristic wall-shear viscosity for simple tube flow of the viscoelastic fluid at the same flow rate. Indeed, nearly all of the detailed discussion above for systems 1 - 4 may be carried over to the viscoelastic case. The only major exception is the magnitudes of $(\Delta P^{+} R_o/\mu_o \bar{V})$ which appear to be somewhat lower than for the Newtonian problem at larger σ, but somewhat larger (less negative) in the case of low σ.

This last point is illustrated in figure 9 where we have compared results for equal values of the deformation (flow rate) parameter $\Gamma^{-1}(=13.3)$ and approximately equal pairs of σ values from the Newtonian and from the corresponding viscoelastic case. The extra pressure drop is considerably lower for $\sigma=3.7$ in the viscoelastic fluid, than for $\sigma=2.04$ in a Newtonian fluid. Similar behavior is observed for $\sigma\simeq1$, although the difference is less pronounced. Finally, for $\sigma\simeq0.15$, the situation is reversed, i.e. the viscoelastic fluid actually shows a larger value of $(\Delta P^{+} R_o/\mu_o \bar{V})$ than the Newtonian fluid. At present, we can give no firm explanation for this phenomena. We would simply recall that a substantial transition in the qualitative shape was also observed (compared to the Newtonian case) for the viscoelastic fluid as σ was varied, and it seems likely that the two features are connected. However,

any simple minded argument based on the shape of the drops without the consideration of the actual flow field and of other properties (e.g. shear thinning, normal stresses, extensional viscosity) of the viscoelastic fluid would only be fortuitous, and of little fundamental value.

4. Conclusion

We have presented results for the additional pressure drop, the drop velocity, the drop shape and streamlines of a train of neutrally buoyant drops suspended concentrically in a cylindrical tube. Reasonable agreement was found on comparing available theoretical and experimental reports in literature with our present work on the limiting behavior of drop shape, $U/\overline{V}$ and ΔP^+ at high and low values of λ and at certain data points. Also, we were able to qualitatively explain the results for intermediate values of λ. This study also points out the differences observed between the cases of a viscoelastic and Newtonian suspending fluid. In particular, the use of a viscoelastic fluid caused a substantial transition in the shape of the drops (compared to the Newtonian case) as the viscosity of the suspended drop was varied; and caused $(\Delta P^+ R_o/\mu_o \overline{V})$ to be reduced for high values of σ ($\gtrsim 0.58$) but increased for low values of σ as compared to the Newtonian case. It may be noted, however, that in comparing the viscoelastic and Newtonian systems, the former was characterized only by an apparent viscosity at the wall shear rate which is relevant for simple tube flow of the pure suspending fluid. A systematic variation of the viscoelastic properties (and also purely viscous properties, e.g. shear thinning) was not attempted and probably such an attempt is necessary

before any qualitative explanation on the role of visco-elasticity can be achieved. Nevertheless the present study on the role of viscoelasticity should be helpful in understanding two-phase flow in porous media, transport of two-phase fluids in tubes and the macroscopic modeling of blood flow in capillaries and moreover, induce further study on this area of research.

REFERENCES

Brenner, H. 1971 Pressure drop due to the motion of neutrally buoyant particles in duct flows. II. Spherical droplets and bubbles. Ind. Engng. Chem. Fund. 10, 537.

Bretherton, F. P. 1960 The motion of long bubbles in tubes. J. Fluid Mech. 10, 166.

Coleman, B. D., Markovitz, H. & Noll, W. 1966 Viscometric Flows of Non-Newtonian Fluids. Springer-Verlag.

Goldsmith, H. L. & Mason, S. G. 1963 The flow of suspensions through tubes. II. Single large bubbles. J. Colloid Sci. 18, 237.

Hetsroni, G., Haber, S. & Wacholder, E. 1970 The flow field in and around a droplet moving axially within a tube. J. Fluid Mech. 41, 689.

Ho, B. P. 1975 Ph.D. thesis, California Institute of Technology.

Hochmuth, R. M. & Sutera, S. P. 1970 Spherical caps in low Reynolds-number tube flow. Chem. Engng. Sci. 25, 593.

Huppler, J. D., Ashare, E. & Holmes, L. A. 1967a Rheological properties of three solutions. Part I. Non-Newtonian viscosity normal stresses, and complex viscosity. Trans. Soc. Rheol. 11, 159.

Huppler, J. D., MacDonald, I. F., Ashare, E., Spriggs, T. W. Bird, R. B. & Holmes, L. A. 1967b Rheological properties of three solutions. Part II. Relaxation and growth of shear and normal stresses. Trans. Soc. Rheol. 11, 181.

Hyman, W. A. & Skalak, R. 1969 Viscous flow of a suspension of liquid drops in a cylindrical tube. Tech. Rept. 3, Project NR062-393. Columbia University, New York.

Hyman, W. A. & Skalak, R. 1970 Viscous flow of a suspension of deformable liquid drops in a cylindrical tube. Tech. Rept. 5, Project NR062-393. Columbia University, New York.

Leal, L. G., Skoog, J. & Acrivos, A. 1971 On the motion of gas bubbles in a viscoelastic fluid. Canadian J. Chem. Engng. 49, 569.

Prothero, J. & Burton, A. C. 1961 The physics of blood flow in capillaries. I. The nature of the motion. Biophysical J. 1, 566.

ibid. 1962a II. The capillary resistance to flow. Biophysical J. 2, 199.

ibid. 1962b III. The pressure required to deform erythrocytes in acid-citrate-dextrose. Biophysical J. 2, 213.

Savins, J. G. 1969 Non-Newtonian flow through porous media. Ind. & Engng. Chem. 61, 18.

Sutera, S. P. & Hochmuth, R. M. 1968 Large scale modeling of blood flow in the capillaries. Biorheology 5, 45.

Taylor, G. I., 1960 Deposition of a viscous fluid on the wall of a tube. J. Fluid Mech. 10, 161.

FIGURE CAPTIONS

Figure 1. Schematic diagram of experimental set-up (not to scale): (1) constant temperature bath (2) micrometer syringe (3) bulk fluid storage (4) test section (5) pressure hole (6) Thermo-couple probe (7) camera and moving mechanism (8) by-pass valve (9) pressure transducer (10) transducer indicator and recorder (11) thermocouple reading (12) withdrawal and infusion pump (13) waste storage (14) storage reservoir.

Figure 2. Drop shapes of systems 1a, 1b, 4a, 4b, 5b, 5d, 8b, and 8d.

Figure 3. Streamline pictures of system 1b: a single drop and the leading drop of a train; system 2d: a train of drops; system 6b: a train of drops; system 7b: a single drop and a train of drops.

Figure 4. Relative velocity of drops ($U/\bar{V}$-2) versus drop size. In (a): ◆, system 1a; ●, system 2a; ▼, system 3a; ■, system 4a; ○, results of Hyman & Skalak (1969) for undeformed drops and σ=1; ———, equation (1) (Hetsroni, et.al. (1970)) for σ=2.04, 0.93, 0.58, and 0.19. In (b): ●, system 2a; ◀ system 2b; ▲, system 2c;

▶ , system 2d; results of Hyman & Skalak (1970) for deformed drops, $\sigma=1$ and for $\Gamma^{-1}=10$ (◁) and $\Gamma^{-1}=4$ (▷).

Figure 5. Dimensionless extra pressure drop, $(\Delta P^{+} R_o/\mu_o \bar{V})$ versus λ for systems 1a, b, c, d; 3a, b, c, d; 4a, b, c, d; — — —, equation (3) (Brenner (1971)) for $\sigma=2.04$, 0.58, and 0.19; ----, estimation of extra pressure drop by assuming increase of λ is equivalent to increase of an annular core starting from $\lambda=0.985$.

Figure 6. Dimensionless extra pressure drop, $(\Delta P^{+} R_o/\mu_o \bar{V})$ versus λ for systems 5a, b, c, d; 7a, b, c, d; 8a, b, c, d.

Figure 7. $(\Delta P^{+} R_o/\mu_o \bar{V})$ versus λ for systems 2a, b, c, d; system 6a, b, c, d; — — —, equation (3) for $\sigma=0.93$. Results of Hyman & Skalak (1969, 1970) for $\sigma=1$: ○ , undeformed drops; ◁ , $\Gamma^{-1}=10$ and ▷ , $\Gamma^{-1}=4$ for deformed drops.

Figure 8. $(\Delta P^{+} R_o/\mu_o \bar{V})$ versus $\Gamma(=\mu_o \bar{V}/\gamma)$ for system 1.

Figure 9. A comparison of extra pressure drop between Newtonian and viscoelastic systems for $\Gamma^{-1}=13.3$.

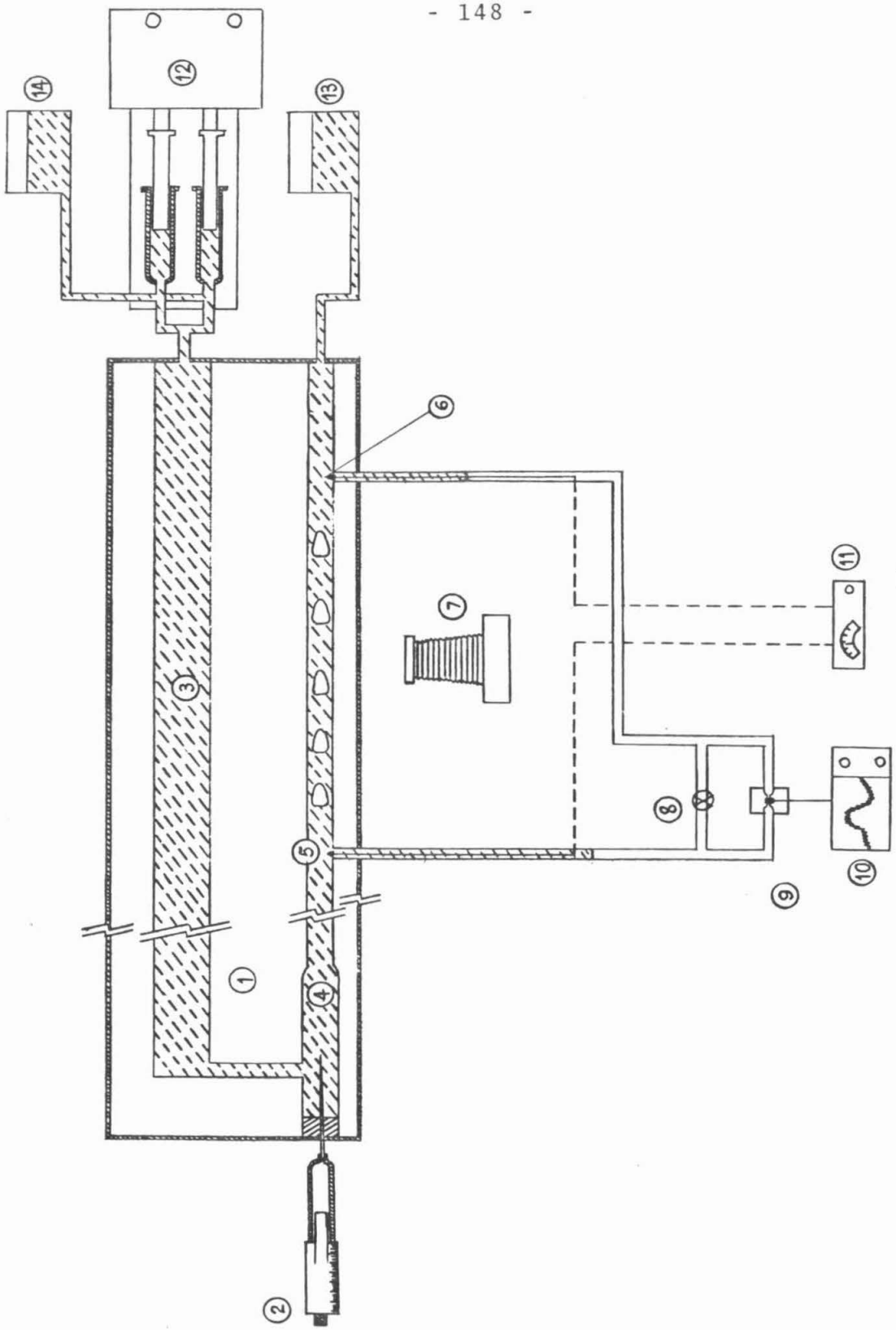

Figure 1.

Figure 2.


λ = .726
λ = .831
λ = .914
λ = .985
λ = 1.046
λ = 1.102
(1a) σ = 2.04 Γ⁻¹ = 13.3
(1b) σ = 2.04 Γ⁻¹ = 9.9
(4a) σ = .19 Γ⁻¹ = 13.3
(4b) σ = .19 Γ⁻¹ = 9.9
(5b) σ = 3.7 Γ⁻¹ = 13.3
(5d) σ = 4.9 Γ⁻¹ = 10.1
(8b) σ = .13 Γ⁻¹ = 13.3
(8d) σ = .17 Γ⁻¹ = 10.1

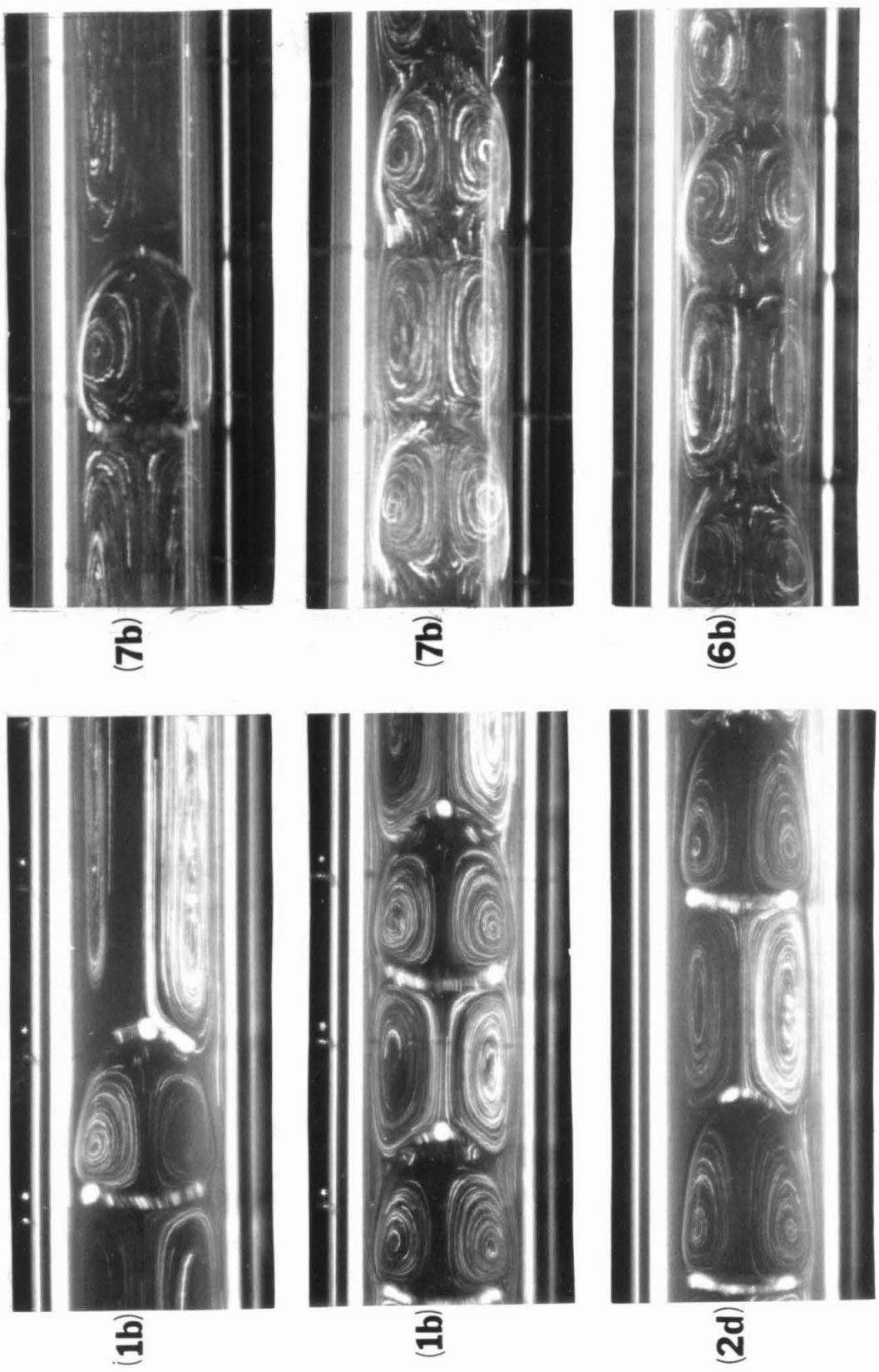

Figure 3.

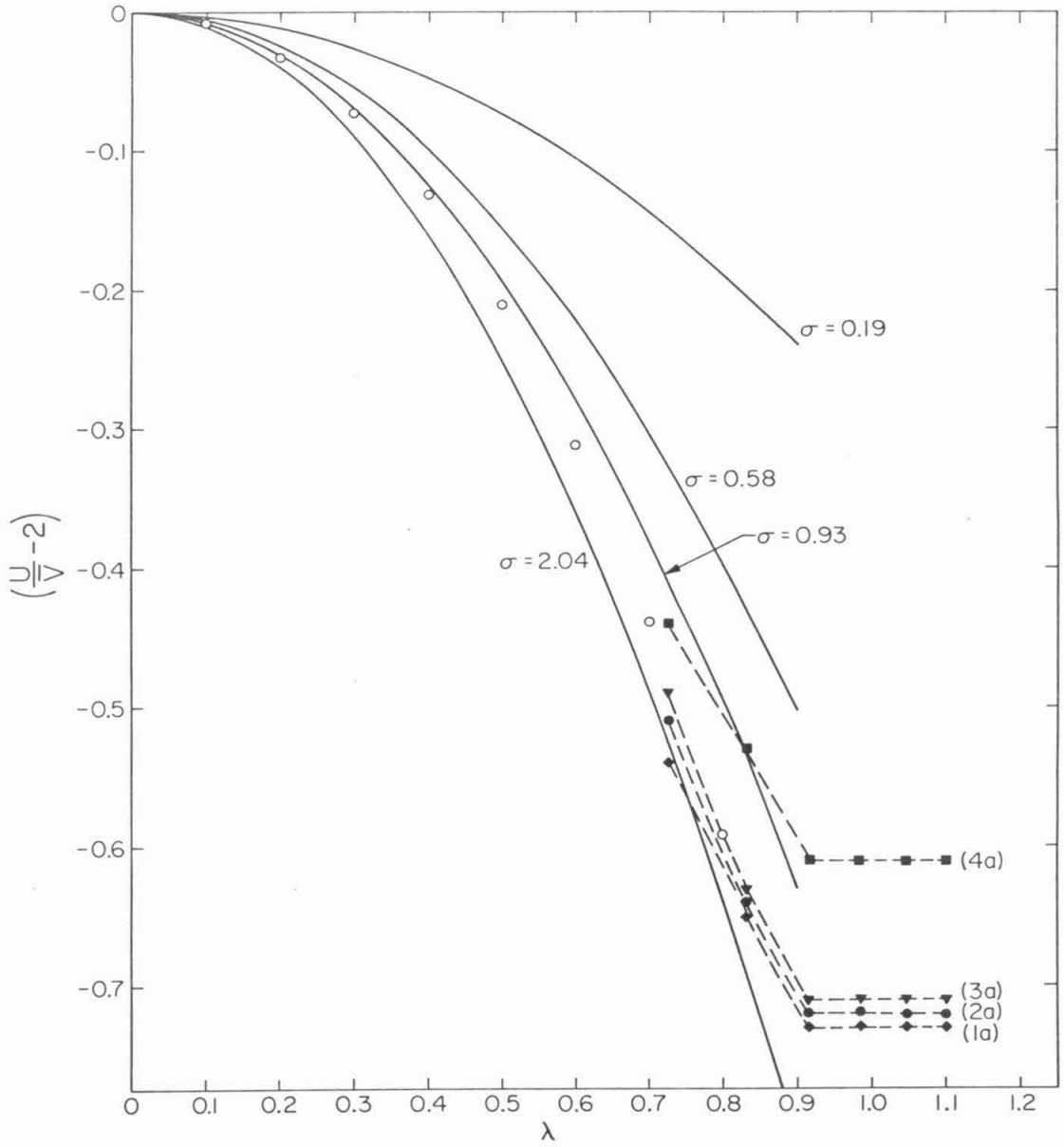
0
-0.1
-0.2
-0.3
-0.4
-0.5
-0.6
-0.7
$\left(\frac{U}{V}-2\right)$
0
0.1
0.2
0.3
0.4
0.5
0.6
0.7
0.8
0.9
1.0
1.1
1.2
λ
σ = 0.19
σ = 0.58
σ = 0.93
σ = 2.04
(4a)
(3a)
(2a)
(1a)

Figure 4 a.

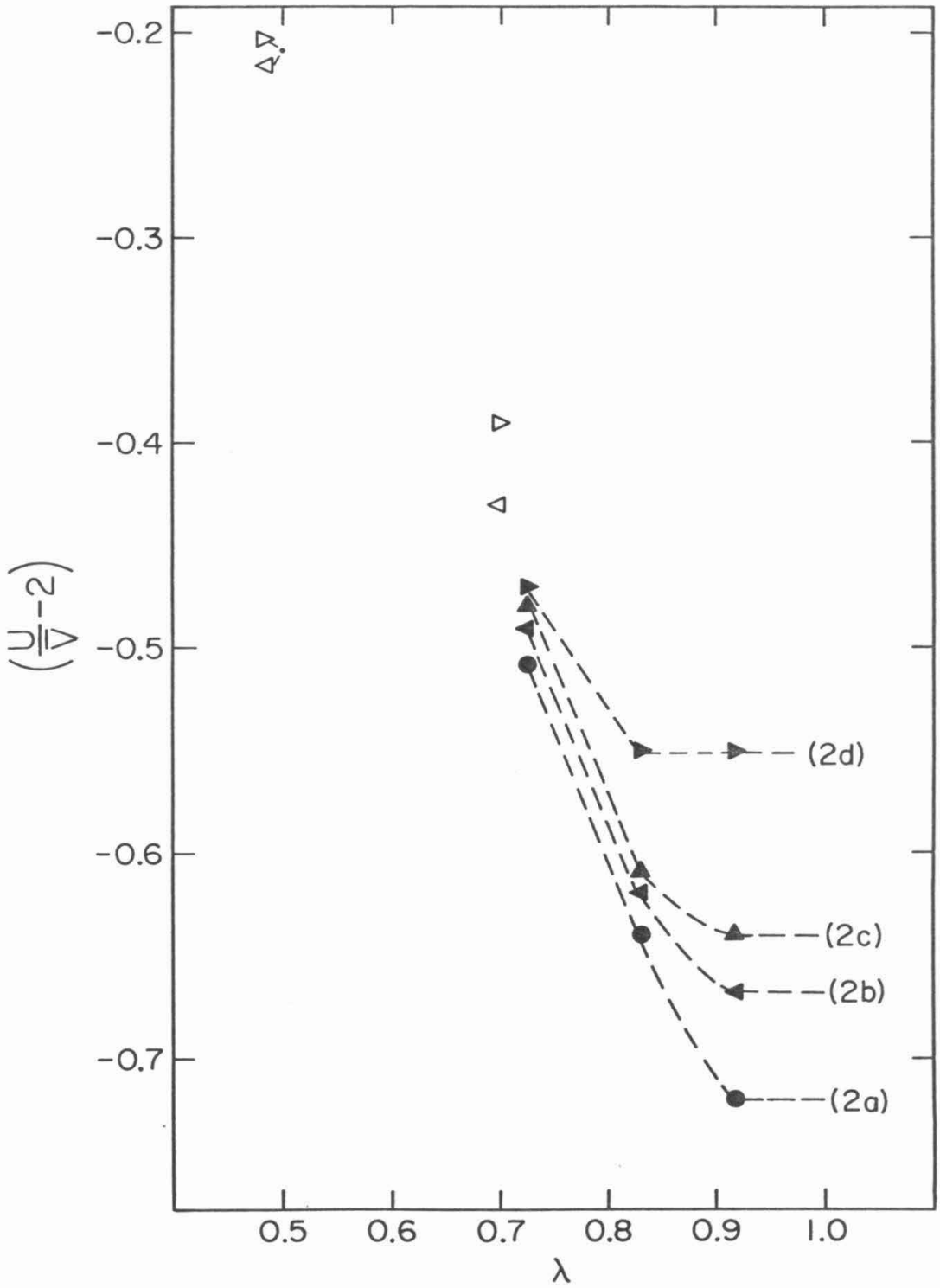

Figure 4b.

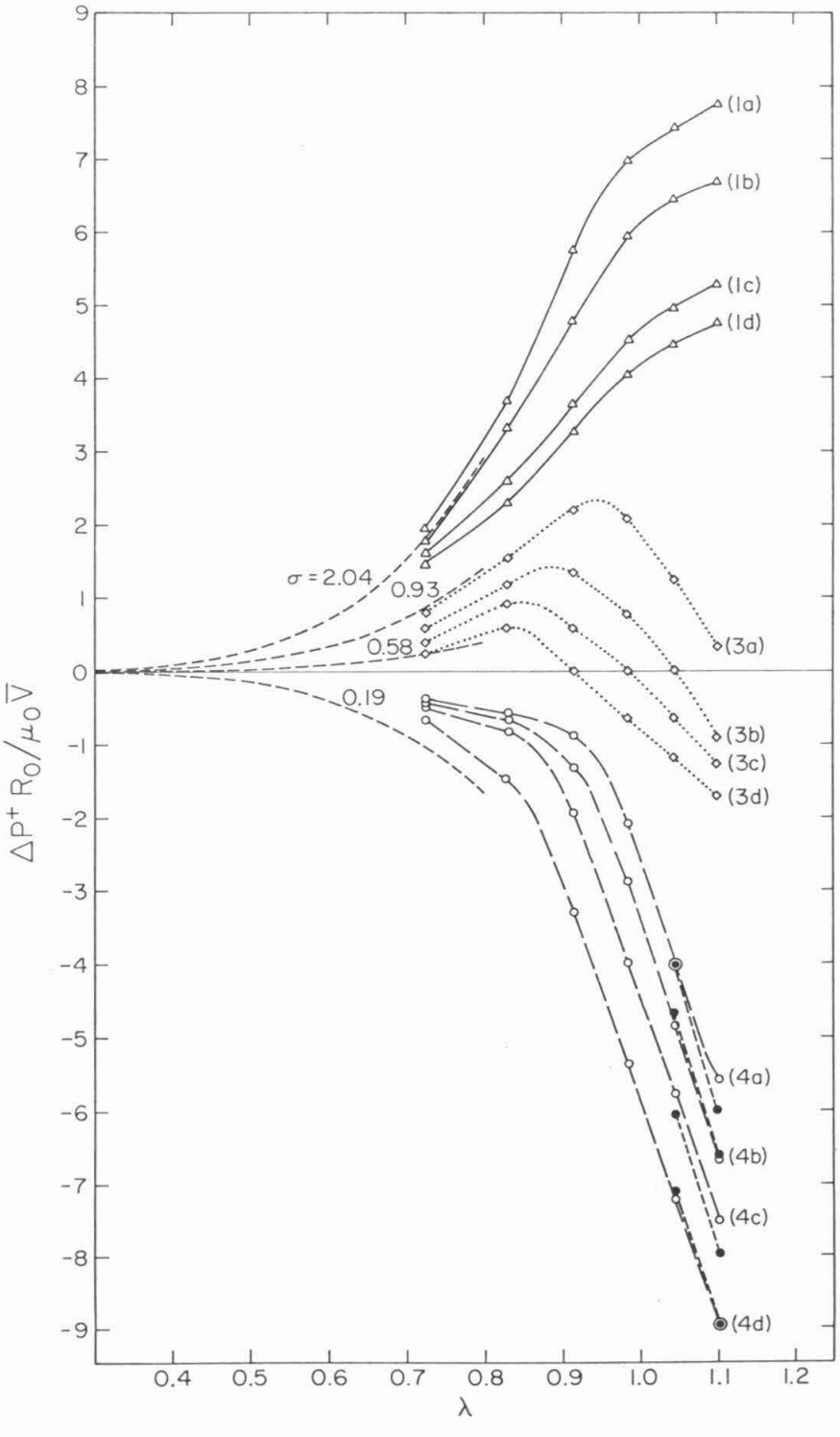
(1a)
(1b)
(1c)
(1d)
σ = 2.04
0.93
0.58
0.19
(3a)
(3b)
(3c)
(3d)
(4a)
(4b)
(4c)
(4d)
ΔP⁺ R₀/μ₀V̄
λ
9
8
7
6
5
4
3
2
1
0
-1
-2
-3
-4
-5
-6
-7
-8
-9
0.4
0.5
0.6
0.7
0.8
0.9
1.0
1.1
1.2

Figure 5.

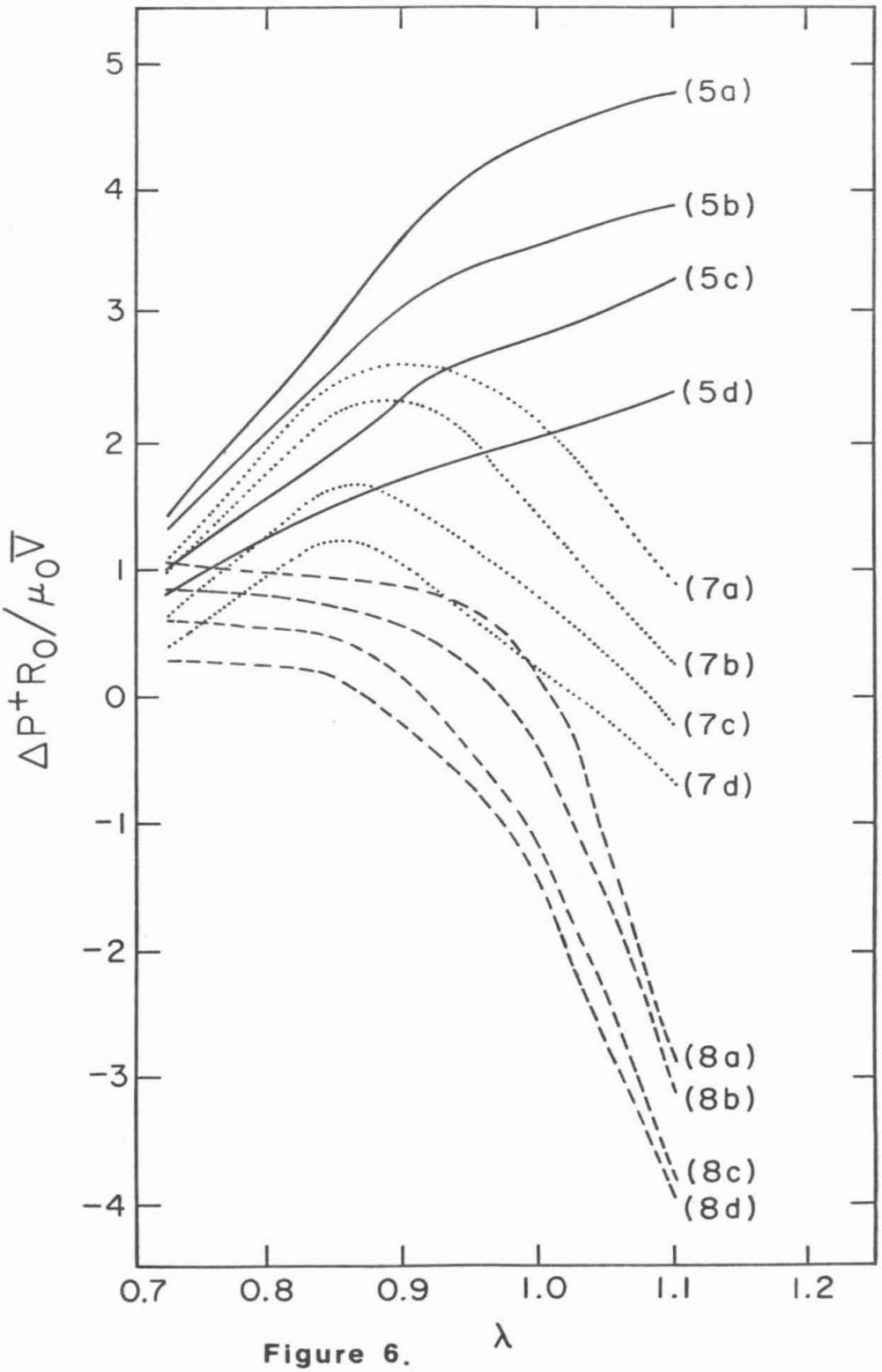
5
4
3
2
1
0
-1
-2
-3
-4
0.7
0.8
0.9
1.0
1.1
1.2
λ
$\Delta P^+ R_0/\mu_0 \bar{V}$
(5a)
(5b)
(5c)
(5d)
(7a)
(7b)
(7c)
(7d)
(8a)
(8b)
(8c)
(8d)

Figure 6.

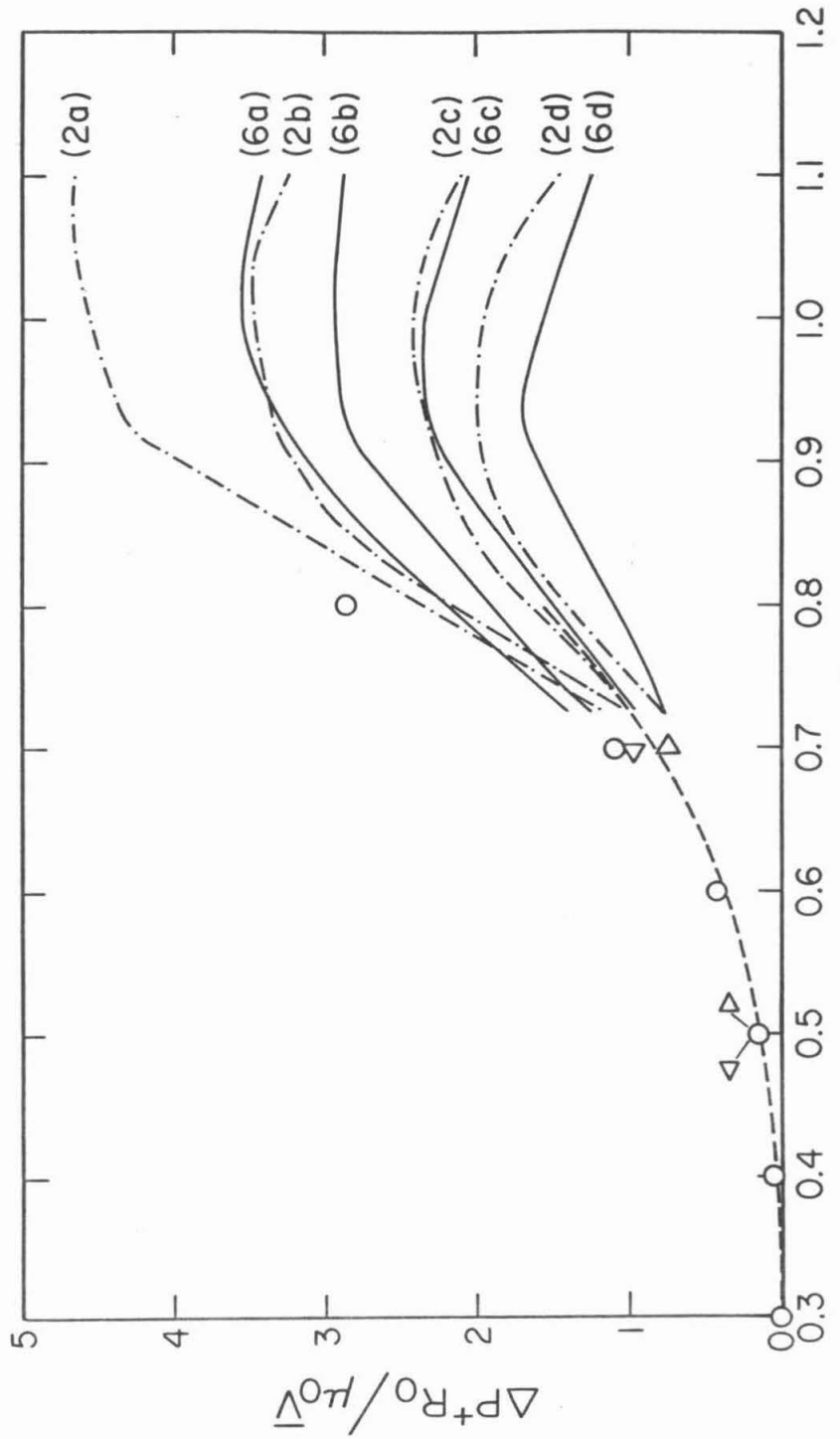
(2a)
(6a)
(2b)
(6b)
(2c)
(6c)
(2d)
(6d)
$\Delta P^+ R_o / \mu_o \bar{V}$
λ
0
1
2
3
4
5
0.3
0.4
0.5
0.6
0.7
0.8
0.9
1.0
1.1
1.2

Figure 7.

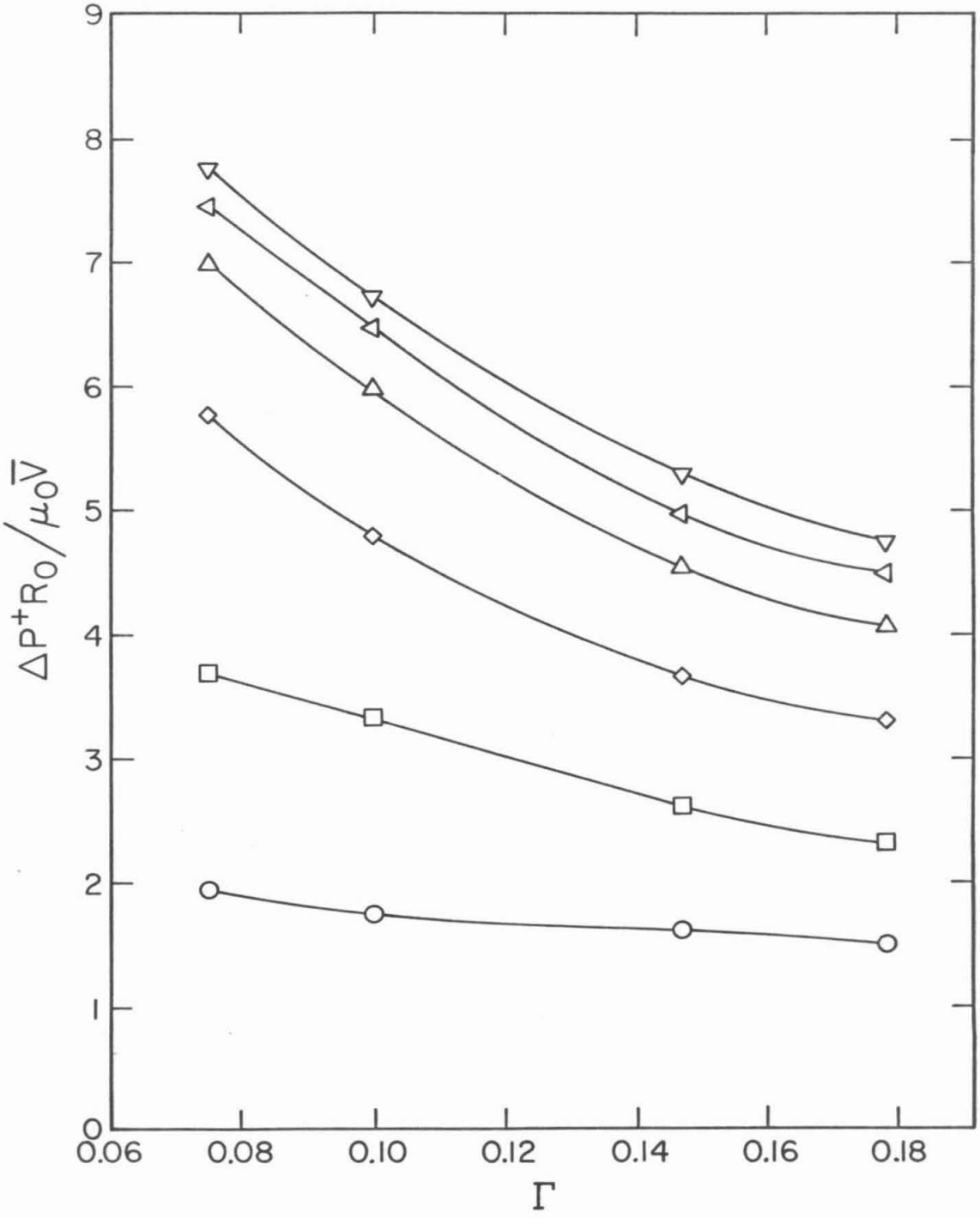

Figure 8.

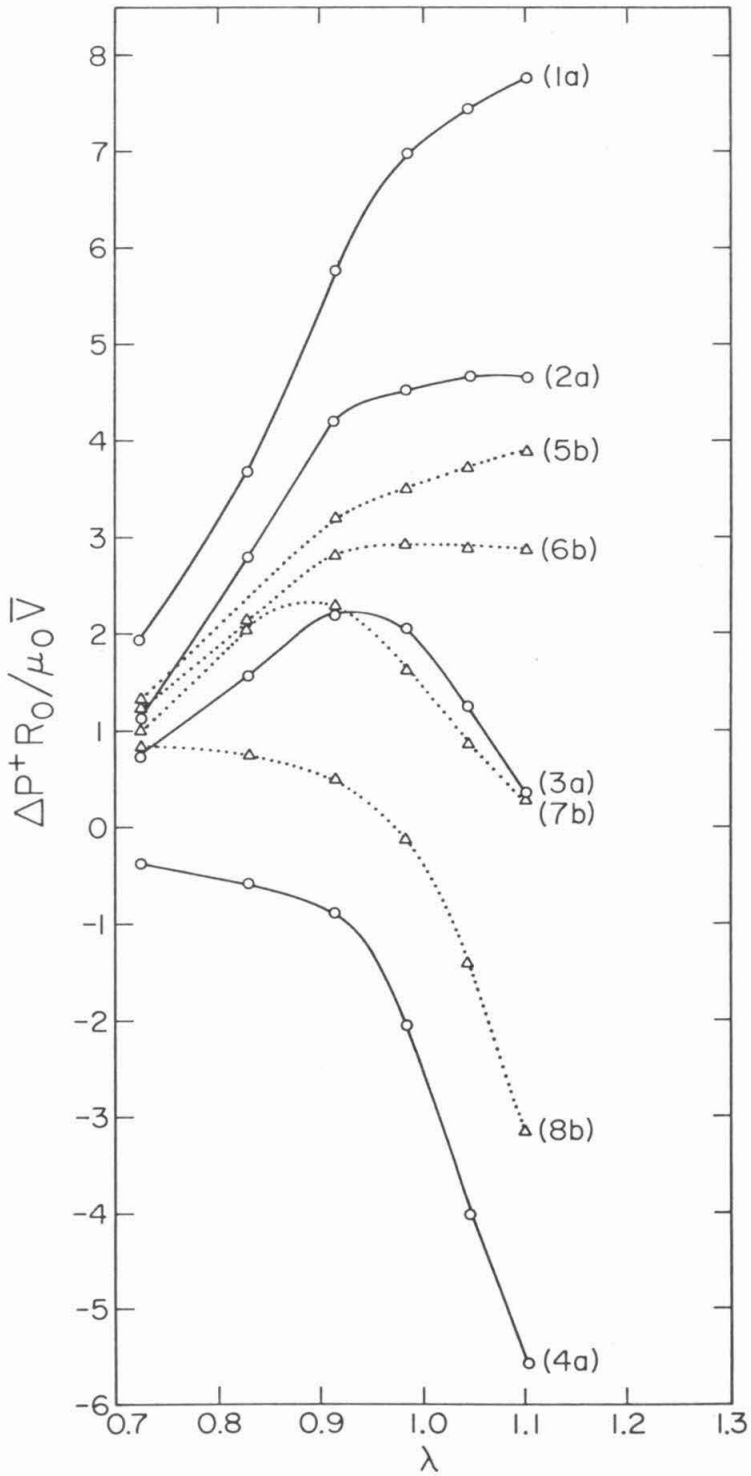
8
7
6
5
4
3
2
1
0
-1
-2
-3
-4
-5
-6
0.7
0.8
0.9
1.0
1.1
1.2
1.3
λ
$\Delta P^+ R_0/\mu_0 \bar{V}$
(1a)
(2a)
(5b)
(6b)
(3a)
(7b)
(8b)
(4a)

Figure 9.

TABLE CAPTIONS

Table 1. Conditions of experiments.

Table 2. Velocity of drops relative to the average flow rate, $(U/\bar{V})$.

TABLE 1. CONDITIONS OF EXPERIMENTS

		Quantities Independent of Flow Rate	Quantities Dependent on Flow Rate			
			(a)	(b)	(c)	(d)
Flow Rate V cm./sec.		-	.390	.525	.756	.920
Newtonian Systems	Wall shear rate β_w sec.$^{-1}$	-	3.13	4.20	6.05	7.36
	Suspending fluid viscosity μ_o poise	4.25	-	-	-	-
	Bulk Reynolds number $(\rho V R_o)/\mu_o$	-	0.05	0.06	0.09	0.1
	Deformation Parameter Γ^{-1}	-	13.3	9.9	6.8	5.6
	Viscosity ratio, σ — System 1 (μ_i=8.65 p.)	2.04	-	-	-	-
	Viscosity ratio, σ — System 2 (μ_i=3.97 p.)	0.93	-	-	-	-
	Viscosity ratio, σ — System 3 (μ_i=2.45 p.)	0.58	-	-	-	-
	Viscosity ratio, σ — System 4 (μ_i=0.80 p.)	0.19	-	-	-	-
Visco-elastic Systems	Wall shear rate β_w sec.$^{-1}$	-	4.10	5.50	7.93	9.65
	Suspending fluid viscosity μ_o poise	-	6.54	5.46	4.47	4.08
	Suspending fluid first normal stress difference N_1, dyne/cm^2	-	40.0	50.0	70.0	80.0
	Bulk Reynolds number $(\rho V R_o)/\mu_o$	-	0.03	0.05	0.09	0.1
	Deformation Parameter Γ^{-1}	-	14.9	13.3	11.2	10.1
	Viscosity ratio, σ — System 5 (μ_i=20.1 p.)	-	3.1	3.7	4.5	4.9
	Viscosity ratio, σ — System 6 (μ_i=6.9 p.)	-	1.1	1.3	1.5	1.7
	Viscosity ratio, σ — System 7 (μ_i=2.4 p.)	-	.37	.44	..54	.59
	Viscosity ratio, σ — System 8 (μ_i=.69 p.)	-	.11	.13	.15	.17

TABLE 2. RELATIVE VELOCITY OF DROPS ($U/\bar{V}$)

System number	v (ml.)					
	.2	.3	.4	.5	.6	.7
1a	1.46	1.35	1.27	1.27	1.27	1.27
1b	1.46	1.35	1.30	1.30	1.30	1.30
1c	1.46	1.35	1.32	1.32	1.32	1.32
1d	1.47	1.39	1.39	1.39	1.39	1.39
2a	1.49	1.36	1.28	1.28	1.28	1.28
2b	1.51	1.38	1.33	1.33	1.33	1.33
2c	1.52	1.39	1.36	1.36	1.36	1.36
2d	1.53	1.45	1.45	1.45	1.45	1.45
3a	1.51	1.37	1.29	1.29	1.29	1.29
3b	1.52	1.41	1.35	1.35	1.35	1.35
3c	1.54	1.42	1.39	1.39	1.39	1.39
3d	1.58	1.49	1.49	1.49	1.49	1.49
4a	1.56	1.47	1.39	1.39	1.39	1.39
4b	1.57	1.48	1.41	1.41	1.41	1.41
4c	1.59	1.50	1.48	1.48	1.48	1.48
4d	1.65	1.55	1.55	1.55	1.55	1.55
5a	1.37	1.31	1.26	1.26	1.26	1.26
5b	1.38	1.35	1.29	1.29	1.29	1.29
5c	1.41	1.35	1.32	1.32	1.32	1.32
5d	1.47	1.39	1.36	1.36	1.36	1.36
6a	1.37	1.31	1.26	1.26	1.26	1.26
6b	1.38	1.36	1.29	1.29	1.29	1.29
6c	1.42	1.38	1.32	1.32	1.32	1.32
6d	1.47	1.39	1.36	1.36	1.36	1.36
7a	1.38	1.31	1.28	1.28	1.28	1.28
7b	1.38	1.36	1.31	1.31	1.31	1.31
7c	1.44	1.38	1.36	1.36	1.36	1.36
7d	1.49	1.39	1.39	1.39	1.39	1.39
8a	1.40	1.33	1.32	1.32	1.32	1.32
8b	1.42	1.38	1.34	1.34	1.34	1.34
8c	1.47	1.41	1.41	1.41	1.41	1.41
8d	1.51	1.43	1.43	1.43	1.43	1.43

APPENDIX C

Photographs of the eight systems at all flow rates and drop volumes were taken during the course of the experiments. Only a limited number of pictures relevant to depict the differences in shapes due to changes in σ and flow rate, and the differences between Newtonian and viscoelastic systems were presented in section 3(i). The rest of the pictures are given here in figures C1, C2, C3, and C4.

(1c) (1d) (2a) (2b) (2c) (2d)

Figure C1.

(3a) (3b) (3c) (3d) (4c) (4d)

Figure C2.

Figure C 3.

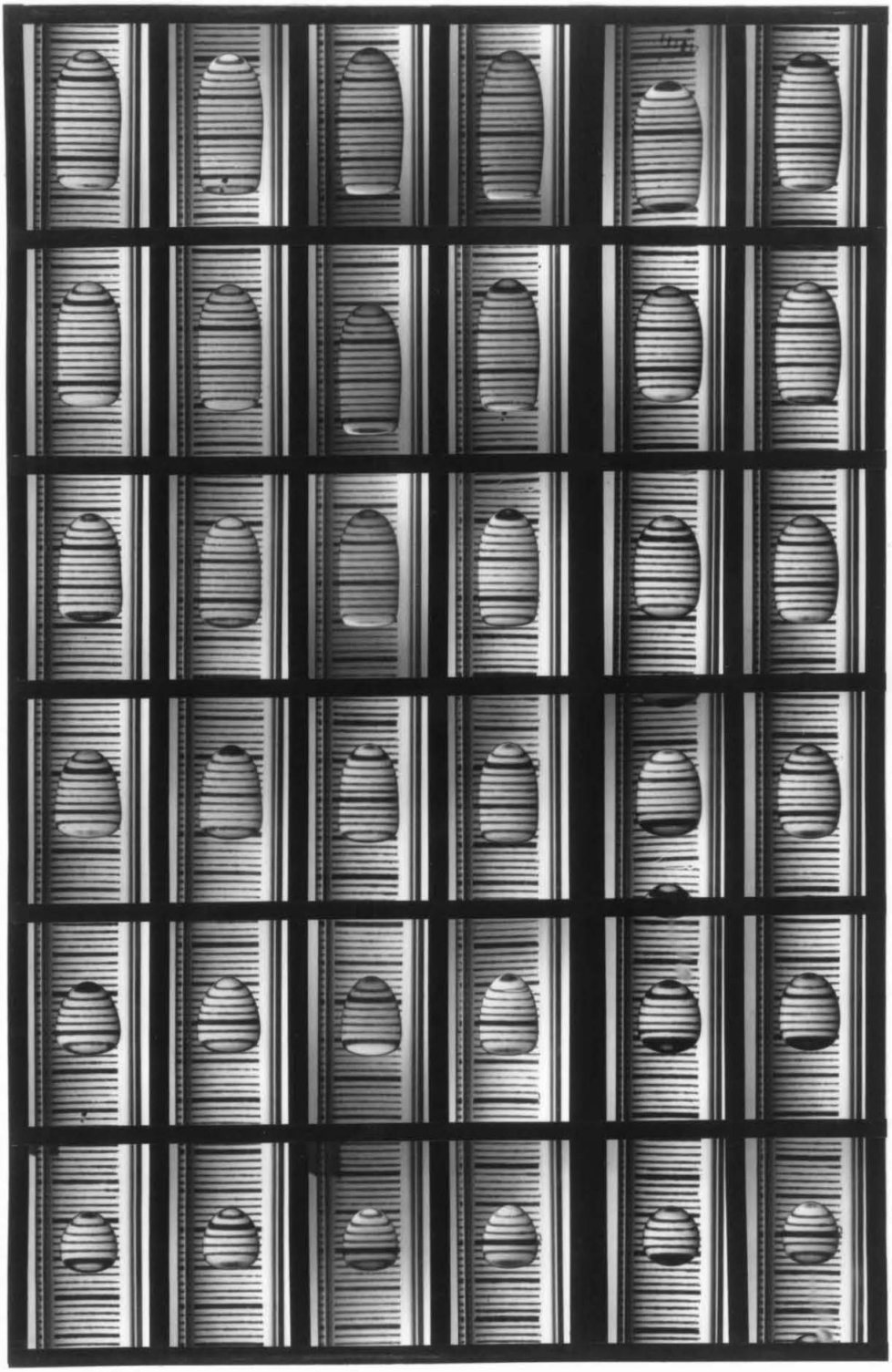

(7a) (7b) (7c) (7d) (8a) (8c)

Figure C4.

CHAPTER V

CONCLUSION

The lateral migration of a neutrally buoyant rigid sphere in two-dimensional unidirectional flows was investigated theoretically. In Chapter II, it was found that the sphere influenced by small, but not negligible, fluid inertia and by the presence of the bounding walls, migrates across streamlines. A result for the lateral velocity was obtained for a general unidirectional flow between two parallel plane walls. A sphere in simple shear migrates to the center midway between the walls, whereas in plane Poiseuille flow, it migrates to distances from both walls corresponding to 20% of the wall separation. In Chapter III, the normal stress effect of a second-order fluid was found to cause lateral migration even in the absence of fluid inertia. Results for the lateral velocity were obtained for a general two-dimensional unidirectional flow. In contrast to the results of Chapter II, the bounding walls do not affect the lateral migration and no migration was found in the case of simple shear. By using normal stress data for viscoelastic fluids, it was found that a sphere migrates to the position of minimum shear rate.

The theoretical results were found to agree with the experimental data reported in the literature. In addition, the effective viscosity (in plane Poiseuille flow) of a suspension of spheres under the influence of inertia-induced migration and translational Brownian motion was obtained. For the case of normal stress-induced migration, the results were applied to spheres suspended in a screw extruder.

In Chapter IV, experimental results on the extra pressure drop, drop velocity and shape, and streamlines were obtained for the motion of large neutrally buoyant drops in a cylindrical tube. Both Newtonian and visco-elastic suspending fluids were considered with distinct differences in the drop shape and extra pressure drop being found between the two cases.

It is hopeful that the fundamental knowledge provided in this dissertation will be useful in future technological applications.